Colloidal Nanoparticles as Catalysts and Catalyst Precursors for Nitrite Hydrogenation

Yingnan Zhao

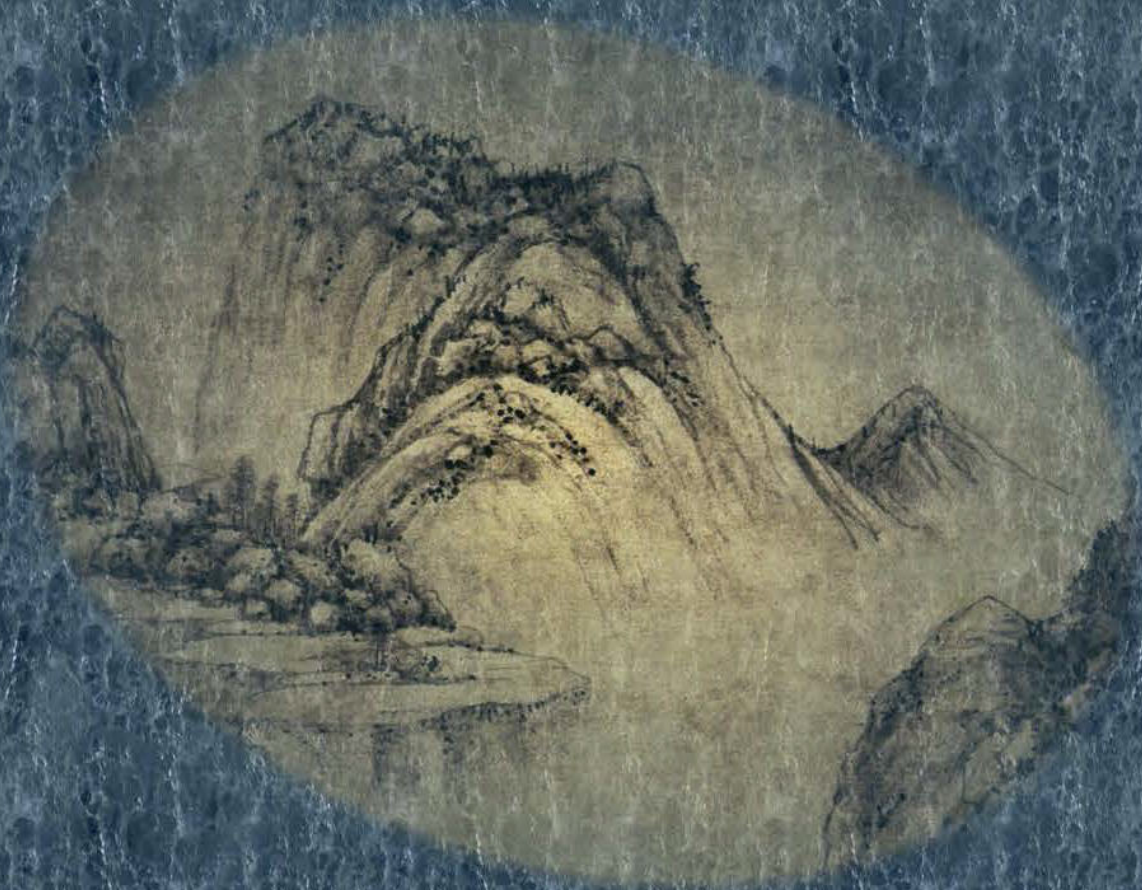

COLLOIDAL NANOPARTICLES AS CATALYSTS AND CATALYST PRECURSORS FOR NITRITE HYDROGENATION

Yingnan Zhao

Promotion committee

Prof. dr. ir. J.W.M. Hilgenkamp	Chairman	University of Twente	The Netherlands
Prof. dr. ir. L. Lefferts	Promoter	University of Twente	The Netherlands
Prof. dr. ir. J.E. ten Elshof		University of Twente	The Netherlands
Prof. dr. G. Mul		University of Twente	The Netherlands
Prof. dr. J.J.L.M. Cornelissen		University of Twente	The Netherlands
Prof. dr. Y.D. Li		Tianjin University	China
Prof. J. Ross		University of Limerick	Ireland
Prof. M.A. Gilarranz		Universidad Autónoma de Madrid	Spain

The research described in this thesis was carried out the *Catalytic Processes and Materials* (CPM) group of the University of Twente, The Netherlands. I acknowledge financial support for my PhD study from *China Scholarship Council* (CSC).

Cover design: Yingnan Zhao

Motivation: The idea of the cover design raised when my friend, Bert Geerdink, suggested me to find some artistic likeness of the catalysts prepared for this research. An image of Chinese classical ink painting came to my mind when looking at the TEM images for the Pd nanoparticles supported on activated carbon. The image showing on the front cover is part of the painting "Peaceful moment on a water-flow pavilion" (水阁清幽图) by Huang Gongwang (黄公望, 1269 – 1354), a great painter born during the later Song Dynasty. The trees on the mountains have some similarity with the image of blank Pd nanoparticles distributed on sheet-like carbon material. Furthermore, the mountains also implies the long journey I have taken during the five-year PhD study, like the maxim on the back cover, given by Qu Yuan (屈原) more than 2000 years ago: "The journey will be endless and tough, and I will seek my beauty high and low with my will unbending" (路漫漫其修远兮，吾将上下而求索). The Chinese calligraphy was written by my grandfather, Zhao Dizun (赵弟尊).

Publisher: Wöhrmann Print Service, The Netherlands

ISBN: 978-90-365-3820-6

DOI: 10.3990/1.9789036538206

COLLOIDAL NANOPARTICLES AS CATALYSTS AND CATALYST PRECURSORS FOR NITRITE HYDROGENATION

DISSERTATION

to obtain
the degree of doctor at the University of Twente,
on the authority of the rector magnificus,
Prof. dr. H. Brinksma
on account of the decision of the graduation committee,
to be publicly defended
on Thursday January 15th 2015 at 16:45

by

Yingnan Zhao

born on July 14th 1984
in Heze, Shandong, China

This dissertation has been approved by the promoter

Prof. dr. ir. L. Lefferts

献给我们的父母，

和我爱的银儿。

Dedicated to our parents,

and to my Yin

with love.

Table of content

Chapter 1

Introduction

1. Catalyst preparation via colloidal methods

The conception "colloid" is primarily about size. A colloid always consists of at least two phases, either gas, liquid or solid, while the dispersed phase has dimensions within the range of 1 nm to 1μm traditionally [1]. There are eight possible phase combinations for a colloidal system, as classified in Table 1, the only exception being two gas phases, which always mix molecularly. In this thesis, the study is focused on colloidal system consisting of Pd nanoparticles (1 – 5 nm) synthesised and dispersed in aqueous phase.

Table 1. Type of colloidal systems (with typical examples) (Adapted from literature [1]).

Continuous phase	Dispersed phase		
	Gas (bubbles)	**Liquid (droplets)**	**Solid (particles)**
Gas		Liquid aerosol (mist)	Solid aerosol (smoke)
Liquid	Foam (Shampoo)	Emulsion (milk)	Sol (ink)
Solid	Solid foam (packaging)	Gel (butter)	Solid sol (stained glass)

The attempts to stabilize colloid go back to the time of Faraday [2]. Zsigmondy et al. reported a study on the stabilization of Au colloid by using stabilizers as glues, gums and starches in 1901 [3]. Over a century, the study of colloids was limited to very few kinds (e.g., silver chloride, gold) exclusively dispersed in aqueous phase, and most of the samples were troubled by problems such as polydispersed particle sizes and poor defined morphologies [4]. Due to these limitations, there were only quite a few applications of colloidal methods for catalytic purpose before the 1990s [5-7]. The last decade has witnessed a breakthrough of using colloids in catalytic applications, primarily attributed to the development of methods for colloid preparation [8-10]; nanoparticles of transition-metal and metal oxide with monodispersed sizes and shapes can be prepared in aqueous as well as in organic liquid solvents [11, 12]. Another attribute to the application came from the development of theory of particle growth control, colloid stabilization and agglomeration [4, 8, 13-15]. Nowadays researchers can manipulate nanostructured size and morphology easily using electrostatic ("inorganic") and/or steric ("organic") stabilization.

Nanoparticles (NPs), especially those smaller than 5 nm, are known as outstanding catalytic materials with high activity due to the large fraction of surface atom, being accessible for reactants. It is also well known that nanoparticles differ from bulk materials in terms of structure, including low coordination numbers of atoms in the surface, as well as electronic

structure [16, 17]. Traditionally, metal nanoparticles on catalyst support materials (metal oxides, zeolites, carbon, solid polymer, etc.) are prepared via methods such as impregnation, precipitation, ion-exchange, etc. [18-22]. With these methods, the particle size of the metal nanoparticles is usually influenced strongly by the preparation procedure, such as the choice of metal-precursors, metal loading, property of support, and calcination conditions, often resulting in a relatively broad particle size distribution. Furthermore, the shape of the nanoparticles is also poorly defined usually.

There is a wide range of catalytic reactions for which the activity per active site depends on the size of the metal particle, termed "structure-sensitive" reactions [23-25]. These reactions include hydrogenations [26-30], oxidations [31, 32], Suzuki or Heck couplings [33, 34], and electron transfer reactions [35]. In many cases, structure sensitivity has been studied using single crystal surfaces as model catalyst under ultra-high vacuum conditions, which is very different as compared to any realistic conditions for catalytic conversion, i.e. high pressure or in liquid phase [36]. The application of colloidal methods can achieve monodispersed metal nanoparticles with significant surface area, as opposed to single crystals, which can be tested under realistic reaction conditions. Under the condition that also the surface structure of the exposed planes in nanoparticles can be controlled, this approach holds the promise to bridge the material gap, connecting academic and industrial catalysis studies [37, 38].

2. Pd colloidal catalyst preparation

Pd nanoparticles can serve as good catalyst for hydrogenation and dehydrogenation [39-43], as well as cracking and carbon-carbon bond forming reactions such as Suzuki or Heck couplings [44-47]. These reactions have often been reported as "structure-sensitive", i.e., turnover frequency is influenced significantly by Pd particle size [33, 48-50]. However, there are also several specific reactions of these types that are claimed to be size-independent [51-53]. In some cases, structure sensitivity also depends on the reaction conditions and on the range of particle sizes [25]. The development of colloid methods opens the possibility to prepare monodispersed nanoparticles for model catalytic studies, in order to clarify the structure-sensitivity within specific size range.

2.1. Precursors

The most commonly used precursor for preparation of Pd colloids is Na_2PdCl_2, because of its stability in air and good solubility in a variety of solvents [4, 54, 55]. H_2PdCl_4 is another Pd precursor frequently used in literature, normally freshly prepared by dissolving $PdCl_2$ in HCl solution [56, 57]. The Cl^-, either released during reduction as the colloid prepared or as added HCl, is also reported as an oxidative etching agent, inducing recrystallization of e.g. multiply twinned particles to single crystals [58]. $Pd(NO_3)_2$ is also a precursor commercially available for colloid preparation; however, it is hygroscopic and tends to hydrolyse to $Pd(OH)_2$, thus less preferred for preparation with high purity requirements [59]. Organic palladium complexes, such as $Pd(acac)_2$, have also been used as colloid precursor when the synthesis is performed in organic liquid phase [60].

2.2. Reduction agents

Pd salts as precursors need to be reduced using reduction agents in liquid phase in order to prepare NPs. In general, alcohols, glycols, as well as hydrazine and hydrides can all serve as reductant, ensuring fast reduction of various Pd precursors [61-63]. The predominant shape of Pd nanoparticles is the Wulff polyhedron (sphere-like NPs) when Pd colloid is prepared via relatively fast reduction.

2.3. Stabilizers

The nanoparticles diffuse randomly in the dispersing liquid phase, and the system is unstable with respect to agglomeration in the absence of any protection of the particles. At short interparticle distances, two nanoparticle would be attracted to each other by van der Waals forces [8]. Stabilizers are needed to prevent agglomeration of nanoparticles. As early in 1965, Thiele et al. have performed a systematic comparison of 22 different protecting agents, both natural and synthetic, with the ability of preventing agglomeration of Au nanoparticles [13].

There are two established classes of nanoparticle stabilizers: (i) electrostatic (or electronic) and (ii) steric stabilizers [64]. Electrostatic stabilization occurs by adsorbing ions on the electrophilic metal surface. This adsorption creates an electrical double layer, resulting in Coulombic repulsion between the nanoparticles, opposing attractive van der Waal forces [19].

Steric stabilization is achieved by a protective barrier composed of large molecules, such as polymers or surfactants, surrounding individual nanoparticles. Steric stabilizers work by chemically bonding with at least part of the metal surface, as well as by physically occupying the interspace between nanoparticles, preventing direct contact between nanoparticles [14].

The latter effect has not been supported directly by clear experimental evidence so far; however it consistent with the thermodynamic mechanism schematically represented in Figure 1, including two aspects: (1) in the interparticle space, the adsorbed stabilizer on two approaching particles would be restrict in motion, preventing high free energy in the system; (2) on the other hand, a high local concentration of polymer in between two particles causes a local high osmotic pressure, inducing attraction of solvent molecules to decrease the local polymer concentration, thus separating the nanoparticles [65]. In summary, a good steric stabilizer requires bonding with the surface of NPs, with sufficient concentration and solubility in the dispersing solvent surrounding the NPs [8].

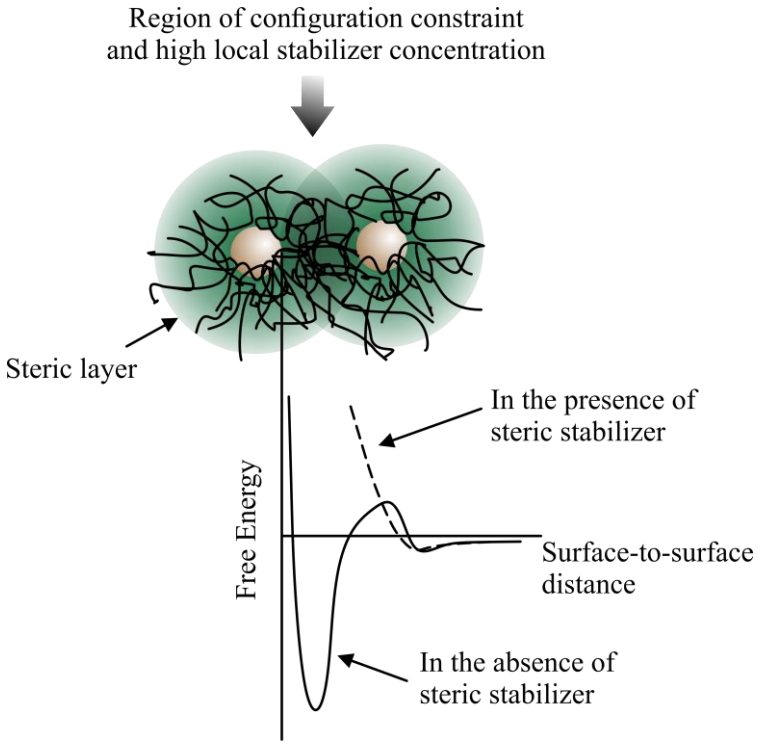

Figure 1. The thermodynamic mechanism of steric stabilization in a colloidal system: the steric layer created by adsorbed steric stabilizer present an energy barrier preventing the approach of two particles; high concentration of steric stabilizer in interparticle space would also cause osmotic effect by solvent.

In fact, electrostatic stabilization is always accompanied by a steric effect. Thus "electrosteric" stabilization (a combination of electrostatic and steric) has therefore been proposed as a third type of stabilization [14, 19].

Besides preventing agglomeration after preparation, several other effects have been reported in Pd nanoparticle preparation via colloidal method. The particle size of the nanoparticles prepared via chemical or electrochemical reduction in liquid phase can be manipulated by the amount and properties of stabilizers. Reetz et al. reported increasing Pd nanoparticle sizes from 2 to 4 nm when changing the electrostatic stabilizer in the order $^{+}N(n\text{-}C_4H_9)_4$ $<^{+}N(n\text{-}C_8H_{17})_4<^{+}$ $N(n\text{-}C_{18}H_{37})_4$ in a electrochemical colloid preparation procedure. Teranishi et al. reported that Pd nanoparticle sizes decrease in the range from 3 to 1.7 nm when increasing the amount of PVP stabilizer using alcohol as reducer [66], and Kim et al. reported similar effect on Pd NPs in the range between 3.5 and 7 nm with trioctylphosphine (TOP) as stabilizing surfactant [60].

The interaction between stabilizer and nanoparticle also influences the catalytic performance of the nanoparticles, including activity and selectivity. It is frequently reported that stabilizers, especially those strongly bonding with the metal surface, block surface sites and deactivate the catalysts [67-71]. Electrostatic stabilizers influence the charge of metal surface; even “neutral” polymer stabilizers, such as polyvinylpyrrolidone (PVP), are reported to induce charge-transfer with transition-metal NPs [72, 73]. In many cases, such interactions introduced by stabilizers remain after immobilizing the NPs on heterogeneous support materials, influencing the catalytic performance of the resulting catalysts, unless the stabilizers are completely removed [69, 74-76].

3. Nitrate and nitrite hydrogenation

3.1. Nitrate and nitrite in groundwater

Nitrate (NO_3^-) contamination of groundwater is a problem for supply of drinking water, because of harmful biological effects, as summarized in Figure 2 [77]. Nitrate is more stable than nitrite (NO_2^-) in the environment [78]. High concentration of nitrate in drinking water is harmful because it can be converted to more toxic nitrite in the human body, decreasing the oxygen-carrying capacity of blood, which can even be fatal to infants. Nitrite can also react with amines and amides resulting in N-nitroso compounds (nitrosamines and nitrosamide), which are suspected to be carcinogenic [78, 79].

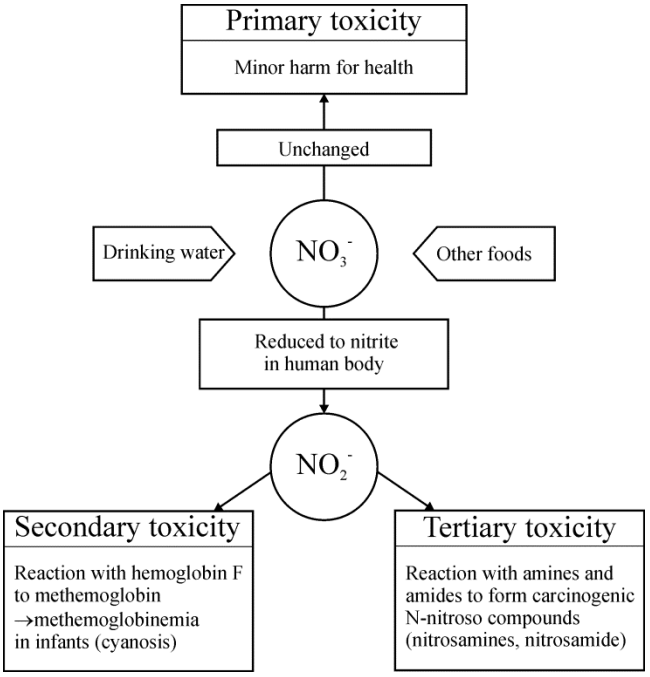

Figure 2. Overview on the toxicity of nitrate (adapted from [77])

Table 2. Causes of nitrate contamination in groundwater [80]

	Agriculture	**Municipal**	**Industrial**
Diffuse sources	• Use of synthetic nitrogen fertilizers • Use of organic fertilizers	• Combustion engines in vehicles • Disposal of municipal effluents by sludge spreading on fields	• Atmospheric emissions (nitric oxide and nitrite discharges) from energy production • Combustion engines in vehicles • Disposal of effluents by sludge spreading on fields
Point and linear sources	• Accidental spills of nitrogen-rich compounds • Absence of slurry storage facilities • Leaking slurry or manure tanks	• Old and badly designed landfills • Septic tanks • Leaking sewerage systems	• Disposal of nitrogen-rich wastes using well-injection techniques • Old and badly designed landfills
	• Nitrogen-rich effluent discharge to rivers with important groundwater connections • Poorly constructed wells which allow an exchange between polluted and non-polluted aquifer layers		

Note: all the activities listed can be result directly or indirectly in groundwater nitrate pollution. In the environment, several different forms of nitrogen (NO_2, NH_4^+, NH_3) can potentially be transformed into nitrate.

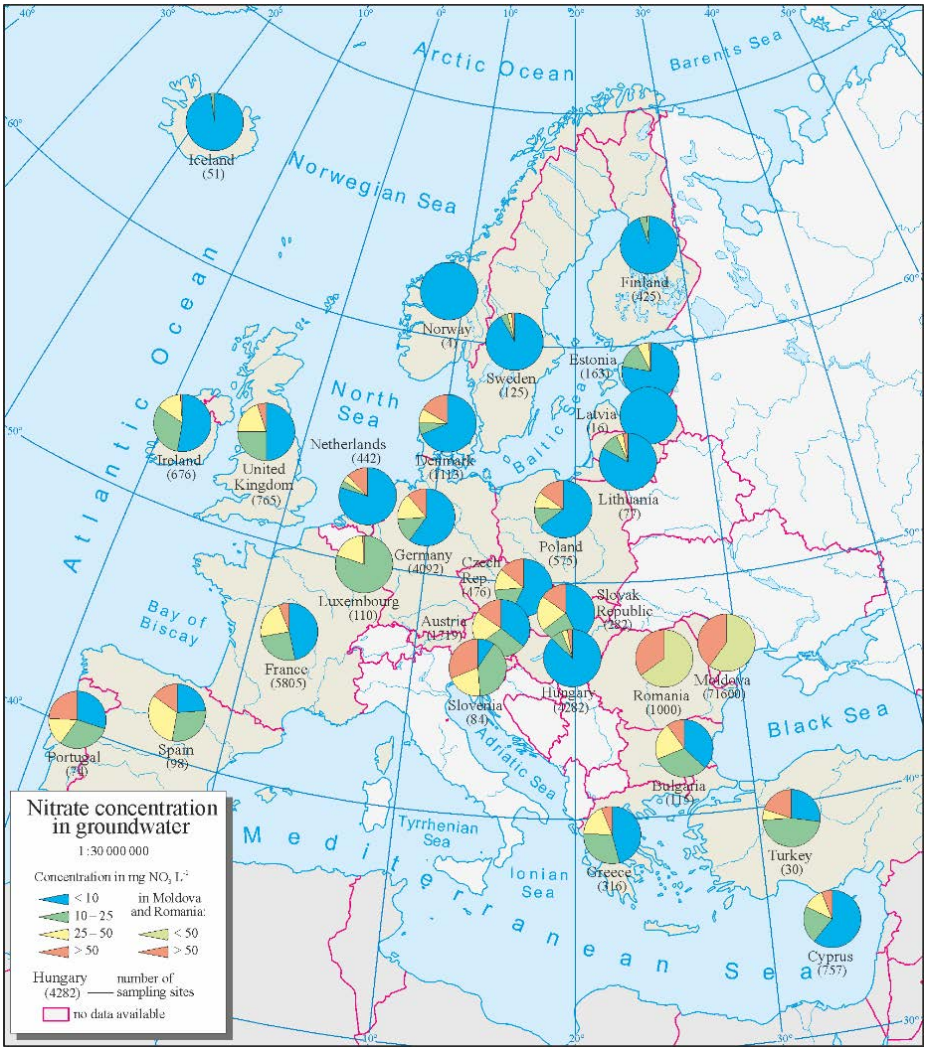

Figure 3. Nitrate concentration (mg nitrate L^{-1}) in groundwater in Europe (updated at 2002, by European Environment Agency [81]).

The World Health Organisation (WHO) defined guideline values in 2008 for nitrate and nitrite in drinking water as 50 mg nitrate L^{-1} (806 µmol L^{-1}) and 3 mg nitrite L^{-1} (65 µmol L^{-1}), respectively, to protect bottle-fed infants with short-term exposure. A provisional guideline value for nitrite has also been proposed as 0.2 mg nitrite L^{-1} (4 µmol L^{-1}) for long-term exposure [78].

The causes of nitrate contamination in ground water are summarized in Table 2, where agriculture pollutants via over-fertilization are the major source of contamination in general [78, 80-82], endangering safety of drinking water particularly in rural area. Figure 3 shows nitrate concentration in groundwater in European countries; the orange area of the pie chart is

indicating the percentage of sampling sites with nitrate concentrations exceeding the guideline value. Figure 4 shows nitrate concentrations in 628 sampling sites in China, showing that 28% of groundwater sites contain nitrate exceeding the guideline value [82]. It can be seen in both figures that nitrate contamination has become a serious challenge for drinking water safety in both Europe and China.

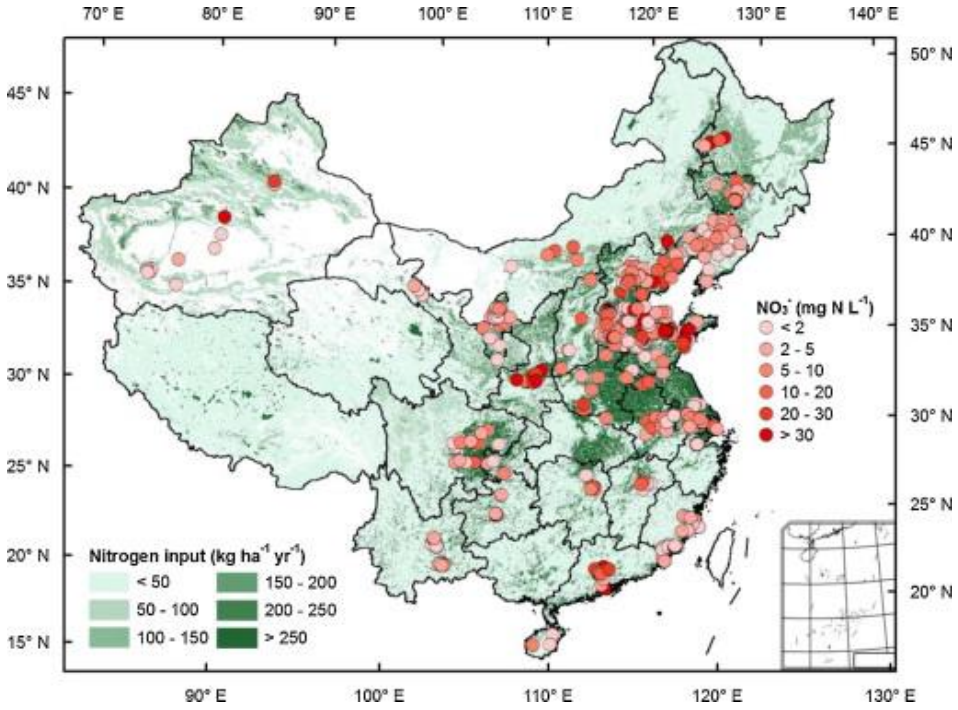

Figure 4. Nitrate concentrations (mg nitrogen L^{-1}) of groundwater in different sampling sites in China (2000–2012) [82]. Please note that the unit of the concentration is different with what are generally used in this thesis, and the guideline value where is 10 mg nitrogen L^{-1} according to WHO's suggestion for drinking water [78]. (Copy right Elsevier)

The most appropriate method to decrease nitrate concentrations, particularly in groundwater, is to prevent contamination [83]. Nitrite is currently converted to nitrate via chlorination, with the obvious disadvantage that the nitrate concentration increases [78]. On the other hand, nitrate concentration can be decreased using biological denitrification [84] or ion exchange [85-87]. However, biological treatment for nitrate is inherently slow and complex, not allowing for high degrees of removal [88]. Ion-exchange, on the other hand, is energy intensive and induces environmental issues because a concentrated brine needs to be discharged [89].

Therefore, catalytic conversion appears to be the most promising option for nitrate/nitrite removal for drinking water, operating under mild conditions (typically around 20ºC and 1 bar) without forming any contaminating by-products.

3.2. Catalysts for nitrate hydrogenation

Nitrate removal via catalytic hydrogenation was first reported by Vorlop and co-workers in the late 1980s, according the following reactions:

$$NO_3^- + H_2 \xrightarrow{Pd\text{-}Cu} NO_2^- + H_2O \qquad \text{(Eq. 1.1)}$$

$$2NO_2^- + 3H_2 + 2H^+ \xrightarrow{Pd} N_2 + 4H_2O \qquad \text{(Eq. 1.2)}$$

$$NO_2^- + 3H_2 + 2H^+ \xrightarrow{Pd} NH_4^+ + 2H_2O \qquad \text{(Eq. 1.3)}$$

Nitrogen (N_2) is clearly the preferred product, while nitrite was observed as an intermediate product whereas ammonium is an undesired by-product [77, 90]. The authors demonstrated the necessity of using bimetallic catalysts for nitrate hydrogenation, composed of a noble metal (Pd or Pt) and a base metal (Cu, Fe, Co, Ni, Ag). The base metal is mainly functional for nitrate converting to nitrite, as Pd is insufficient oxophilic to remove the first oxygen atom from nitrate [91]. In contrast, nitrite can be hydrogenated on the noble metal. Since then, various metal-metal combinations with different ratios have been tested in order to optimize activity and selectivity to N_2, minimizing the formation of ammonium [88, 89, 91-93]. The most frequently test system is Pd-Cu nanoparticles supported on alumina and other materials [94-104]. It is believed that close proximity of the two metals is necessary for effective transport of hydrogen atoms from the noble metal to the base metal in order to keep the latter in a low oxidation state, which is necessary after oxidation of the base metal during the conversion of nitrate to nitrite [105, 106].

3.3. Catalysts for nitrite hydrogenation

Nitrate hydrogenation can be described according the equations 1.1 to 1.3, with nitrate reduction to nitrite (Eq. 1.1) as the rate limiting step, based on the pioneering work of Vorlop, et al. [77, 107, 108]. Nitrite hydrogenation (Eq. 1.2 and 1.3), on the other hand, is critical for the selectivity to N_2 and ammonium. Thus, insight in the mechanism of nitrite hydrogenation contributes to understand the mechanism of the complete reaction and, based on that, to

optimize selectivity to N_2. Monometallic Pd catalysts have been found most efficient for nitrite hydrogenation [53, 109].

The selectivity of nitrite hydrogenation is influenced by the concentrations of the reactants. Low nitrite concentration and high H_2 pressure favour ammonium formation over N_2, based on both kinetics [77, 101] as well as infrared spectroscopy studies on adsorbed intermediates on the Pd surface [110]. It should be noted that in a semi-batch reaction, the NO_2^-/H_2 concentration ratio continuously decreases as the hydrogen pressure is kept constant whereas the NO_2^- is consumed, resulting in increasing selectivity to ammonium with time and conversion level [101]. It is also important to compare the selectivity to N_2 at the same conversion level for catalyst tested in a fixed bed reactor.

It has been reported that pH is also an important parameter influencing the activity and the selectivity: the more acidic the solution, the higher activity and lower ammonium formation [101, 111]. Obviously, for the preparation of drinking water this is not a practical variable. It is also important to notice that nitrite hydrogenation consumes protons during the reaction (Eq 1.2 and 1.3), causing the pH to increase. Therefore, buffers are frequently used in order to study catalyst performance at close to constant pH value, e.g. by buffering with CO_2 [101, 103, 112-114] or formic acid [97, 115]. Formic acid has also been used as reductant in such studies.

Kinetics studies also show that catalytic performance for nitrite hydrogenation is influenced by reaction temperature [77, 101, 116]. Both Vorlop et al. and Pintar et al. reported that reaction rate increases with increasing temperature from 2 to 25°C in semi-batch reaction with Pd/γ-Al_2O_3 catalysts. Ammonium formation is also enhanced by rising temperature [77, 101]. Similar changes in activity and selectivity were also observed between 25°C and 50°C in fixed bed reaction with Pd catalyst supported on carbon nanofibers (CNF), as reported by Chinthaginjala et al. [116].

Nitrite hydrogenation is a fast reaction and mass transfer limitation is frequently reported, implying concentration gradients especially inside porous catalyst support materials [101, 109, 112, 117]. The molecular diffusivities of the reactants increase in the sequence of $NO_2^- < H_2 < H^+$ in magnitude of 10^{-5} cm^2 s^{-1} in aqueous phase, suggesting that the NO_2^-/H_2 ratio will decrease deeper in the pores of the catalyst [77, 108]. Indeed, Strukul et al. reported that using large Pd/Al_2O_3 catalyst particles (> 0.5 mm) enhanced ammonium formation [118]. However, this effect also explained by some other researchers with sluggish diffusion of protons in the absence of a buffer, which would induce high pH values inside the catalyst particles, increasing

the selectivity to ammonium in that way [119]. Commonly, no quantum effect has been considered in this model [120, 121]. In contrast, using support material with "open" pore structure such as entangled carbon nanofibers (CNF), suppressing concentration gradient inside the catalyst particles, can improve the level of control [52, 116]. In any case, mass transfer limitation should be carefully avoided in order to discuss intrinsic catalytic performance for nitrite hydrogenation, and also to optimize the performance, by offering all metal particles in the catalyst identical concentrations of reactants including protons, independent of their position in the support.

Pd particle size is an important parameter influencing the catalyst performance. It has been claimed in literature that turn over frequency (TOF) of nitrite hydrogenation on supported Pd catalysts is size independent for particle between 1.5 and 20 nm [52, 53]. Interestingly, a recent study by Shuai et al. reports that the TOF for nitrite hydrogenation varies with Pd particle size of Pd-PVP colloid particles [63]. On the other hand, the relationship of the selectivity to N_2 and particle size is still under debate. Yoshinaga et al. reported large Pd particles are favourable for selectivity to N_2 in nitrite hydrogenation, proposing that N_2 formation proceeds on terraces, whereas ammonium formation is supposed to proceed on low coordination Pd sites on edges, corners and defects [98]. This is supported by the observations with Pd/CNF catalysts that ammonium formation increases with decreasing Pd particle size, reported by Shuai et al [53]. In contrast, Mendez et al. reported higher ammonium selectivity with large Pd NPs (10 nm) than with small Pd NPs (2 nm) supported on γ-Al_2O_3 [122]. Interestingly, Sá et al. claimed that poisoning low coordination sites on Pd surface with Bi atoms, has no effect on selectivity to ammonium [123].

4. Scope and outline of the thesis

The objective of the research described in this thesis is to obtain better understanding of nitrite hydrogenation reaction by using model catalysts with monodispersed Pd NPs via colloidal method in aqueous phase. Complications arising from the application of colloids, including blocking of surface sites and otherwise influencing the catalytic performance by any remaining polymer stabilizer, will be either minimized or just accepted and studied.

Chapter 2 describes a novel method to remove resident polymer stabilizer (polyvinyl alcohol (PVA)) from Pd surface after the colloid immobilized on activated carbon (AC). It is

shown that the choice of acid (HCl or H_2SO_4), used to induce electrostatic adsorption of the Pd colloid on AC, has a significant effect on the final coverage of the Pd surface by PVA. Furthermore, thermal decomposition of PVA in H_2 or inert atmosphere has also been studied, and the results show different decomposition temperature for PVA located on Pd surface as compared with PVA adsorbed on AC. The optimized amount of HCl will be discussed in **Chapter 5**, in order to optimize the catalytic performance of the resulting catalyst. It is shown that chlorine influences selectivity to ammonium without significant effect on activity.

The effect of polymer stabilizer on catalytic performance of Pd catalyst for nitrite hydrogenation is described in **Chapter 3**. Unsupported colloidal Pd NPs are used directly as catalyst in aqueous phase in order to rule out any support effect. Polymer stabilizers, PVA and PVP, containing different functional groups, have been used with varying molar ratios of polymer-monomer and Pd, in order to achieve different particle sizes and coverages of the Pd surface by polymer. It is found that both PVA and PVP block Pd sites, limiting the apparent activity of the catalyst. However, PVP influences the activity per Pd surface atom not covered with PVP. PVP also influences the selectivity to ammonium, probably by influencing reaction intermediates adsorbed on the available Pd sites. In contrast, PVA shows no such effects.

Chapter 4 explained the general high selectivity to N_2 for nitrite hydrogenation with Pd catalysts. It is found that the major conversion of nitrite to N2 on only minor Pd sites, with high reaction rate. In contrast, majority of Pd surface sites covers with nitrogen atoms, which are responsible for the formation of ammonium, via NO_xH_y species as intermedia, with relatively much lower reaction rate.

In **Chapter 6** the results will be summarized and remaining open questions will be formulated. Especially, options to improve practical catalysts for nitrate and nitrite removal based on the new knowledge, acquired in this thesis, will be discussed.

References

[1] J. Goodwin, Colloids and Interfaces with Surfactants and Polymers, Second Edition, John Wiley & Sons Ltd, in United Kingdom (2009).

[2] M. Faraday, Philos. Trans. R. Soc. London, 147 (1857) 145-181.

[3] R. Zsigmondy, Fresenius, Zeitschrift f. anal. Chemie, 40 (1901) 697-719.

[4] Y. Xia, Y. Xiong, B. Lim, S.E. Skrabalak, Angew. Chem. Int. Ed., 48 (2009) 60-103.

[5] J.B. Michel, J.T. Schwartz, in: P.G.P.A.J. B. Delmon, G. Poncelet (Eds.) Stud. Surf. Sci. Catal., Elsevier, (1987), pp. 669-687.

[6] K.J. Klabunde, Y.X. Li, B.J. Tan, Chem. Mater., 3 (1991) 30-39.

[7] A. Henglein, Chemical Reviews, 89 (1989) 1861-1873.

[8] J.S. Bradley, in: G. Schmid (Ed.) Clusters and Colloids: From Theory to Applications, VCH Publishers, New York (1994).

[9] N. Semagina, L. Kiwi-Minsker, Catal. Rev., 51 (2009) 147-217.

[10] J.H. Fendler, F.C. Meldrum, Adv Mater, 7 (1995) 607-632.

[11] M.R. Mucalo, R.P. Cooney, Journal of the Chemical Society, Faraday Transactions, 87 (1991) 1221-1227.

[12] J.D. Aiken III, Y. Lin, R.G. Finke, J. Mol. Catal. A: Chem., 114 (1996) 29-51.

[13] H. Thiele, H.S. von Levern, Journal of Colloid Science, 20 (1965) 679-694.

[14] L.S. Ott, R.G. Finke, Coord. Chem. Rev., 251 (2007) 1075-1100.

[15] W. Hoogsteen, L.G.J. Fokkink, J Colloid Interf Sci, 175 (1995) 12-26.

[16] R. Pool, Science, 248 (1990) 1186-1188.

[17] L. Guczi, G. Petö, A. Beck, Z. Pászti, Top. Catal., 29 (2004) 129-138.

[18] M. Králik, A. Biffis, J. Mol. Catal. A: Chem., 177 (2001) 113-138.

[19] J.D. Aiken Iii, R.G. Finke, J. Mol. Catal. A-Chem., 145 (1999) 1-44.

[20] K.E. Gonsalves, H. Li, R. Perez, P. Santiago, M. Jose-Yacaman, Coord. Chem. Rev., 206–207 (2000) 607-630.

[21] M.L. Toebes, J.A. van Dillen, Y.P. de Jong, J. Mol. Catal. A-Chem., 173 (2001) 75-98.

[22] B. Corain, P. Centomo, S. Lora, M. Kralik, J. Mol. Catal. A: Chem., 204–205 (2003) 755-762.

[23] M. Boudart, A. Aldag, J.E. Benson, N.A. Dougharty, C. Girvin Harkins, J. Catal., 6 (1966) 92-99.

[24] M. Boudart, in: H.P. D.D. Eley, B.W. Paul (Eds.) Adv. Catal., Academic Press, (1969), pp. 153-166.

[25] G.A. Somorjai, J. Carrazza, Ind Eng Chem Fund, 25 (1986) 63-69.
[26] Á. Molnár, A. Sárkány, M. Varga, J. Mol. Catal. A: Chem., 173 (2001) 185-221.
[27] A. Borodziński, Catal. Lett., 71 (2001) 169-175.
[28] J. Silvestre-Albero, G. Rupprechter, H.-J. Freund, J. Catal., 240 (2006) 58-65.
[29] C.M. Pradier, T. Birchem, Y. Berthier, G. Cordier, Catal. Lett., 29 (1994) 371-378.
[30] C.E. Gigola, H.R. Aduriz, P. Bodnariuk, Appl Catal, 27 (1986) 133-144.
[31] M. Arenz, K.J.J. Mayrhofer, V. Stamenkovic, B.B. Blizanac, T. Tomoyuki, P.N. Ross, N.M. Markovic, J Am Chem Soc, 127 (2005) 6819-6829.
[32] F. Şen, G. Gökağaç, J. Phys. Chem. C, 111 (2007) 5715-5720.
[33] Y. Li, E. Boone, M.A. El-Sayed, Langmuir, 18 (2002) 4921-4925.
[34] J. Le Bars, U. Specht, J.S. Bradley, D.G. Blackmond, Langmuir, 15 (1999) 7621-7625.
[35] R. Narayanan, M.A. El-Sayed, J. Phys. Chem. B, 108 (2004) 5726-5733.
[36] F. Zaera, Progress in Surface Science, 69 (2001) 1-98.
[37] R.M. Rioux, H. Song, M. Grass, S. Habas, K. Niesz, J.D. Hoefelmeyer, P. Yang, G.A. Somorjai, Top. Catal., 39 (2006) 167-174.
[38] H.J. Freund, H. Kuhlenbeck, J. Libuda, G. Rupprechter, M. Bäumer, H. Hamann, Top. Catal., 15 (2001) 201-209.
[39] I. I. Moiseev, M. N. Vargaftik, New J Chem, 22 (1998) 1217-1227.
[40] H.-U. Blaser, A. Indolese, A. Schnyder, H. Steiner, M. Studer, J. Mol. Catal. A: Chem., 173 (2001) 3-18.
[41] R.A.W. Johnstone, A.H. Wilby, I.D. Entwistle, Chemical Reviews, 85 (1985) 129-170.
[42] A. Borodziński, G.C. Bond, Catalysis Reviews, 48 (2006) 91-144.
[43] A. Tungler, G. Fogassy, J. Mol. Catal. A: Chem., 173 (2001) 231-247.
[44] A.M. Trzeciak, J.J. Ziółkowski, Coord. Chem. Rev., 249 (2005) 2308-2322.
[45] N. Miyaura, A. Suzuki, Chemical Reviews, 95 (1995) 2457-2483.
[46] A.M. Trzeciak, J.J. Ziółkowski, Coord. Chem. Rev., 251 (2007) 1281-1293.
[47] V. Farina, Adv Synth Catal, 346 (2004) 1553-1582.
[48] C. Ornelas, L. Salmon, J. Ruiz Aranzaes, D. Astruc, Chem. Commun., (2007) 4946-4948.
[49] N. Semagina, A. Renken, D. Laub, L. Kiwi-Minsker, J. Catal., 246 (2007) 308-314.
[50] S.-K. Oh, Y. Niu, R.M. Crooks, Langmuir, 21 (2005) 10209-10213.
[51] J. Silvestre-Albero, G. Rupprechter, H.-J. Freund, Chem. Commun., (2006) 80-82.
[52] J.K. Chinthaginjala, J.H. Bitter, L. Lefferts, Appl. Catal., A, 383 (2010) 24-32.

[53] D. Shuai, J.K. Choe, J.R. Shapley, C.J. Werth, Environ Sci Technol, 46 (2012) 2847-2855.

[54] Y. Zhao, L. Jia, J.A. Medrano, J.R.H. Ross, L. Lefferts, ACS Catal., 3 (2013) 2341-2352.

[55] M. Hähnlein, U. Prüße, J. Daum, V. Morawsky, M. Kröger, M. Schröder, M. Schnabel, K.D. Vorlop, Stud. Surf. Sci. Catal., 118 (1998) 99-107.

[56] M.M. Telkar, C.V. Rode, R.V. Chaudhari, S.S. Joshi, A.M. Nalawade, Applied Catalysis A: General, 273 (2004) 11-19.

[57] Y. An, M. Suzuki, T. Koyama, K. Hanabusa, H. Shirai, M.-Y. Huang, Y.-J. Jiang, Polym Advan Technol, 7 (1996) 652-656.

[58] Y. Xiong, J. Chen, B. Wiley, Y. Xia, S. Aloni, Y. Yin, J Am Chem Soc, 127 (2005) 7332-7333.

[59] Y. Sun, B. Mayers, Y. Xia, Adv Mater, 15 (2003) 641-646.

[60] S.-W. Kim, J. Park, Y. Jang, Y. Chung, S. Hwang, T. Hyeon, Y.W. Kim, Nano Lett, 3 (2003) 1289-1291.

[61] B. Veisz, Z. Király, Langmuir, 19 (2003) 4817-4824.

[62] Y. Xiong, J.M. McLellan, J. Chen, Y. Yin, Z.-Y. Li, Y. Xia, J Am Chem Soc, 127 (2005) 17118-17127.

[63] D. Shuai, D.C. McCalman, J.K. Choe, J.R. Shapley, W.F. Schneider, C.J. Werth, ACS Catal., 3 (2013) 453-463.

[64] J.T.G. Overbeek, in: J.W. Goodwin (Ed.) Colloidal Dispersions, Royal Society of Chemistry, London (1981), pp. 1-23.

[65] B. Vincent, J. Edwards, S. Emmett, A. Jones, Colloids and Surfaces, 18 (1986) 261-281.

[66] T. Teranishi, M. Miyake, Chem. Mater., 10 (1998) 594-600.

[67] Y. Li, M.A. El-Sayed, J. Phys. Chem. B, 105 (2001) 8938-8943.

[68] J.N. Kuhn, C.-K. Tsung, W. Huang, G.A. Somorjai, J. Catal., 265 (2009) 209-215.

[69] A. Quintanilla, V.C.L. Butselaar-Orthlieb, C. Kwakernaak, W.G. Sloof, M.T. Kreutzer, F. Kapteijn, J. Catal., 271 (2010) 104-114.

[70] L.R. Baker, G. Kennedy, J. Krier, M. Spronsen, R. Onorato, G. Somorjai, Catal. Lett., 142 (2012) 1286-1294.

[71] J.K. Chinthaginjala, A. Villa, D.S. Su, B.L. Mojet, L. Lefferts, Catal. Today, 183 (2012) 119-123.

[72] Y. Borodko, S.M. Humphrey, T.D. Tilley, H. Frei, G.A. Somorjai, J. Phys. Chem. C, 111 (2007) 6288-6295.

[73] Y. Borodko, S.E. Habas, M. Koebel, P. Yang, H. Frei, G.A. Somorjai, J. Phys. Chem. B, 110 (2006) 23052-23059.

[74] C. Lange, D. De Caro, A. Gamez, S. Storck, J.S. Bradley, W.F. Maier, Langmuir, 15 (1999) 5333-5338.

[75] I. Dodouche, F. Epron, Appl. Catal., B, 76 (2007) 291-299.

[76] M. Okamoto, T. Hirao, T. Yamaai, J. Catal., 276 (2010) 423-428.

[77] T. Tacke, Dissertation, Technischen Universität Carolo-Wilhelmina (1991).

[78] World Health Organization, Guidelines for drinking-water quality, 3rd version, 1, in Geneva (2008).

[79] J.O. Lundberg, E. Weitzberg, M.T. Gladwin, Nat Rev Drug Discov, 7 (2008) 156-167.

[80] A. Scheidleder, J. Grath, G. Winkler, U. Stärk, C. Koreimann, C. Gmeiner, S. Nixon, J. Casillas, P. Gravesen, J. Leonard, M. Elvira, European Environment Agency (EEA) (1999).

[81] European Environment Agency (EEA), http://www.eea.europa.eu/data-and-maps/figures/nitrate-concentration-in-groundwater (Last updated 01 Jan 2002).

[82] B. Gu, Y. Ge, S.X. Chang, W. Luo, J. Chang, Global Environmental Change, 23 (2013) 1112-1121.

[83] O. Schmoll, G. Howard, J. Chilton, I. Ghorus, Protecting Groundwater for Health, on behalf of the World health Organization by IWA Publishing, in London (2006).

[84] E. Wąsik, J. Bohdziewicz, M. Błaszczyk, Process Biochem, 37 (2001) 57-64.

[85] M. Boumediene, D. Achour, Desalination, 168 (2004) 187-194.

[86] B.-U. Bae, Y.-H. Jung, W.-W. Han, H.-S. Shin, Water Res, 36 (2002) 3330-3340.

[87] S. Samatya, N. Kabay, Ü. Yüksel, M. Arda, M. Yüksel, Reactive and Functional Polymers, 66 (2006) 1206-1214.

[88] A. Kapoor, T. Viraraghavan, Journal of Environmental Engineering, 123 (1997) 371-380.

[89] N. Barrabés, J. Sá, Appl. Catal., B, 104 (2011) 1-5.

[90] K.-D. Vorlop, T. Tacke, Chemie Ingenieur Technik, 61 (1989) 836-837.

[91] F. Gauthard, F. Epron, J. Barbier, J. Catal., 220 (2003) 182-191.

[92] J.C. Fanning, Coord. Chem. Rev., 199 (2000) 159-179.

[93] M. Shrimali, K.P. Singh, Environ Pollut, 112 (2001) 351-359.

[94] Y. Matatov-Meytal, V. Barelko, I. Yuranov, L. Kiwi-Minsker, A. Renken, M. Sheintuch, Appl. Catal., B, 31 (2001) 233-240.

[95] U. Matatov-Meytal, M. Sheintuch, Catal. Today, 102–103 (2005) 121-127.

[96] A. Pintar, J. Batista, Catal. Today, 53 (1999) 35-50.

[97] U. Prüsse, M. Hähnlein, J. Daum, K.-D. Vorlop, Catal. Today, 55 (2000) 79-90.
[98] Y. Yoshinaga, T. Akita, I. Mikami, T. Okuhara, J. Catal., 207 (2002) 37-45.
[99] U. Prüsse, K.-D. Vorlop, J. Mol. Catal. A: Chem., 173 (2001) 313-328.
[100] A. Pintar, J. Batista, J. Levec, T. Kajiuchi, Appl. Catal., B, 11 (1996) 81-98.
[101] A. Pintar, G. Berčič, J. Levec, Aiche J., 44 (1998) 2280-2292.
[102] Y.-X. Chen, Y. Zhang, G.-H. Chen, Water Res, 37 (2003) 2489-2495.
[103] I. Mikami, Y. Sakamoto, Y. Yoshinaga, T. Okuhara, Appl. Catal., B, 44 (2003) 79-86.
[104] A. Pintar, J. Batista, I. Muševič, Appl. Catal., B, 52 (2004) 49-60.
[105] F. Epron, F. Gauthard, C. Pinéda, J. Barbier, J. Catal., 198 (2001) 309-318.
[106] J. Sá, S. Gross, H. Vinek, Applied Catalysis A: General, 294 (2005) 226-234.
[107] C.G.M.v.d. Moesdijk, Dissertation, Eindhoven University of Technology (1979).
[108] J.K. Chinthaginjala, Dissertation, University of Twente (2010).
[109] S. Hörold, K.D. Vorlop, T. Tacke, M. Sell, Catal. Today, 17 (1993) 21-30.
[110] S.D. Ebbesen, B.L. Mojet, L. Lefferts, J. Catal., 256 (2008) 15-23.
[111] S. Hörold, T. Tacke, K.D. Vorlop, Environmental Technology, 14 (1993) 931-939.
[112] M. D'Arino, F. Pinna, G. Strukul, Appl. Catal. B-Environ., 53 (2004) 161-168.
[113] A. Pintar, M. vetinc, J. Levec, J. Catal., 174 (1998) 72-87.
[114] K.A. Guy, H. Xu, J.C. Yang, C.J. Werth, J.R. Shapley, J. Phys. Chem. C, 113 (2009) 8177-8185.
[115] A. Roveda, A. Benedetti, F. Pinna, G. Strukul, Inorg Chim Acta, 349 (2003) 203-208.
[116] J.K. Chinthaginjala, L. Lefferts, Appl. Catal., B, 101 (2010) 144-149.
[117] A.J. Lecloux, Catal. Today, 53 (1999) 23-34.
[118] G. Strukul, F. Pinna, M. Marcella, L. Meregalli, M. Tomaselli, Catal. Today, 27 (1996) 209-214.
[119] N. Krawczyk, S. Karski, I. Witońska, Reaction Kinetics, Mechanisms and Catalysis, 103 (2011) 311-323.
[120] D. Marx, A. Chandra, M.E. Tuckerman, Chemical Reviews, 110 (2010) 2174-2216.
[121] M.E. Tuckerman, D. Marx, M. Parrinello, Nature, 417 (2002) 925-929.
[122] C.M. Mendez, H. Olivero, D.E. Damiani, M.A. Volpe, Appl. Catal., B, 84 (2008) 156-161.
[123] J. Sá, J. Montero, E. Duncan, J.A. Anderson, Appl. Catal., B, 73 (2007) 98-105.

Chapter 2

Supported Pd catalysts prepared via colloidal method: the effect of acids

Organic capping agents are necessary for metallic nanoparticle preparation via colloidal method, however complete removal of the capping agent and cleaning the metal surface is a well-known challenge in application. In this chapter, polyvinyl alcohol (PVA) stabilized palladium nanoparticles (Pd NPs) were prepared and immobilized on activated carbon (AC).Different acids (HCl and H_2SO_4) were used in order to adjust the pH, thus enhancing the adsorption of the colloid on the support. The catalysts were characterized by TEM, CO-chemisorption, XRF, N_2 physisorption, XPS, TGA and TPR-MS. Activity of the catalyst was tested using nitrite hydrogenation in aqueous phase and formic acid decomposition in gas phase as probe reactions. The results showed that chlorine, introduced via HCl, efficiently suppressed the interaction of the Pd-NPs with PVA. Clean Pd NPs were obtained without any significant sintering after reduction in H_2/N_2 at mild temperature (200°C). The influence of acid on PVA thermal stability was also investigated. Differences in catalytic activity in gas phase versus liquid aqueous phase indicated that the extent of PVA covering the Pd-NPs is phase dependent.

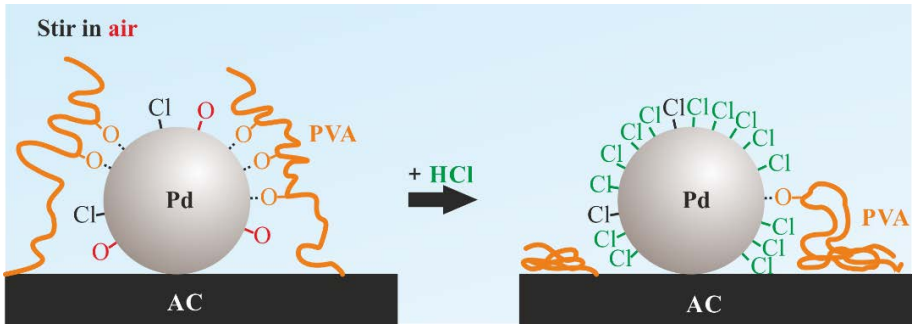

This part of work has been published as Research Article: Y. Zhao, L. Jia, J.A. Medrano, J.R.H. Ross, L. Lefferts, ACS Catal., 3 (2013) 2341-2352.

1. Introduction

Colloid immobilization has widely been used to prepare nanoparticles (NPs) for catalytic applications. Many benefits have been reported regarding this method, namely accurate control over particle size and shape, as well as resulting of high active and selective catalyst as compared to catalyst prepared *via* traditional methods (*e.g.* impregnation) [1-4]. Capping agents such as long carbon chain compounds, surfactants and organic ligands are commonly used as stabilizers to prepare colloids. The nanoparticle size and shape can be manipulated by altering the chain length of the capping agent, nature of associated counter ion, concentration and affinity toward specific crystal facets [5]. However, the capping agent can also constitute a protective layer, which in many cases limits the accessibility of the active sites for the reactants in both gas and liquid phase operation [3, 6, 7]. Therefore the capping agent on the NPs should be removed as completely as possible.

Capping agent removal has been developed following several approaches involving oxidation or thermal treatment. Aliaga *et al.* proposed treatment by UV-ozone to remove organic capping agents from Pt nanoparticles deposited on silicon wafers [8]. For colloids immobilized on porous support materials, thermal treatments in oxidative, inert or reductive atmosphere are widely used at temperature above 300^{o}C to remove the capping agent. High temperature and exothermal procedures, however, can result in significant change of nanoparticle size *via* agglomeration, especially for mono-metallic Pd NPs [4, 9-11]. Furthermore, remaining carbonaceous deposits after thermal treatment might affect the catalytic performance [12]. Recently, Lopez-Sanchez *et al*. established a new approach to partially remove capping polyvinyl alcohol (PVA) from Au and Au/Pd alloy immobilized on TiO_2, *via* refluxing the catalyst slurry in water at 90^{o}C [13]. However, this approach would not be applicable in the case of weak interaction of the colloid particles with the support (*e.g.* on activated carbon (AC)), resulting in metal loss during refluxing. Furthermore, weak interaction between Pd NPs with the support implies relatively poor protection against sintering[14], so that mild temperatures during any treatment becomes even more critical.

In this Chapter, Pd NPs with narrow particle size distribution supported on AC were prepared *via* colloidal immobilization using PVA as capping agent. During the immobilization, acid (usually sulfuric acid, H_2SO_4) needs to be added to adjust the pH, in order to enhance adsorption of the colloid on the support material. This study is reporting on an unexpected effect of the type of acid, *i.e.* H_2SO_4 *versus* HCl, on the accessibility of the Pd NPs.

2. Experimental

2.1. Chemicals

Sodium tetrachloropalladate(II) (Na_2PdCl_4 ≥ 99.995% (metal basis)), polyvinyl alcohol (PVA, average MW = 13000 – 23000, 87% – 89% hydrolyzed), sodium borohydride ($NaBH_4$, ≥ 96% (gas-volumetric)), and formic acid (98% - 100%) were purchased from Sigma-Aldrich. Sodium nitrite (>99%) was purchased from Merck. Activated carbon (AC, SX Ultra 94031-8, S_{BET} = 1100 $m^2 g^{-1}$) was supplied by Norit, and sieved in the range of 38 – 45 μm in diameter. All the aqueous solutions were prepared using ultra purified water obtained on water purification system (Millipore, Synergy).

2.2. Pd nanoparticle synthesis

Palladium nanoclusters were synthesized according to a method described in literature [15], which can be summarized as follows. PVA was dissolved in water at 70°C with stirring for at least 2 hours. The solution (2 wt %) was then cooled down to room temperature. Aqueous solution of Na_2PdCl_4 (20 mL, containing 0.086 mmol Pd) and 1.76 mL of freshly prepared PVA solution were added to 240 mL water, obtaining a yellow-brown solution. After 3 min, $NaBH_4$ solution (1.72 mL, 0.172 mmol) was added under vigorous stirring. The brown Pd colloid solution was immediately formed. The final pH was typically 8 – 8.5.

2.3. Catalyst preparation

Preparation of 1 wt% Pd supported on activated carbon. Activated carbon (0.75 g) was added to the Pd colloid solution (260 mL, 3.3×10^{-4} mol L^{-1}) immediately after preparation. Solution of acid, either hydrochloric or sulfuric, was added to adjust the pH to 2. The slurry was agitated exposing to air for 2 h at room temperature, filtered and thoroughly washed with water. After that, the catalysts were dried in vacuum at 40°C overnight.

Thermal treatment. Catalysts prepared using different acid were carefully treated in a tube furnace. In a typical procedure, the temperature was raised to 200°C at a rate of 5°C min^{-1}, then kept for 1 h at 200°C, in either 10 vol% H_2/90 vol% N_2. Then the sample was flushed in N_2 for 30 min at 200°C, and cooled down at a rate of 20°C min^{-1} to room temperature in the same

atmosphere. The catalysts were flushed in N_2 for 24 h before exposure to air. In the following, the sample notation will be used as shown in Table 2.1.

Table 2.1.Sample notations and details of corresponding preparation procedure (Note that the first two samples do not contain Pd)

Sample	Preparation procedure
PVA/AC_Cl	AC impregnated with PVA solution using HCl to adjust pH to 2
PVA/AC_S	AC impregnated with PVA solution using H_2SO_4 to adjust pH to 2
Pd-PVA/AC_Cl	Pd-PVA colloid immobilized on AC using HCl to adjust pH to 2
Pd-PVA/AC_Cl_H	Pd-PVA/AC_Cl treated in H_2/N_2 at 200°C for 1 h
Pd-PVA/AC_Cl_N	Pd-PVA/AC_Cl treated in N_2 at 200°C for 1 h
Pd-PVA/AC_S	Pd-PVA colloid immobilized on AC using H_2SO_4 to adjust pH to 2
Pd-PVA/AC_S_H	Pd-PVA/AC_S treated in H_2/N_2 at 200°C for 1 h

2.4. Characterization

Pd particle size distribution was determined using TEM (Philips CM300ST-FEG) with a resolution of 1 nm. The AC supported catalysts were firstly ground into sub-micron fragments and dispersed in ethanol. Then the suspension was dropped on a copper grid covered with hollow carbon for TEM image taking. At least five of these ground fragments were randomly selected for determination of Pd particle sizes, and typically 300 Pd particles were measured. Note that information on the spatial distribution of nanoparticles through the support cannot be obtained. The metal loading on the supports were analyzed by XRF. The total surface area of samples were calculated based on N_2 physisorption data, using the BET method for p/p_0 values between 0.03 and 0.13 following the recommendations of Rouquerol *et al*. [16] with a typical error margin of 5%.

CO chemisorption at room temperature was used to determine metal surface area that is accessible in gas phase. Typically, the sample was pre-reduced at 100°C in hydrogen and then flushed in He at the same temperature. After cooling down, CO was introduced as pulses and the response was recorded using a TCD detector. We assumed that the stoichiometric ratio of number of adsorbed CO molecules and number of accessible Pd surface atoms is 1 : 1. The Pd dispersion (*Pd disp*.) was defined as

$$Pd\ disp. = \frac{\text{number of Pd atoms in the surface of NPs}}{\text{number of Pd atoms in total}}$$

The surface of the catalysts was analyzed by X-ray photoelectron spectroscopy (XPS, Quantera SXM, Al *K*α (1486.6 eV)). The powder samples were stored in air without any further pretreatment before analysis. Typically a few microgram sample was pressed into an indium foil, and four spots (600×300 μm^2) on the sample were randomly selected for measurements to

rule out the inhomogeneity in the catalysts. The accuracy of the resulting peak positions was within 0.2 eV. The spectra were fitted using the software "Multipak v.9.4.0.7". Typically, the banding energy in all spectra was first calibrated using the carbon 1s peak at 284.8 eV as an internal reference. The spectra detected from the four spots of one sample were averaged in order to improve the signal-to-noise ratio, followed with Shirley background subtraction. The Pd peaks were fitted using an asymmetric model, caused by interaction of the photoelectron with valence band electrons [17], whereas the S and Cl peaks were fitted using mixed Gaussian-Lorentzian model, as suggested by Handbook of X-ray Photoelectron Spectroscopy [18]. The peaks for each sample (Pd 5d, Cl 2p and S 2p) were fitted with sets of doublets with identical FHWM. Both width and peak position were allowed to optimize. The distance within the doublets was fixed with the data suggested in handbook [18].

Thermal gravimetric analysis (TGA) was performed in either Ar or 10 vol% H_2/90 vol% Ar (flow rate 50 mL min^{-1}). The sample was first heated to 70^{o}C and kept at this temperature for 1h to remove the major part of water. Then the temperature was increased from 70 to 600^{o}C at a rate of 5^{o}C min^{-1}. The weight change was calculated based on the weight of the dried sample at 70^{o}C.

Temperature programmed reduction/desorption (TPR or TPD) analyses were carried out using a home-build setup. The sample was first flushed in Ar at 70^{o}C for 1 h, and then cooled down to room temperature. TPR and TPD were performed using 20 ml min^{-1} flow of 5% H_2/95% Ar or pure Ar, respectively, and using a heating rate of 5^{o}C min^{-1}. Mass spectrometry (MS) was used to analyze qualitatively the composition of the resulting gas stream.

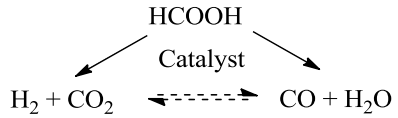

Scheme 2.1. Formic acid decomposition

2.5 Catalytic activity

2.5.1. Formic acid decomposition in gas phase. The activity of catalysts for formic acid catalytic decomposition (Scheme 2.1) was determined in a home-build continuously operated fixed bed reactor [19]. Typically, 50 mg of catalyst was loaded in a fixed bed quartz tubular

reactor (4 mm in diameter). The catalyst was first re-reduced in a 1 vol% H_2/Ar mixture for 1 h at 25ºC to remove adsorbed oxygen introduced during storage in air, then a stream of He was passed through a formic acid trap before being introduced into the reactor. The typical feeding concentration of formic acid in the gas phase was 2.0 vol%. The total flow rate of the gas mixture was 51 mL min^{-1}. The reaction was performed at 120ºC in steady state. The concentrations of formic acid and products were determined by gas chromatography. The conversion of formic acid was kept below 20%.

The activity per total amount of Pd in the catalyst ($mol_{HCOOH}\ mol_{Pd}^{-1}\ min^{-1}$) was defined as:

$$R_{W,\,HCOOH} = -\frac{C_{HCOOH} - C_{HCOOH,\,0}}{W/F_{HCOOH}}$$

Where C_{HCOOH} is formic acid concentration (mol L^{-1}), $C_{HCOOH,\,0}$ is feeding formic acid concentration (mol L^{-1}), W is total mole of Pd atoms (mol), F_{HCOOH} is feeding flow rate of formic acid (L min^{-1}).

Alternatively, assuming identical accessibility of the Pd surface sites for chemisorbed CO and formic acid in gas phase, the activity can also be expressed as per accessible Pd surface sites ($mol_{HCOOH}\ mol_{Pd}^{-1}\ min^{-1}$):

$$R_{S,\,HCOOH} = -\frac{C_{HCOOH} - C_{HCOOH,\,0}}{S/F_{HCOOH}}$$

Where S is defined as the amount of accessible Pd based on CO chemisorption in gas phase (mol).

$$S = W \times Pd\ disp.$$

2.5.2. Nitrite hydrogenation in liquid phase. The activity of catalysts for nitrite hydrogenation (Eq. 1.2 and 1.3) was determined in a continuous operated fixed bed reactor made of PEEK. Typically, 40 mg of catalyst powder was packed in a 4 mm diameter reactor, resulting in a bed height of approximately 10 mm. The feed stream contained 515 μmol L^{-1} (23.7 $mg_{nitrite}\ L^{-1}$) sodium nitrite and 432 μmol L^{-1} hydrogen in water. The hydrogen concentration was obtained by saturating the solution with 60 vol% H_2/Ar at 1 bar. In this way, the catalyst is contacted with aqueous solution only and no gas-phase is present in the reactor, excluding any effects of gas-liquid transfer on the kinetic data obtained. The flow was set at 3.5 mL min^{-1} using an HPLC pump (DIONEX, Ultimate 3000), resulting in space time τ = 28

min^{-1} (τ = (Flow rate)/(catalyst bed volume)) and a pressure drop of typically 1 bar. Nitrite concentrations were measured by ion chromatography (DIONEX, ICS 1000) by injecting a 25 μL sample of the liquid stream leaving the reactor through a 6-port valve. The reaction was performed under differential conditions, keeping the conversion of nitrite at about 5%.

$$2NO_2^- + 3H_2 + 2H^+ \xrightarrow{Pd} N_2 + 4H_2O \qquad \text{(Eq. 1.2)}$$

$$NO_2^- + 3H_2 + 2H^+ \xrightarrow{Pd} NH_4^+ + 2H_2O \qquad \text{(Eq. 1.3)}$$

The activity per total amount of Pd in the catalyst ($mol_{nitrite}\ mol_{Pd}^{-1}\ min^{-1}$) was defined as:

$$R_{W,\,nitrite} = -\frac{C_{nitrite} - C_{nitrite,\,0}}{W/F_{nitrite}}$$

Where $C_{nitirite}$ is nitrite concentration (μmol L^{-1}), $C_{nitirite,\,0}$ is initial nitrite concentration (μmol L^{-1}), $F_{nitrite}$ is flow rate (L min^{-1}).

Alternatively, assuming identical accessibility of the Pd surface sites in both gas– and liquid–phase, the activity can also be expressed as per accessible Pd surface sites ($mol_{nitrite}\ mol_{Pd}^{-1}\ min^{-1}$):

$$R_{S,\,nitrite} = -\frac{C_{nitrite} - C_{nitrite,\,0}}{S/F_{nitrite}}$$

3. Results

3.1. Elemental analysis

The Pd, Cl and S loadings were measured with XRF. All catalysts had the same Pd loading of 1.1 wt%. As shown in Table 2.2, the commercial AC support contained a minor amount of chlorine as low as 0.13 wt%. After using HCl to adjust pH of the aqueous slurry and stirring for 2 h, the chlorine loadings increased to about 1.0 wt%, and the absence or presence of PVA had no significant effect. Interestingly, when H_2SO_4 was used to impregnate PVA onto AC, the chlorine loading was even lower than that in the original AC. For as-prepared Pd catalyst using HCl, the loading of chlorine was as high as 1.4 wt%, and was decreased to 0.85 wt% after reduction in H_2/N_2 at 100°C, decreasing even further to 0.16 wt% after reduction at 200°C. Thermal treatment in N_2 at 200°C caused removal of only a minor fraction of the chlorine, to

1.1 wt%. Correspondingly, when H_2SO_4 was used, the chlorine loading decreased from 0.54 wt% to 0.08 wt% after reduction in H_2/N_2 at 200°C. The sulfur content in the original AC was negligible. When PVA was impregnated on AC using H_2SO_4, the sulfur content increased to 0.71 wt%. Unlike chlorine, the sulfur loading was not significantly increased by the presence of Pd.

Table 2.2. Summary of XRF elemental analysis, CO chemisorption, and TEM

Sample	Treatment	C_{Cl} (wt %)	C_S (wt %)	Particle size[(a)] (nm)	*Pd disp.* (%)	
					TEM	CO chem.[(c)]
AC		0.13±0.01	-			
AC_Cl		1.0±0.1				
PVA-AC_Cl		0.85±0.08				
	H_2/N_2, 200°C	0.34±0.03				
	N_2, 200°C	0.35±0.03				
PVA-AC_S		0.04±0.01	0.71±0.07			
Pd-PVA/AC_Cl		1.4±0.1		2.8±0.8	38	6[(b)]
	H_2/N_2, 100°C	0.85±0.08				31
	H_2/N_2, 200°C	0.16±0.02		3.0±0.9	35	36
	N_2, 200°C	1.1±0.1		3.0±0.8	35	8[(b)]
Pd-PVA/AC_S		0.54±0.05	0.44±0.02	2.9±0.9	36	4[(b)]
	H_2/N_2, 100°C					10
	H_2/N_2, 200°C	0.08±0.01	0.42±0.02	3.0±0.8	35	17
	H_2/N_2, 250°C			3.1±1.0	34	22

(a) Observed in TEM.
(b) The sample was reduced at room temperature for 1 h before CO chemisorption, which is known to be sufficient for removal of adsorbed oxygen from Pd catalyst [20, 21].
(c) Please note that apparent Pd dispersions were obtained by CO chemisorption, because part of the Pd surface was not accessible for CO due to PVA blocking and Cl poison, as discussed below.

3.2. Pd particle size

Figure 2.1 shows a narrow particle size distribution in as-prepared catalysts according to TEM. The mean particle size of the catalyst prepared with HCl was 2.8 nm, and was very similar to that of catalyst prepared using H_2SO_4 (2.9 nm). An example of the particle size distribution in thermally treated catalysts is shown in Figure 2.1e and 2.1f, showing that the particle size remained in the range of 3 nm after thermal treatment in H_2/N_2 or in N_2 at 200°C. The particle size distributions were not significantly influenced by any of the thermal treatments, as shown in Table 2.2. All the nanoparticles were sphere-like shaped as observed with TEM, as shown in Figure 2.1.

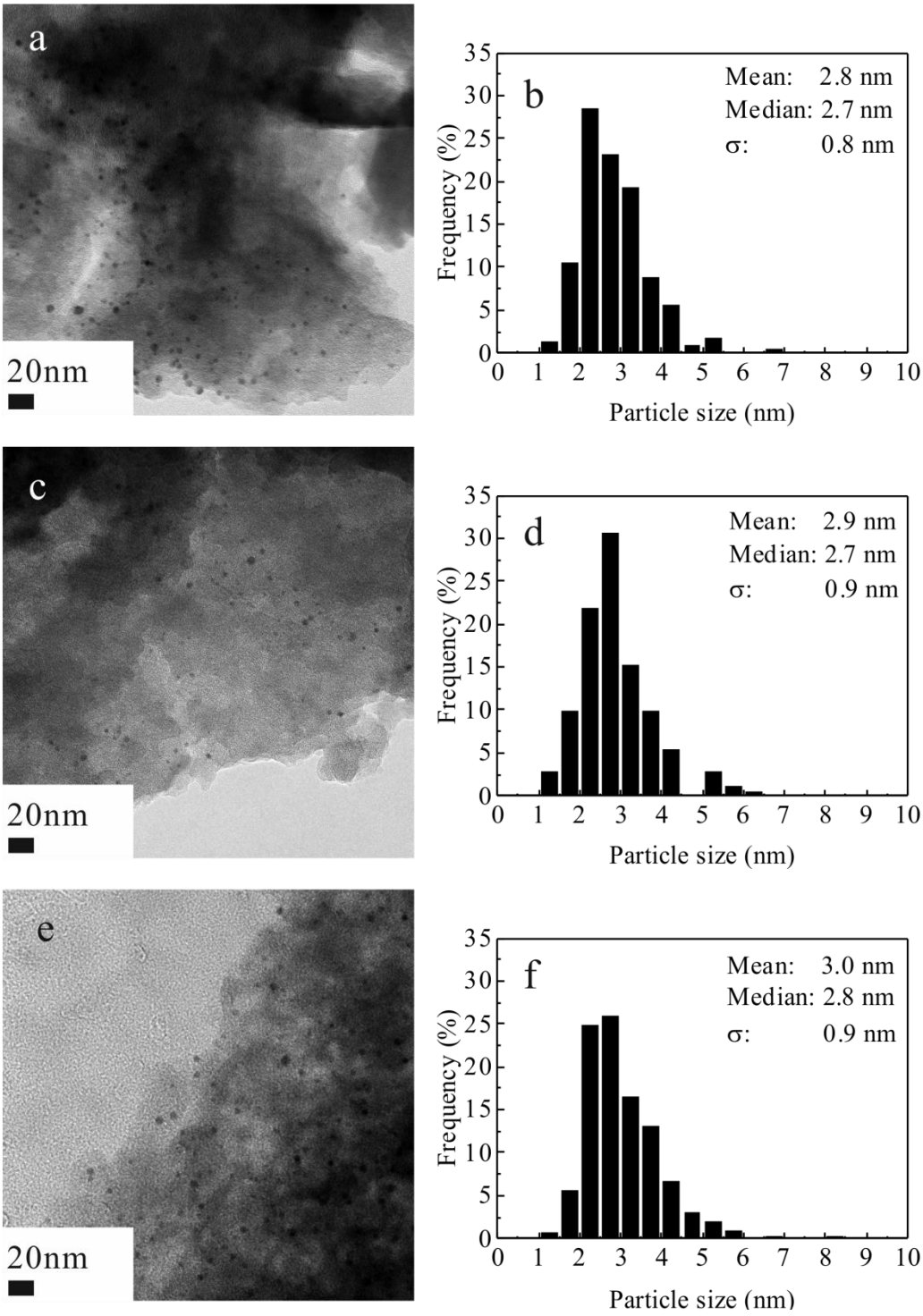

Figure 2.1. TEM image and corresponding Pd particle size distribution of Pd-PVA/AC_Cl (a and b), Pd-PVA/AC_S (c and d), and Pd-PVA/AC_Cl_H (e and f).

3.3. CO chemisorption

CO chemisorption was used to determine the accessibility of Pd atoms in gas phase. As shown in Table 2.2, the apparent Pd dispersion of these samples were quite different according to CO chemisorption, although the particle sizes and Pd loadings were almost the same for all samples. According to CO chemisorption, the apparent Pd dispersion was as low as 6% for as-prepared catalyst prepared using HCl; this apparent dispersion increased to 31% and further to 36% after reduction at 100°C and 200°C, respectively, in H_2/N_2 atmosphere. However, thermal treatment in N_2 did not significantly change the apparent Pd dispersion (8%).

The as-prepared catalyst prepared using H_2SO_4 also showed a low apparent Pd dispersion of 4%. After reduction at 100°C, the apparent Pd dispersion was still as low as 10%. And it increased to 17% and further to 22% as the result of reduction at 200°C and 250°C in H_2/N_2, respectively.

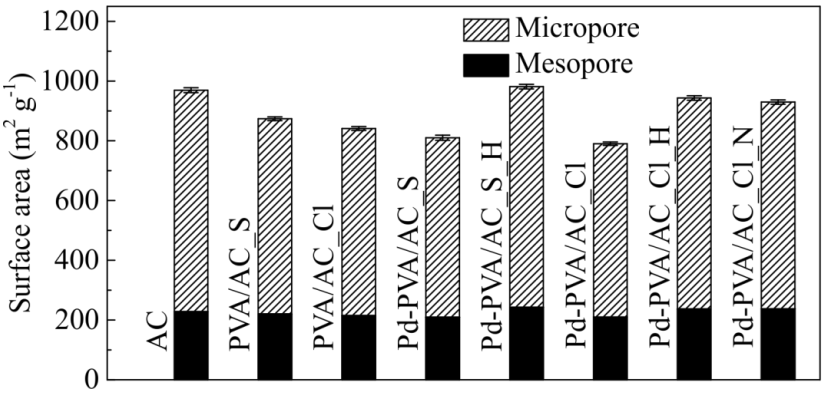

Figure 2.2. Surface area of micro- and mesopores. The surface area of micropores was calculated by t-plot method using data of N_2 physical adsorption. The mesopore surface area was estimated based on the difference between BET surface area and micropore surface area.

3.4. Porosity

Both the total surface area as well as the surface area of the micropores (< 2 nm) were calculated based on N_2 physisorption isotherms. Figure 2.2 shows the effect of PVA, including various pretreatments, on the surface area of both the micropores and mesopores. Micropore surface areas decreased in the order AC > PVA/AC_S > PVA/AC_Cl > Pd-PVA/AC_S > Pd-PVA/AC_Cl. After the thermal treatments, micropore surface areas of the catalysts increased

to values similar to the original AC. In contrast, the effect of PVA on the surface area of mesopores was not significant within experimental error.

3.5. XPS

Figure 2.3a shows the effect of thermal treatments of catalyst prepared with HCl on the oxidation state of Pd according XPS. Table 2.3 presents the full data set of peak positions resulting from the fitting procedure as well as the ratio values for Pd^{2+}/Pd^{0}, showing that the as-prepared catalyst contained 38% Pd^{2+}. Thermal treatment in H_2/N_2 at 100°C and 200°C resulted in partly and almost complete reduction, respectively, as shown in Table 2.3b. Interestingly, the thermal treatment in inert atmosphere at 200°C also partly reduced oxidized Pd, as shown in Figure 2.3a and Table 2.3b. Table 2.3b also shows that in as-prepared catalyst using H_2SO_4, the Pd^{2+} content was significantly lower as compared to the catalyst prepared using HCl. Similar in the case of using HCl, thermal treatment in H_2/N_2 at 100°C and 200°C resulted in partly and almost complete reduction, respectively. However, thermal treatment in inert atmosphere did not influence the amount of oxidized Pd significantly, in contrast to the catalyst prepared with HCl.

Catalyst prepared using HCl contained two types of chlorine with formal charge Cl^{-}, as shown in Figure 2.3c and Table 2.3a, which can be attributed to Cl bonded to Pd (*ca.* 198 eV) and Cl in organic compounds (*ca.* 200 eV), respectively [22]. After thermal treatments at 200°C in either H_2/N_2 or N_2, the relative amount of Cl bonded to carbon increased (Table 2.3b).

Sulfur in as prepared Pd-PVA/AC_S is mainly observed as S^{6+}, as shown in Figure 2.3b, indicating the presence of sulfate, sulfonic acid or sulfone species [23]. Thermal treatment in H_2/N_2 results in reduction of S^{6+} to zero or negative charged sulfur species, typically elemental sulfur, sulfide, disulfide, thiol, or thiophene [23, 24], especially at higher temperature, as shown in Table 2.3b.

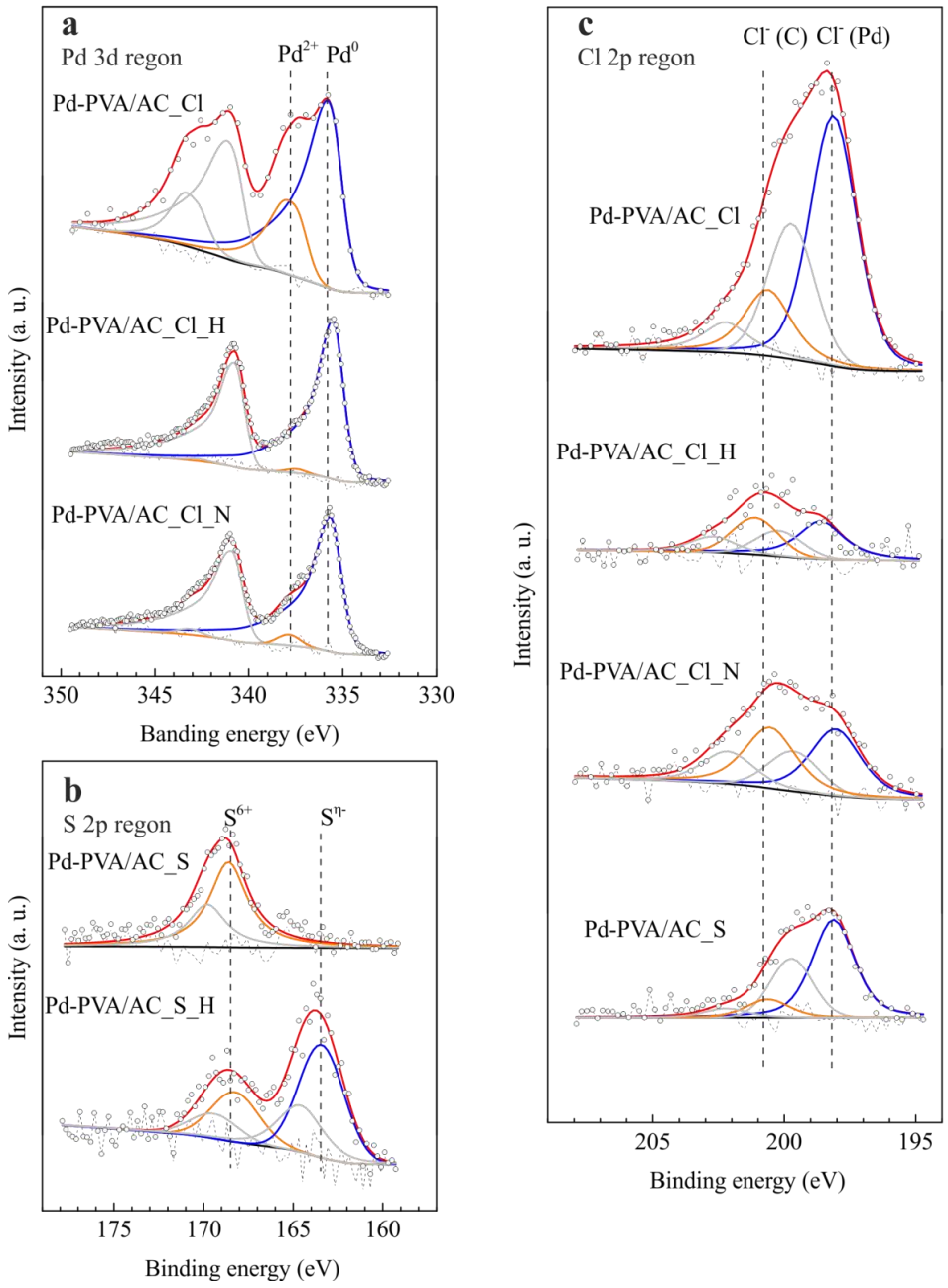

Figure 2.3. XPS spectra of activated carbon supported Pd-PVA colloids. (a) Pd 3d spectra; (b) S 2p spectra; (c) Cl 2p spectra. Original data (hollow dots) was subtracted with Shirley background (black line) and fitted using method described in section 2.4. The fitted Pd 3d5/2 peaks, Cl 2p3/2 peaks and S 2p3/2 peaks are highlighted (blue and orange) for comparison. The sum of all fitted peaks showed as red line with error showed as dash line.

Table 2.3. Summary of XPS data on Pd, Cl and S oxidation-states and surface concentrations.

Thermal treatment	a. Oxidation states					
	Pd $3d_{5/2}$ (eV)		Cl $2p_{3/2}$ (eV)		S $2p_{3/2}$ (eV)	
	Pd^0	Pd^{2+}	Cl (Pd)	Cl (C)	S^{6+}	$S^{\eta-}$ (a)
Pd-PVA/AC_Cl						
-	335.7	337.4	198.1	200.6		
H_2/N_2,100°C	335.6	337.1	198.2	200.7		
H_2/N_2, 200°C	335.5	337.3	198.1	200.8		
N_2, 200°C	335.7	337.3	198.0	200.5		
Pd-PVA/AC_S						
-	335.7	337.7	198.2	200.7	168.6	-
H_2/N_2, 100°C	335.7	337.1	198.1	200.5	168.6	163.0
H_2/N_2, 200°C	335.8	337.3	-	-	168.3	163.5
H_2/N_2, 250°C	335.7	337.3	-	-	168.4	163.3

Thermal treatment	b. Relative molar concentration		
	Pd^{2+}/Pd	Cl (C)/Cl	$S^{\eta-}/S$
Pd-PVA/AC_Cl			
-	0.38	0.21	
H_2/N_2,100°C	0.21	0.37	
H_2/N_2, 200°C	0.03	0.57	
N_2, 200°C	0.12	0.50	
Pd-PVA/AC_S			
-	0.13	0.15	-
H_2/N_2, 100°C	0.06	0.39	0.22
H_2/N_2, 200°C	0.03	-	0.61
H_2/N_2, 250°C	0.02	-	0.71

(a) $0 \leq \eta \leq 2$

3.6. TGA-DTG study

TGA was used to study desorption and decomposition of PVA. Figure 2.4a, b and c show TGA-DTG results in Ar atmosphere of original commercial AC, and AC treated with HCl or H_2SO_4, respectively. Table 4 summarizes the results in terms of peak position and weight loss at 200°C, showing weight loss in the same temperature window for original AC and AC treated in HCl solution (pH = 2). However, the sample treated in HCl lost much more weight (1.62 wt %) as compared to the original AC (0.34 wt %). This difference might be due to desorption of HCl. The AC treated in H_2SO_4 showed hardly any desorption below 160°C; instead, a clear weight loss was observed around 240°C. The presence of H_2, instead of Ar only, had no influence on any of these experimental results as shown in Table 2.4.

As shown in Figure 2.4d, a mechanical mixture of PVA and AC showed mainly weight loss around 340°C, similar to results obtained with PVA only (data not shown). The products

detected in the gas phase, as indicated in Table 2.4, included H_2O, CO_2, and $–CH_3$ fragment (m/z = 18, 44 and 15, respectively). The presence of the CO_2 and $–CH_3$ fragment can be attributed to the formation of carboxyl acids as decomposition product originating from acetyl groups in PVA (87 – 89% hydrolyzed) [25]. The $–CH_3$ fragment observed at 400°C, however, indicates an alternative decomposition pathway of PVA [26].

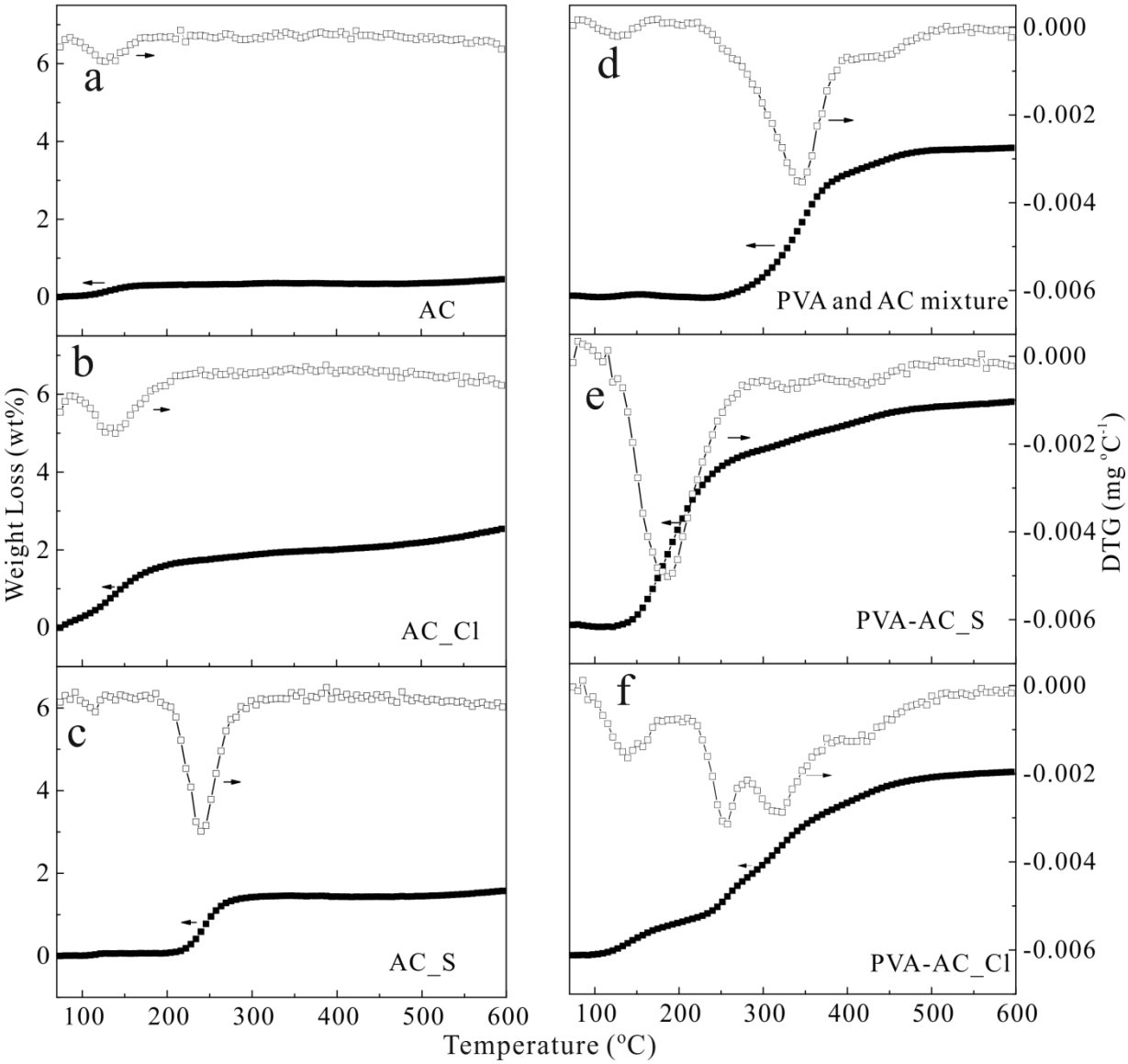

Figure 2.4. TGA-DTG in Ar atmosphere. (a) activated carbon; (b) activated carbon treated in HCl at pH=2; (c) activated carbon treated in H_2SO_4 at pH=2; (d) PVA and AC mechanical mixture; (e) PVA/AC_S; (f) PVA/AC_Cl.

The stability of PVA on AC was strongly affected by the acid, *i.e.*H_2SO_4 or HCl, used during colloid immobilization. As shown in Figure 2.4e, PVA/AC_S showed major weight loss at a significantly lower temperature around 190°C. The compounds produced were identical to those observed with PVA only according to MS (Table 2.4). Therefore, these products were likely to originate from PVA decomposition. When HCl was used instead, four weight loss steps were observed, as shown in Figure 2.4f. The weight loss at 120°C was due to physically adsorbed H_2O and/or HCl, similar as observed on the HCl treated AC. The two following weight loss steps at 315°C and 400°C were similar to the decomposition pattern of PVA (not shown) as well as the PVA and AC mechanical mixture (Figure 4d); also the products detected in gas phase were identical (Table 2.4). Additionally, a new weight loss step appeared around 250°C as shown in Figure 2.4d and Table 2.4; the volatile products detected were again similar to PVA decomposition. It should be noted that HCl was never detected with MS; however, it cannot be ruled out that any HCl released or formed would be adsorbed on the stainless steel tubing, preventing its detection.

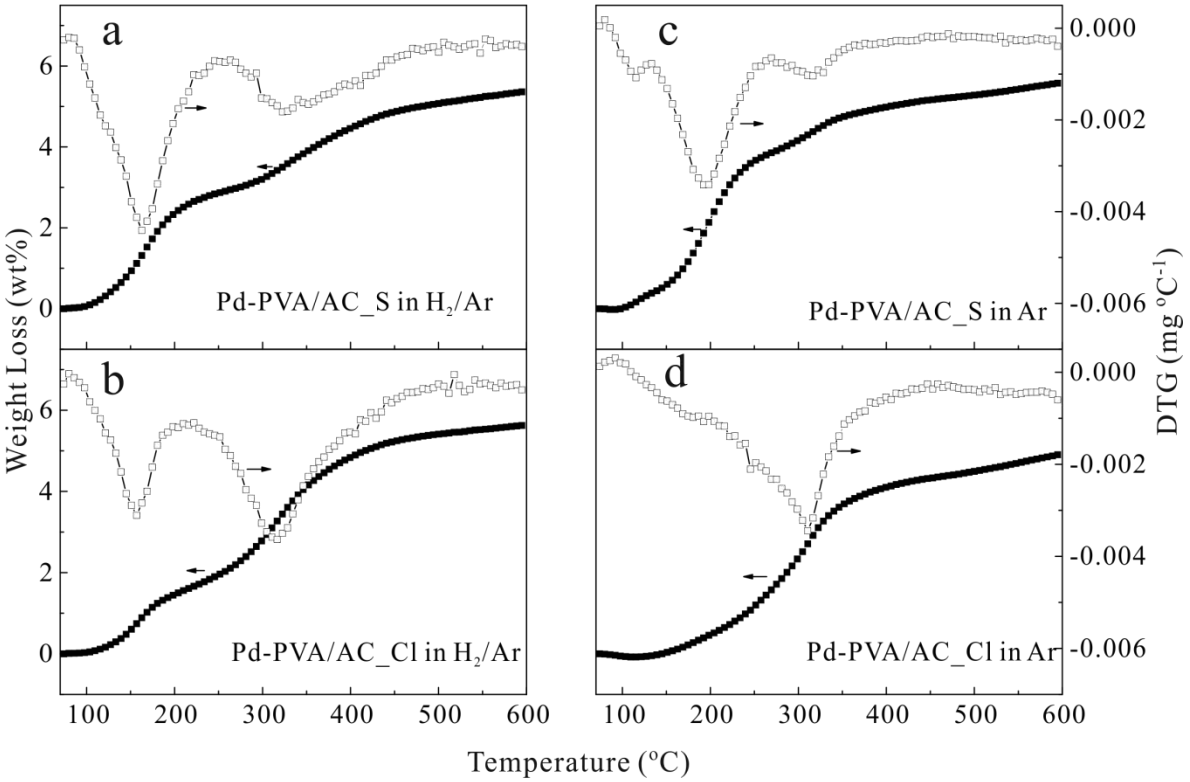

Figure 2.5. Weight loss and DTG of sample containing PVA in H_2/Ar (left) and Ar (right) atmosphere.

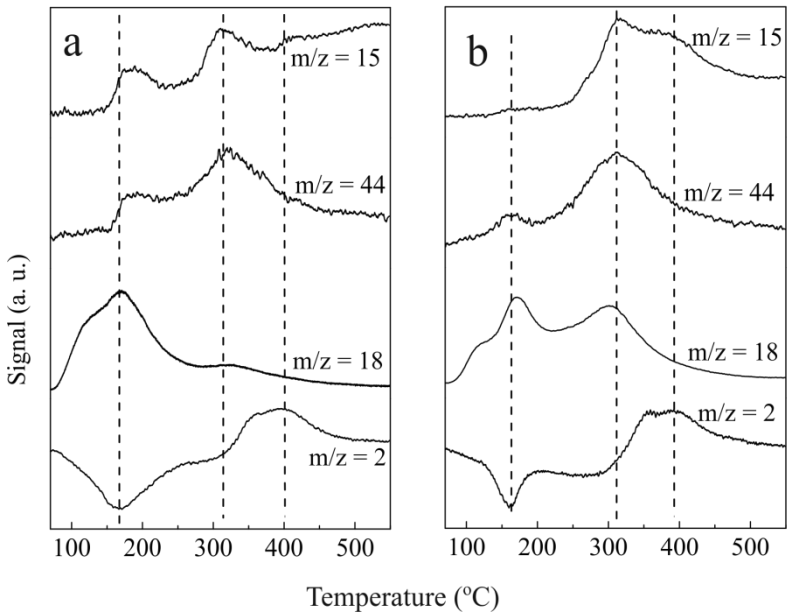

Figure 2.6. Trends in selected m/z values as detected with MS downstream during H_2-TPR of (a) Pd-PVA/AC_S, (b) Pd-PVA/AC_Cl. Gas composition 5% H_2/95% Ar. Heating rate 5°C min^{-1}.

In the presence of Pd, the TGA plots of as-prepared catalysts clearly depended on the choice of gas (H_2/Ar *versus* Ar), as shown in Figure 2.5. The major weight loss of the catalyst prepared using H_2SO_4 shifted 30°C lower when H_2 was introduced in Ar flow (Figure 2.5a and c). The volatile products were again similar to those produced from bulk PVA decomposition at 340°C (Table 2.4). Additionally, MS results indicate H_2 consumption at 160°C, whereas H_2 production occurred at 320°C and 400°C (Figure 2.6a, Table 2.4). H_2 consumption and production was also observed with the sample prepared using HCl (Figure 2.6b, Table 2.4). However, the main weight loss was around 310°C (Figure 2.5b and d), similar to PVA and PVA/AC_Cl (Figure 2.4d and f). This trend was different as compared to the observations for catalysts prepared with H_2SO_4 (Figure 2.5a and c), although the volatile compounds detected by MS were again similar (Table 2.4).

Table 2.4. Summary of TGA-DTG results

Sample	Atmosphere	Weight loss at 200°C (wt %)	Weight loss position		Related gas products according to MS
			Peak range (°C)	Peak position (°C)	
AC	H_2/Ar	0.35	90-160	120	H_2O
	Ar	0.34	90-160	120	H_2O
AC_Cl	H_2/Ar	1.58	90-190	130	
	Ar	1.62	90-190	130	
AC_S	H_2/Ar	0.04	210-280	240	
	Ar	0.05	210-280	240	
PVA and AC mechanical mixture	H_2/Ar	0.10	250-450	120	H_2O
				340	H_2O, CO_2, $-CH_3$
				400	$-CH_3$
	Ar	0.08	250-450	120	H_2O
				340	H_2O, CO_2, $-CH_3$
PVA-AC_S	H_2/Ar	2.91	120-300	190	H_2O, CO_2, $-CH_3$
	Ar	2.88	120-300	190	H_2O, CO_2, $-CH_3$
PVA-AC_Cl	H_2/Ar	0.82	220-450	120	H_2O
				250	H_2O, CO_2, $-CH_3$
				315	H_2O, CO_2, $-CH_3$
				400	$-CH_3$
	Ar	0.84	220-450	120	H_2O
				250	H_2O, CO_2, $-CH_3$
				315	H_2O, CO_2, $-CH_3$
				400	$-CH_3$
Pd-PVA/AC_S	H_2/Ar	2.38	90-450	160	H_2 (negative), H_2O, CO_2 and $-CH_3$
				320	H_2, H_2O, CO_2, $-CH_3$
				400	H_2, $-CH_3$
	Ar	2.26	130-450	190	H_2O, CO_2, $-CH_3$
				315	H_2O, CO_2, $-CH_3$
				400	H_2, $-CH_3$
Pd-PVA/AC_Cl	H_2/Ar	1.47	90-400	155	H_2 (negative), H_2O, CO_2
				315	H_2, H_2O, $-CH_3$
				400	H_2, $-CH_3$
	Ar	0.48	90-400	310	H_2O, CO_2, $-CH_3$
				400	H_2, $-CH_3$

3.7. Catalytic performance

The catalysts exhibited stable activities on the time scale of hours after initial stabilization time. A typical example of activity as function of time on stream is presented in Figure. A2.2.

3.7.1. Formic acid decomposition. The activities of the catalysts for formic acid decomposition at 120°C, defined per total Pd as well as per surface Pd according to CO chemisorption, are presented in Figure 2.7a and b. In all experiments CO_2 and H_2 were the major products. The reaction rate per total Pd for the catalyst prepared using HCl significantly increased after reduction at 200°C. Same effect was also observed for the catalyst prepared using H_2SO_4, although the resulting activity was only half as compared to the H_2 reduced catalyst prepared using HCl.

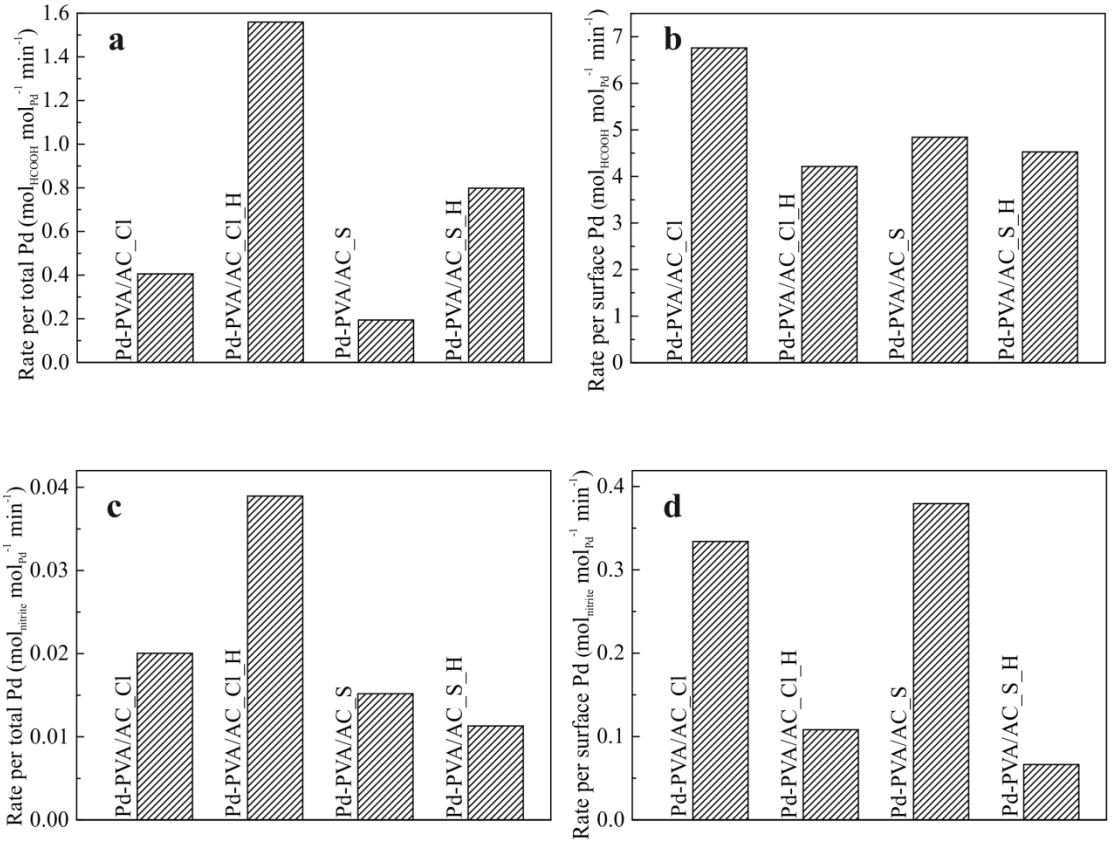

Figure 2.7. Reaction rate per total Pd (a) and per surface Pd determined by CO chemisorption (b) for formic acid catalytic decomposition at 120ºC, and reaction rate per total Pd (c) and per surface Pd determined by CO chemisorption (d) for nitrite hydrogenation at 25ºC.

The reaction rates per surface Pd were quite similar for the reduced catalysts using either HCl or H_2SO_4, as well as for the as-prepared catalyst prepared using H_2SO_4, as shown in Figure 2.7b. As-prepared catalyst using HCl showed higher reaction rate per surface Pd at 120ºC, as compared to all other catalysts.

3.7.2. Nitrite hydrogenation. The activities of the catalysts for nitrite hydrogenation in aqueous phase at 25ºC are also compared, as shown in Figure 2.7c and d. The reaction rate per total Pd of the catalyst prepared using HCl (Figure 2.7c) was significantly enhanced after the reduction treatment. In contrast, the reaction rate per total Pd for the catalyst prepared using H_2SO_4 did not show any increase after the reduction treatment.

The activity calculated based on the amount of surface Pd atoms, according to CO chemisorption, strongly decreased as a result of the reduction treatment, independent of the acid used in the catalyst preparation procedure, as shown in Figure 2.7d.

4. Discussion

4.1. Oxidation and blocking of the surface of Pd NPs

Figure 2.1 and Table 2.2 show that the Pd particle sizes are identical when either HCl or H_2SO_4 were used to immobilize the colloid, for any of the thermal treatments applied. However, it is also shown in Table 2.2 that the apparent Pd dispersion, according to CO chemisorption, in as-prepared catalysts were significantly lower than the results calculated from TEM. Additionally, the catalytic activity per total Pd in as-prepared catalysts was always low, as shown in Figure 2.7. The obvious explanation is that PVA blocked the surface of Pd NPs, as reported by many other researchers [3, 6, 27]. Thermal treatment in different atmosphere has been often suggested to remove the capping polymer [4, 28]. However, complete removal has been reported to be difficult to achieve, and in any case temperature above 300^{o}C is needed, easily causing sintering [9, 12]. Surprisingly, the data in table 2.2 show that it was possible to clean the Pd NPs completely in H_2/N_2 at 200^{o}C, but only when HCl had been used in the catalyst preparation. In contrast, catalyst prepared with H_2SO_4 could not be cleaned to the same extent. The CO chemisorption data suggest much lower dispersion as compared to TEM. The effect of the acid on the preparation is therefore discussed in detail below.

Chlorine was present in all catalysts, independently of the acid used during colloid immobilization, as shown in Table 2.2 and confirmed by XPS (Figure 2.3c). It is known that the presence of chlorine in Pd catalysts decreases the capacity of CO chemisorption [29], therefore it is difficult to discern whether the low CO adsorption capacity was due to the presence of Cl or the PVA blocking effect. The presence of small content of chlorine in as-prepared catalyst using H_2SO_4 originated from the Pd precursor, Na_2PdCl_4. It is well known that complete removal of Cl from Pd catalyst prepared with Cl containing precursors is difficult *via* reduction by $NaBH_4$ or even by treatment in H_2 below 100^{o}C [30-32]. Therefore, the presence of Cl on Pd may well contribute to the extremely low CO chemisorption capacity in as-prepared catalysts, as shown in Table 2.2.

When HCl was used instead of H_2SO_4 during colloid immobilization, the chlorine content as well as the fraction of oxidized Pd tripled in the as-prepared catalyst, indicating a strong correlation between the chlorine content and the Pd oxidation state. Obviously, the additional chlorine was introduced by HCl. The immobilization was always performed in the presence of air. We suggest that the presence of HCl enhanced the oxidation of the Pd NPs with O_2, according to the following reaction equations:

$$2Pd + O_2 \longrightarrow 2PdO \qquad \Delta G = -186.82 \text{ kJ} \qquad \text{(Eq. 2.1)}$$

$$PdO + 2Cl^- + 2H^+ \longrightarrow PdCl_2 + H_2O(l) \qquad \Delta G = -41.38 \text{ kJ} \qquad \text{(Eq. 2.2)}$$

The resulting overall reaction is:

$$2Pd + Cl^- + O_2 + 4H^+ \longrightarrow 2PdCl_2 + 2H_2O(l) \qquad \Delta G = -269.57 \text{ kJ} \qquad \text{(Eq. 2.3)}$$

According to the XPS results in Table 2.3, 38% of Pd was oxidized when using HCl, and this percentage was quite similar to the Pd dispersion observed by TEM (38%, Table 2.2). This would indicate that the surface of the Pd NPs was completely oxidized with Cl^- as the counter-ion.

UV-vis spectra of unsupported colloid (Figure A2.1) indicate re-oxidation and re-dissolution of Pd NPs in the presence of O_2 and Cl^-. On the other hand, the Pd particle sizes (TEM in Figure 2.1) and Pd contents (XRF results in Table 2.1) show no difference for AC supported catalysts regardless which acid was used. Thus, the re-dissolution of Pd during colloid immobilization was only a minor effect.

As shown by XRF (Table 2.2) and XPS (Figure 2.3, Table 2.3), chlorine bonded to Pd was removed by the reduction in H_2/N_2, especially at higher temperature, suggesting that $PdCl_x$ was converted to Pd^0 and HCl. The Pd dispersion calculated based on CO chemisorption was comparable with TEM observations after reduction at 200°C in H_2/N_2, indicating that complete exposure of the Pd surface was obtained.

Given the fact that Cl^- interacted significantly with the Pd NPs, we propose that the presence of Cl^- and O_2 during colloid immobilization weakens the interaction between Pd NPs and PVA, explaining that PVA was found to be completely removed by H_2 treatment at 200°C. This proposition is schematically presented in Figure 2.8.

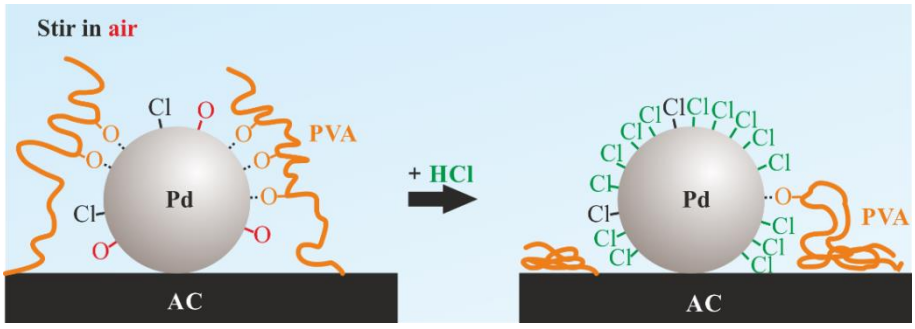

Figure 2.8. Proposed mechanism of chlorine suppressing PVA coverage on Pd NPs.

On the other hand, when H_2SO_4 was used, 13% of Pd was present as Pd^{2+} in as-prepared catalyst, as shown in Table 2.3. The oxidized Pd could be reduced almost completely in H_2/N_2, as only 2% of Pd atoms remained oxidized after reduction at 250°C. However, the Pd surface area accessible for CO chemisorption was still very low as compared to the particle size according to TEM. Therefore, the limited accessibility of the surface of the Pd NPs was caused by other reasons. Before concluding that blocking by PVA is responsible, two alternative explanations will be discussed shortly.

As the mean diameter of the Pd NPs in all catalysts was larger than 2 nm, most of the Pd NPs should be located in mesopores. As shown in Figure 2.2, no blocking of mesopores was observed according to N_2 physisorption results, indicating that PVA did not decrease the accessibility of those pores containing Pd NPs.

Another alternative explanation might be the presence of S in the catalysts prepared with H_2SO_4, as S poisoning of Pd is a well-known phenomenon [33-35]. As shown in Table 2.2, almost all sulfur species originated from H_2SO_4. Reduction of S^{6+} species to S^0/S^{2-} species was observed (Figure 2.3b), accompanied by reduction of Pd^{2+} as well as an increase of the apparent Pd dispersion according to CO chemisorption, as shown in Table 2.2 and 2.3. Both these observations illustrate that the formation of S^0/S^{2-} is not accompanied by formation of PdS on the surface of the Pd particles. Insignificant interaction of the S species with Pd is also illustrated by the fact that the S content in Pd-PVA/AC_S was even lower than in PVA/AC_S.

In summary, PVA blocked the Pd surface of the nanoparticles in the catalyst prepared using H_2SO_4 during colloid immobilization. When HCl was used instead, PVA coverage was suppressed by Cl bonded to Pd, whereas Cl was removed by reduction in H_2/N_2, resulting in clean surface of Pd NPs.

4.2. PVA thermal stability

As shown in Figure 2.4, the choice of acid used for colloid immobilization also influenced the thermal stability of PVA in inert atmosphere. In the presence of H_2SO_4, the decomposition temperature of PVA dispersed on AC (Figure 2.4e) was 150°C lower as compared to PVA in the mechanical mixture (Figure 2.4d). Three reasons can be suggested to explain this. First, PVA decomposition might be promoted catalytically by sulfonic acid on AC or PVA, in a similar way as the catalytic decomposition of cross-linked PVA by sulfosuccinic acid (SSA) in the study of Morancho *et al.* [36]. Second, Yang *et al.* demonstrated decreasing thermal stability when hydrolyzing PVA [25]. The PVA used in this study was produced from polyvinyl acetate [37], and was hydrolyzed to 87 – 89% as purchased. It is quite possible that further hydrolysis of PVA occurred in the presence of H_2SO_4 in aqueous phase, thus decreasing the thermal stability. Finally third, PVA was possibly well dispersed on the AC surface, thus increasing the surface area of PVA, which was likely to enhance its thermal decomposition. Further research would be necessary to distinct between these three options.

In contrast, the TGA results of PVA dispersed on AC prepared with HCl (Figure 2.4f) indicate a much milder effect on promoting PVA decomposition as compared with H_2SO_4. Comparing with the TGA result of PVA in the mechanical mixture (Figure 2.4d), the new weight loss step around 250°C would indicate a lesser influence of the possible reasons discussed above.

Remarkably, PVA decomposition in inert atmosphere was not influenced by the presence of Pd, comparing Figure 2.4e and 2.5c, as well as Figure 2.4f and 2.5d. This indicates that PVA was mainly dispersed on AC, and the interaction with Pd involved only a minor fraction of the PVA in the catalyst. However, in H_2/Ar, the presence of Pd caused an additional weight loss step appeared around 160°C (Figure 2.5b and 2.5d), concurrently with hydrogen consumption and H_2O production (Figure 2.6), indicating hydrogenolysis of PVA catalyzed by Pd NPs, according to the following reaction:

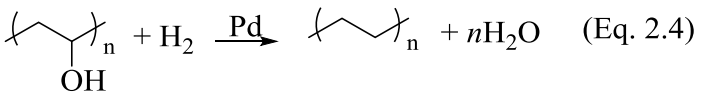

(Eq. 2.4)

The catalyst prepared using H_2SO_4 exhibited more significant weight loss (for both decomposition and hydrogenation) compared to the catalyst prepared using HCl at 200°C (Table 2.4). However, the capacity for CO chemisorption did not increase (Table 2.2). This

indicates again that the majority of the PVA interacted with AC, whereas only a minority fraction was involved in the interaction with Pd NPs, decreasing the accessible Pd surface area.

4.3. Catalytic activity

4.3.1. Activity per total Pd. The influence of the choice of acid and thermal treatment on catalyst performance was studied with reactants in gas phase *vs.* reactants in aqueous phase, using formic acid decomposition and nitrite hydrogenation as model reactions, respectively.

In both reactions, treatment at 200°C in H_2/N_2 increased the reaction rate per total Pd for the catalyst prepared using HCl, as shown in Figure 2.7a and 2.7c, together with increasing apparent Pd dispersion calculated from CO chemisorption in Table 2.2, as well as further reduction of Pd and removal of Cl bonded to Pd as observed by XPS in Table 2.3. As discussed above, this confirms that the thermal treatment in H_2/N_2 together with the use of HCl increased the accessibility of surface Pd atoms on the nanoparticles, enhancing the activity for both reactions.

However, catalysts prepared with H_2SO_4 revealed very different effects on activity in the two reactions after treatment in H_2/N_2. Activity for nitrite hydrogenation decreased slightly after reduction in H_2/N_2 at 200°C (Figure 2.7c), whereas activity for formic acid decomposition increased strongly (Figure 2.7a). All catalysts prepared with H_2SO_4 were much less active as compared to the reduced catalysts prepared using HCl, which can be attributed to remaining capping agent on the Pd NPs. As aforementioned, TGA results (Figure 2.5a) indicate that PVA mostly decomposed at 200°C in H_2/Ar, thus a minor fraction of PVA in the catalysts is responsible for the partial deactivation of the Pd surface.

4.3.2. Activity per surface Pd. Figure 7b shows that the activity per Pd surface atom for formic acid decomposition varied only slightly for all catalysts. Thus the activity scales with the number of sites accessible for CO. Note that CO chemisorption for as-prepared catalyst prepared using HCl was performed after a pretreatment including reduction at room temperature. Possibly Pd was partially reduced by formic acid during the reaction, increasing the actual number of Pd surface active sites as compared to the estimation based on CO chemisorption.

In the case of nitrite hydrogenation in aqueous environment, the activity per surface Pd atom varied significantly after the thermal treatment in H_2/N_2. For the catalyst prepared using HCl, this was probably an artifact: the as-prepared catalyst contained an extremely high chlorine concentration, causing a low CO chemisorption capacity. Probably, part of the chlorine was removed by H_2 during the nitrite hydrogenation, which is supported by the fact that Cl^- was detected in the product liquid initially. As a consequence, the number of Pd surface sites was underestimated, and the activity per Pd surface atom was overestimated.

By comparison, the catalyst prepared using H_2SO_4 showed even more significant decrease in activity per Pd surface atom after reduction in H_2/N_2 at 200°C, as shown in Figure 2.7d. Increasing the number of active sites during reaction was not likely to be the main reason in this case, because the catalyst contained much less chlorine as well as oxidized Pd (Table 2.3). Therefore, it is proposed that the main reason was the effect of the reaction medium (gas *vs.* water) on the arrangement of the PVA molecules on the surface of the Pd NPs. As PVA has high affinity for water, it is expected that PVA will cover the Pd surface more extensively when exposed to gas phase (during CO chemisorption), whereas in aqueous medium (during nitrite hydrogenation), the PVA molecules tend to interact with water, decreasing the coverage of the Pd surface. Consequently, the number of Pd atoms accessible on the surface in water was probably underestimated by CO chemisorption, resulting in an overestimated activity per surface Pd for catalyst prepared using H_2SO_4.

5. Conclusions

The choice of acid during Pd colloid immobilization on activated carbon is critical to achieve complete accessibility of surface Pd atoms. Usage of HCl efficiently suppresses blocking of the surface of the immobilized Pd NPs by PVA. Clean and catalytically active Pd NPs can be achieved after reduction in H_2/N_2 atmosphere at 200^oC without any significant sintering.

In contrast, H_2SO_4 does not induce this suppressing effect and PVA remains blocking a significant part of the Pd surface. The extent of blocking the Pd surface by PVA is less significant in water as compared to in gas-phase, which is addressed to the interaction of PVA with water, suppressing partly the interaction with the metal surface. This is reflected in the catalytic activity for formic acid decomposition in gas phase *versus* nitrite hydrogenation in aqueous phase.

The majority of the PVA molecules interact with the support only and the temperature of PVA decomposition is therefore not a useful parameter for developing methods to obtain clean Pd NPs.

Appendix

A.1. UV-vis

UV-vis spectra of Na_2PdCl_4 aqueous solution and unsupported Pd-PVA colloid were obtained using a Varian CARY 300 scan UV-vis spectrophotometer.

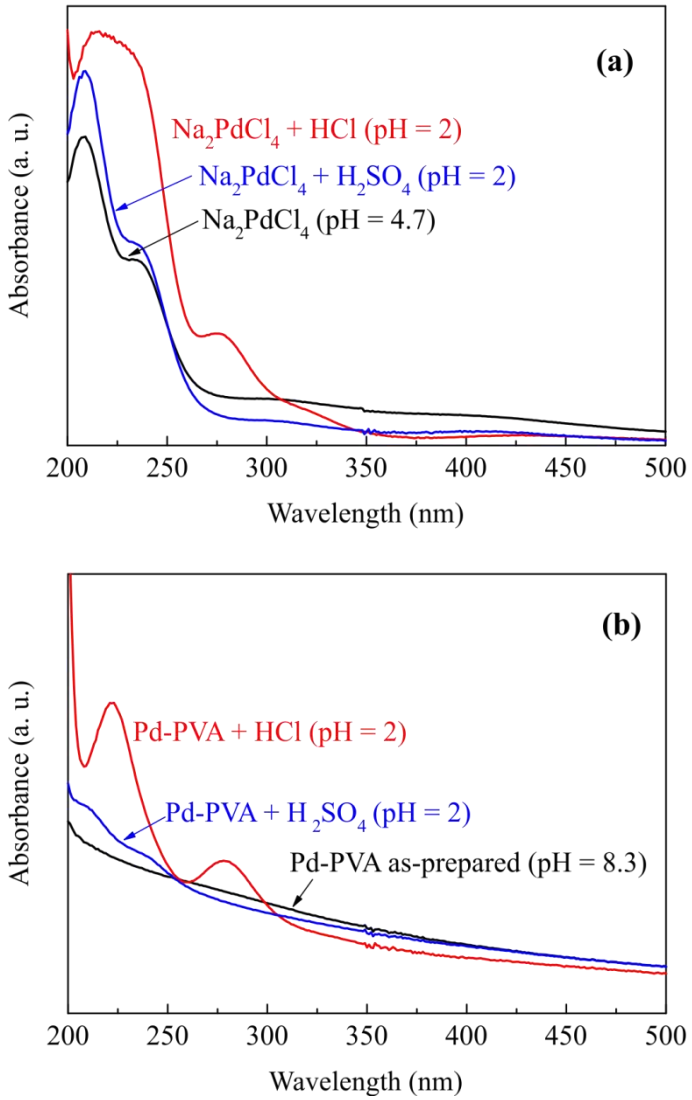

Figure A2.1. (a) UV-vis spectra of Na_2PdCl_4 aqueous solution with HCl, H_2SO_4 and without acid; (b) UV-vis spectra of unsupported Pd-PVA colloid in present of HCl, H_2SO_4 and without acid. The absorption peaks at 207 nm and 236 nm can be attributed to $[PdCl_3(H_2O)]^-$ and peaks at 222 nm and 278 nm to $[PdCl_4]^{2-}$. These assignments are consistent with the literature [38, 39].

As shown in Figure A2.1(a), $[PdCl_3(H_2O)]^-$ was present in original Na_2PdCl_4 solution, and there was no change when H_2SO_4 was added. When HCl was added instead, a red shift of the spectrum occurred probably caused by the increase of Cl^- content.

Pd^{2+} was completely reduced to Pd^0 after colloid preparation, as shown in Figure A2.1(b). When the pH of as-prepared colloid was adjusted to 2 by adding HCl and stirring in air for 2 h, $[PdCl_4]^{2-}$ is detected by UV-vis, indicating that at least part of the reduced Pd on the NPs was re-oxidized and re-dissolved into the aqueous phase. When H_2SO_4 was used instead, the re-dissolving of Pd was less significant, and Pd^{2+} is present as $[PdCl_3(H_2O)]^-$ instead of $[PdCl_4]^{2-}$. This is probably caused by the lower Cl : Pd ratio as compared to when HCl was added.

A.2. Catalyst durability

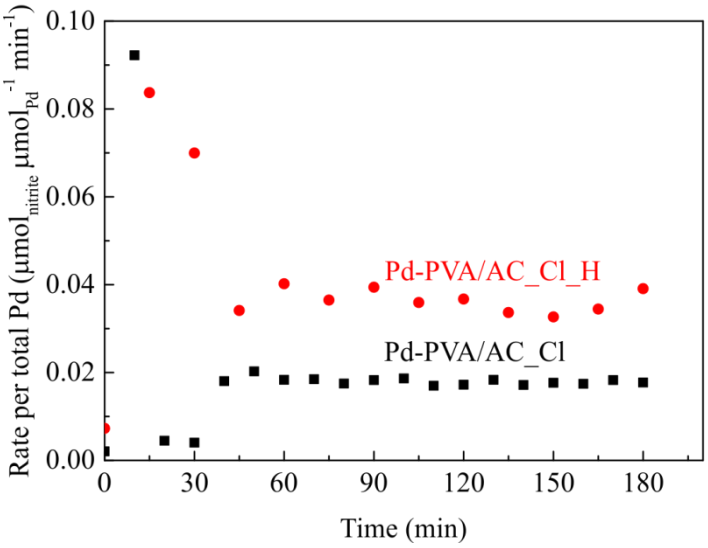

Figure A2.2. Reaction rate per total Pd for nitrite hydrogenation performed in fixed bed reactor at 25ºC.

Catalyst activity for nitrite hydrogenation was measured in continuously operated fixed bed reactors, as shown in Figure A2.2. The activities of the catalysts stabilized after 1 h reaction.

References

[1] Y. Xia, Y. Xiong, B. Lim, S.E. Skrabalak, Angew. Chem. Int. Ed., 48 (2009) 60-103.

[2] N. Semagina, L. Kiwi-Minsker, Catal. Rev., 51 (2009) 147-217.

[3] A. Villa, D. Wang, D.S. Su, L. Prati, Chemcatchem, 1 (2009) 510-514.

[4] E.G. Rodrigues, S.A.C. Carabineiro, J.J. Delgado, X. Chen, M.F.R. Pereira, J.J.M. Órfão, J. Catal., 285 (2012) 83-91.

[5] A.V. Gaikwad, in: Faculty of Science, University of Amsterdam, Amsterdam, 2009.

[6] A. Quintanilla, V.C.L. Butselaar-Orthlieb, C. Kwakernaak, W.G. Sloof, M.T. Kreutzer, F. Kapteijn, J. Catal., 271 (2010) 104-114.

[7] X. Wang, P. Sonström, D. Arndt, J. Stöver, V. Zielasek, H. Borchert, K. Thiel, K. Al-Shamery, M. Bäumer, J. Catal., 278 (2011) 143-152.

[8] C. Aliaga, J.Y. Park, Y. Yamada, H.S. Lee, C.-K. Tsung, P. Yang, G.A. Somorjai, J. Phys. Chem. C, 113 (2009) 6150-6155.

[9] Y. Borodko, H.S. Lee, S.H. Joo, Y. Zhang, G. Somorjai, J. Phys. Chem. C, 114 (2009) 1117-1126.

[10] R.M. Rioux, H. Song, J.D. Hoefelmeyer, P. Yang, G.A. Somorjai, J. Phys. Chem. B, 109 (2004) 2192-2202.

[11] P. Dash, T. Bond, C. Fowler, W. Hou, N. Coombs, R.W.J. Scott, J. Phys. Chem. C, 113 (2009) 12719-12730.

[12] L.R. Baker, G. Kennedy, J. Krier, M. Spronsen, R. Onorato, G. Somorjai, Catal. Lett., 142 (2012) 1286-1294.

[13] J.A. Lopez-Sanchez, N. Dimitratos, C. Hammond, G.L. Brett, L. Kesavan, S. White, P. Miedziak, R. Tiruvalam, R.L. Jenkins, A.F. Carley, D. Knight, C.J. Kiely, G.J. Hutchings, Nat. Chem., 3 (2011) 551-556.

[14] S.D. Lin, Y.-H. Hsu, P.-H. Jen, J.-F. Lee, J. Mol. Catal. A: Chem., 238 (2005) 88-95.

[15] A. Villa, D. Wang, N. Dimitratos, D. Su, V. Trevisan, L. Pratia, Catal. Today, 150 (2010) 8.

[16] F. Rouquerol, J. Rouquerol, K. Sing, in: Adsorption by Powders and Porous Solids, Academic Press, London, 1999, pp. 237-285.

[17] David Briggs, J.T. Grant, IM Publications, Chichester, 2003.

[18] J. F. Moulder, W. F. Stickle, P. E. Sobol, K.D. Bomben, Perkin-Elmer Corporation, Eden Prairie, 1992.

[19] D.A. Bulushev, L. Jia, S. Beloshapkin, J.R.H. Ross, Chem. Commun., 48 (2012) 4184-4186.
[20] C. Amorim, G. Yuan, P.M. Patterson, M.A. Keane, J. Catal., 234 (2005) 268-281.
[21] F. Pinna, F. Menegazzo, M. Signoretto, P. Canton, G. Fagherazzi, N. Pernicone, Applied Catalysis A: General, 219 (2001) 195-200.
[22] P.A. Simonov, A.V. Romanenko, I.P. Prosvirin, E.M. Moroz, A.I. Boronin, A.L. Chuvilin, V.A. Likholobov, Carbon, 35 (1997) 73-82.
[23] A.V. Naumkin, A. Kraut-Vass, S.W. Gaarenstroom, C.J. Powell, in, the National Institute of Standards and Technology.
[24] J.H. Cai, E. Morris, C.Q. Jia, J. Sulfur Chem., 30 (2009) 555-569.
[25] H. Yang, S. Xu, L. Jiang, Y. Dan, J. Macromol. Sci., Part B: Phys., 51 (2011) 464-480.
[26] P. Thomas, J.P. Guerbois, G. Russell, B. Briscoe, J. Therm. Anal. Calorim., 64 (2001) 501-508.
[27] J.K. Chinthaginjala, A. Villa, D.S. Su, B.L. Mojet, L. Lefferts, Catal. Today, 183 (2012) 119-123.
[28] L. Okhlopkova, M. Kerzhentsev, F. Tuzikov, Y. Larichev, Z. Ismagilov, J. Nanopart. Res., 14 (2012) 1-15.
[29] J. Sepúlveda, N. Fígoli, React. Kinet. Catal. Lett., 53 (1994) 155-160.
[30] A.K. Zharmagambetova, V.A. Golodov, Y.P. Saltykov, J. Mol. Catal., 55 (1989) 406-414.
[31] A.K. Zharmagambetova, S.G. Mukhamedzhanova, E.A. Bekturov, React. Polym., 24 (1994) 17-20.
[32] J.M. Badano, M. Quiroga, C. Betti, C. Vera, S. Canavese, F. Coloma-Pascual, Catal. Lett., 137 (2010) 35-44.
[33] S.T. Marshall, J.W. Medlin, Surf. Sci. Rep., 66 (2011) 173-184.
[34] P.A. Gravil, H. Toulhoat, Surf. Sci., 430 (1999) 176-191.
[35] L.-Y. Gan, Y.-X. Zhang, Y.-J. Zhao, J. Phys. Chem. C, 114 (2009) 996-1003.
[36] J.M. Morancho, J.M. Salla, A. Cadenato, X. Fernández-Francos, X. Ramis, P. Colomer, Y. Calventus, R. Ruíz, Thermochim. Acta, 521 (2011) 139-147.
[37] R. Tamaki, Y. Chujo, Appl. Organomet. Chem., 12 (1998) 755-762.
[38] L.I. Elding, Inorg Chim Acta, 6 (1972) 647-651.
[39] C. Drew Tait, D.R. Janecky, P.S.Z. Rogers, Geochim Cosmochim Ac, 55 (1991) 1253-1264.

Chapter 3

Unsupported PVA and PVP stabilized Pd nanoparticles as catalyst for nitrite hydrogenation in aqueous phase

Pd colloids stabilized with polyvinyl alcohol (PVA) and polyvinylpyrrolidone (PVP) have been prepared, characterized with TEM, zeta-potential measurements, CO chemisorption in aqueous phase and ATR-IR spectroscopy using CO as a probe molecule, and finally tested for performance in nitrite hydrogenation as unsupported nanoparticles. Polymer coverage on Pd surface was significant for both Pd-PVA and Pd-PVP colloid, blocking active sites. The turn-over-frequency (TOF) of the remaining sites as well as selectivity to ammonium was not influenced by coverage of the Pd surface with PVA. However, the ammonium selectivity increased with increasing Pd particle size. In contrast, increasing coverage of Pd surface with PVP increased the TOF, while the ammonium formation was suppressed. This has been attributed to an effect of PVP on the surface reaction intermediates, based on the observation that chemisorbed CO was also influenced by PVP.

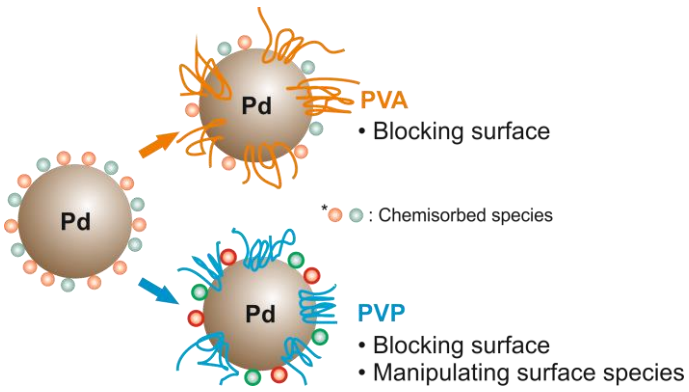

This part of work has been published as Research Article: Y. Zhao, J.A. Baeza, N. Koteswara Rao, L. Calvo, M.A. Gilarranz, Y.D. Li, L. Lefferts, J. Catal., 318 (2014) 162-169..

1. Introduction

Colloidal methods are widely used to prepare model catalyst with accurately controlled particle sizes and shapes [1-3]. Such colloids, containing metallic nanoparticles, can be used either to prepare supported catalysts via immobilization on support material, or to apply directly as a catalyst after dispersion in liquid reaction medium [4].

To prepare colloid, stabilizers are usually necessary during colloid preparation to limit crystal growth and particle agglomeration [3, 5-8]. Polymers, such as polyvinyl alcohol (PVA) and polyvinylpyrrolidone (PVP), are commercially available, relatively inexpensive, well water-soluble, nontoxic, and very effective stabilizers for colloid preparation [9]. These two polymers both contain a long-carbon-chain back-bone with different functional groups, where PVA contains hydroxyl groups whereas PVP contains pyrrolidone groups, as shown in Scheme 3.1.

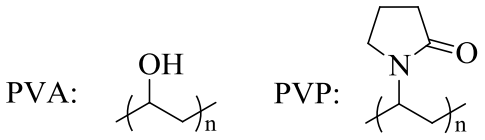

Scheme 3.1. Molecular structure of PVA and PVP

It is widely reported that stabilizers interact with the surface of the nanoparticles competing with reactant molecules, acting as a (partial) surface poison by blocking active sites [10-12]. Therefore, obtaining "clean" particles without significant change of size and shape of the nanoparticles has become a major challenge in the case of supported catalysts prepared via colloidal methods. Methods based on exposure to ozone with UV-light, as well as thermal treatments in oxidative, reducing and inert atmosphere have been explored with limited success, often resulting in deteriorating particle size and shape or incomplete removal and formation of carbonaceous deposits blocking the surface [13-19]. On the other hand, partial removal of polymer stabilizer already increases activity significantly of e.g. Pt/TiO_2 catalyst for CO oxidation in gas phase and alcohol oxidation in liquid phase [20].

Also, favourable effects of polymer stabilizers, such as PVP, on catalyst performance have been reported. Quintanilla et al. reported that PVP increases the activity of Au/Al_2O_3 for liquid phase oxidation of benzyl alcohol [11]. When using colloid metal particles directly, without a support material, stabilizers are clearly necessary to prevent agglomeration during the catalytic experiment, and therefore should not be removed. Evangelisti et al. reported PVP was

responsible for high stereo-selectivity to *cis*-alkenes for hydrogenation of aliphatic alkynes with Pd-PVP colloid [21]. PVP was also reported to enhance activity of Au-PVP colloid for aerobic oxidation of alcohols especially for very small nanoparticles (<1.5 nm) [22, 23].

In this chapter, unsupported Pd-PVA and Pd-PVP colloids were used as catalysts to ensure absence of any support effect in nitrite hydrogenation. Colloids with different Pd particle sizes were prepared by altering the concentration of these two commonly used polymer stabilizers. It will be shown that the functional groups influence the catalytic performance of the Pd colloid.

2. Experimental

2.1. Chemicals

Sodium tetrachloropalladate (II) (Na_2PdCl_4 ≥ 99.995% (metal basis)), polyvinyl alcohol (PVA, average MW = 13000 – 23000, 87% – 89% hydrolyzed), polyvinylpyrrolidone (PVP, average MW = 40000), and sodium borohydride ($NaBH_4$, ≥ 96% (gas-volumetric) were purchased from Sigma-Aldrich. Sodium nitrite (> 99%) was purchased from Merck. All the aqueous solutions were prepared using ultra purified water obtained on water purification system (Millipore, Synergy).

2.2. Pd-PVA Colloid Preparation

PVA was dissolved in water at 70ºC with stirring for 2 hours. The solution (2 wt %) was then cooled down to room temperature. Aqueous solution of Na_2PdCl_4 (20 mL, containing 0.086 mmol Pd) and 1.76 mL of freshly prepared PVA solution were added to 240 mL water, obtaining a yellow-brown solution. After 3 min, $NaBH_4$ solution (1.72 mL, 0.172 mmol) was added with a syringe pump under vigorous stirring. Brown Pd colloid solution was immediately formed. The final pH was around 9. The procedure as described leads to a molar ratio of polymer-monomer/Pd ($polymer_{mono}$/Pd) equal to 9.3 (mol/mol); this ratio was varied between 1.2 and 9.3 by varying the volume of the polymer solution.

2.3. Pd-PVP Colloid Preparation

Similar to Pd-PVA colloid preparation, PVP aqueous solution (5.04 wt %) was prepared at room temperature. Aqueous solution of Na_2PdCl_4 (20 mL, containing 0.086 mmol Pd) and 1.76 mL of freshly prepared PVP solution were added to 240 mL water ($polymer_{mono}$/Pd = 9.3, mol/mol). After 3 min, $NaBH_4$ solution (1.72 mL, 0.172 mmol) was added with a syringe pump under vigorous stirring. Brown Pd colloid solution was immediately formed. The final pH was around 9. Also in this case the $polymer_{mono}$/Pd ratio was varied by varying the volume of the polymer solution.

2.4. Electron Microscopy

Pd particle size distribution was determined using TEM (Philips CM300ST-FEG) with a resolution of 1 nm. Typically 2 µL colloidal suspension was dropped and dried on a copper grid covered with hollow carbon for TEM image taking. Pd particle sizes were determined with ImageJ at minimal 7 locations on the grid, and at least 500 Pd particles were measured. A Cu grid covered with graphene modified lacey carbon was used instead when HRTEM images was taken on the same apparatus.

2.5. Zeta Potential

The zeta potential of the Pd colloid dispersed in the reaction suspension after reaction at pH = ~8.5 was characterized by a Zetasizer Nano ZS ZEN3600 instrument (Malvern Instruments) at 25^{o}C using laser with wavelength of 633 nm.

2.6. ATR-IR of Adsorbed CO

The as-prepared colloidal suspension was sprayed on a ZnSe crystal (Internal Reflection Element) to form a catalyst layer of a few micron thick. Then the crystal was mounted in a home-build *in-situ* ATR-IR(Attenuated Total Reflection Infrared Spectroscopy) cell which has been described in detail elsewhere [24]. The cell was mounted in the sample compartment of an infrared spectrometer (Bruker Tensor 27) equipped with a MCT detector. All the measurements were done at room temperature (21 ± 1^{o}C) with a resolution of 4 cm^{-1}. Typically the sample was reduced in a H_2 flow for 2 h, followed by flushing in Ar for 30 min. The last

spectrum in Ar was used as background. IR spectra were recorded every minute with 128 scans during exposing the sample to pure CO for 30 min, followed by flushing with Ar for 30 min.

2.7. CO Chemisorption in Aqueous Phase

The accessibility of surface Pd atoms of the colloid in aqueous phase was characterized by CO chemisorption, in a home-built apparatus equipped with a glass vial and a Teflon coated magnetic stir-bar with a stirring rate of at least 500 rpm. 4 mL of 3.3×10^{-4} mol_{Pd} L^{-1} of Pd colloid was first reduced in H_2 flow for 1 h followed by flushing in He for 30 min. Then CO pulses were introduced via a six-port valve with a 50 μL loop and the response in the exiting gas stream was measured on-line with a quadrupole mass spectrometer (MS, Pfeiffer AG Balzers, OmniStar, (m/z=28)). The amount CO in every pulse was estimated based on the integrated area of the response signal recorded as a function of time. Pulsing was repeated until saturation occurred, implied by that the peak area of subsequent CO peaks became constant and equal to the peak area of the original pulse. The total amount of chemisorbed CO was calculated by summing the amounts of CO adsorbed during each individual pulse. All the measurements performed at 21 ± 1°C with colloidal suspension pH = 8.5 ± 0.5, identical to the conditions of the catalytic experiments as described below. A typical result is shown in Figure. A3.2 in the Appendix.

2.8. Nitrite Hydrogenation

The reactions involved in nitrite hydrogenation are given in Eq. 1.2 and 1.3.

$$2NO_2^- + 3H_2 + 2H^+ \xrightarrow{Pd} N_2 + 4H_2O \qquad \text{(Eq. 1.2)}$$

$$NO_2^- + 3H_2 + 2H^+ \xrightarrow{Pd} NH_4^+ + 2H_2O \qquad \text{(Eq. 1.3)}$$

All the as-prepared colloids were stored in a refrigerator and were used in catalytic experiments without any further separation or washing. The reaction was performed at 21 ± 1°C in a home-build apparatus including a glass tank reactor (ϕ 98 mm with four 5 mm baffles), equipped with a mechanical 6-blade-stirrer (ϕ 44 mm, 1000 rpm) with the propeller positioned at the centre of liquid. Typically, 70 mL as-prepared colloidal suspension was mixed with 230 mL phosphate (KH_2PO_4 + NaOH) buffer solution under vigorous stirring in 40 vol% H_2 in He

(total flow rate 100 mL min^{-1}) at 1 bar for 1 h, with the Pd content $C_{Pd} = 7.7 \times 10^{-5}$ mol L^{-1} in the reaction suspension. The initial pH of the reaction was 8.5, resulting in significant selectivity to ammonium, in order to obtain accurate data. Then 3 mL 4.4 mmol L^{-1} $NaNO_2$ solution was introduced, starting the reaction. Samples were taken using a 1 mL syringe (BD Plastipak), in which the sample was filtered through 40 mg of α-Al_2O_3 (>99.99%, AKP-30, Sumitomo Chemical) and a syringe filter (PTFE, 0.2 μm, Whatman) in order to remove the colloid. The sample was diluted with a factor of 5 before injection into ion chromatography (DIONEX, ICS 1000) to determine the concentrations of nitrite and ammonium. Selectivity to ammonium of the colloids was defined as:

$$\text{ammonium selectivity (\%)} = \frac{\text{mole of ammonium formed}}{\text{mole of nitrite consumed}} \times 100\% \qquad \text{(Eq. 3.1)}$$

The influence of additional PVA or PVP, added after colloid preparation, on catalyst performance was studied by adding extra polymer after synthesis of Pd NPs via colloidal method. This was done for colloidal catalysts prepared with $polymer_{mono}$/Pd ratio of 9.3 and 1.2, adding same type of polymer to achieve a $polymer_{mono}$/Pd ratio of 37.2, before introducing H_2/He gas into the reactor.

Any G-L mass transfer limitation was experimentally ruled out by varying catalyst amount as shown in Figure. A3.5 in the Appendix.

3. Results

3.1. TEM

Figure. 3.1 shows a typical TEM image and size distribution for Pd-PVP colloid with $polymer_{mono}$/Pd mole ratio of 9.3; similar results were obtained for all catalysts and the results are presented in Figure. A3.1 in the Appendix. These results are summarized in Figure. 3.1(b), showing that the Pd particle size increase with decreasing the amount of polymer, which is in good agreement with previous studies [7, 25]. The polymers act as a protecting agent during colloid synthesis, avoiding uncontrolled nanoparticles growth and preventing aggregation [26, 27]. The particle sizes obtained with PVP are systematically larger as compared to PVA at constant $polymer_{mono}$/Pd mole ratio in this study. In general, relatively small particle size (2 – 4 nm) of Pd NPs were achieved in this study using $NaBH_4$ as reducing agent, as compared to

literature reporting typically Pd particle sizes in the range of 5 to13 nm by using a weaker reducing agent like ethanol or methanol [25], indicating the importance of reduction rate on Pd particle size [7]. The HRTEM image in Figure. 3.2 illustrates that the Pd-polymer colloids as synthesized appear sphere-like shaped and no specific other shapes were observed.

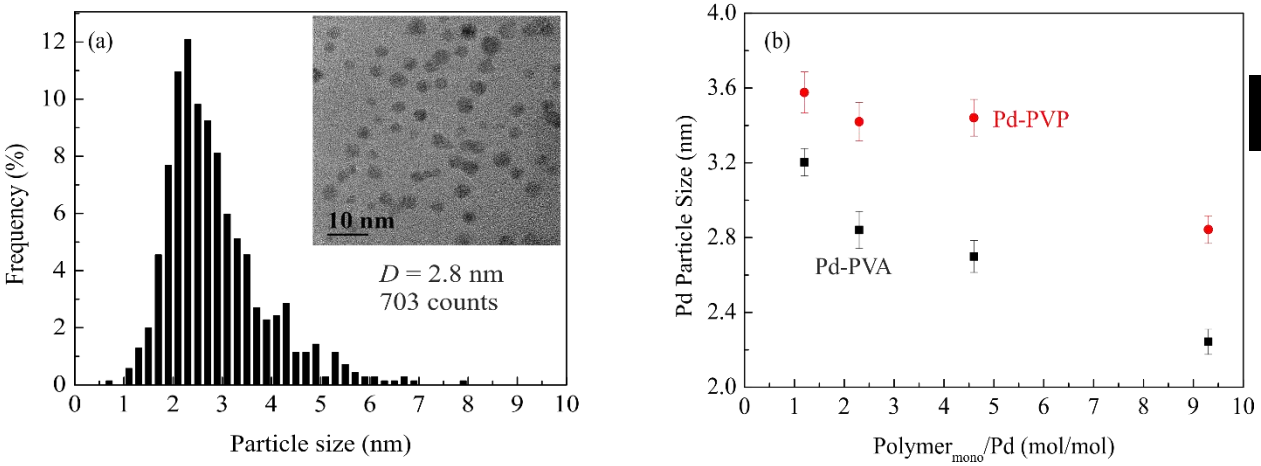

Figure. 3.1. Pd particle size observed by TEM: (a) TEM image and particle size distribution for Pd-PVP colloid with polymer$_{mono}$/Pd = 9.3 (mol/mol); (b) Mean diameters of the Pd colloids prepared using different capping agents and polymer$_{mono}$/Pd mole ratio. The error bars represent error margin of 95% confidential intervals.

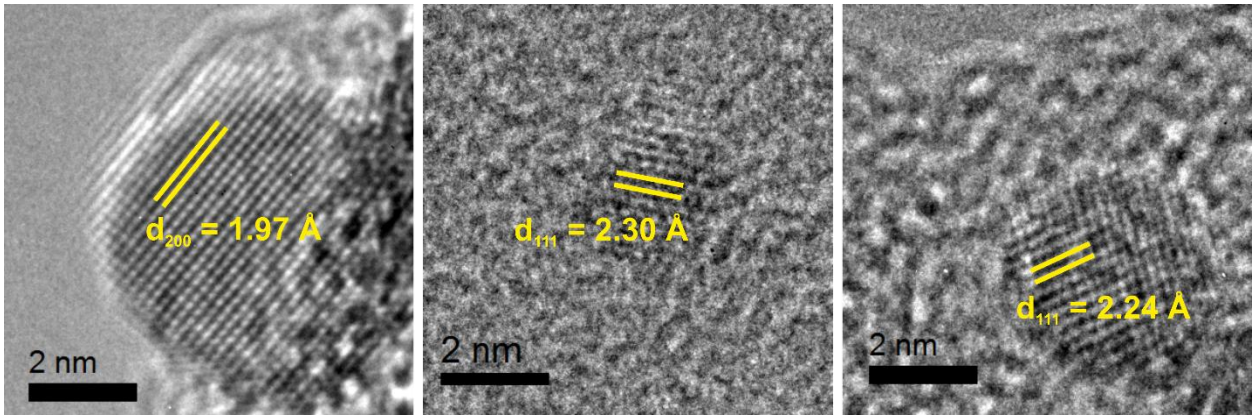

Figure. 3.2. HRTEM images of Pd-PVA colloid (polymer$_{mono}$/Pd = 9.3, mol/mol). The Pd NPs are deposited on a Cu grid covered with graphene modified lacey carbon.

3.2. Zeta potential

The influence of the $polymer_{mono}$/Pd mole ratio on the zeta potential of Pd-polymer colloid is depicted in Figure. 3.3. Both Pd-PVA and Pd-PVP colloids were negatively charged at pH = 8.5, and PVA resulted in lower zeta potential values as compared to PVP. Both Pd-PVA and Pd-PVP revealed decreasing negative charge with increasing amount of polymer and this trend was also observed when additional polymer was added after Pd nanoparticle synthesis. Apparently, polymer is able to partly neutralize the negative charge on Pd nanoparticles after its formation.

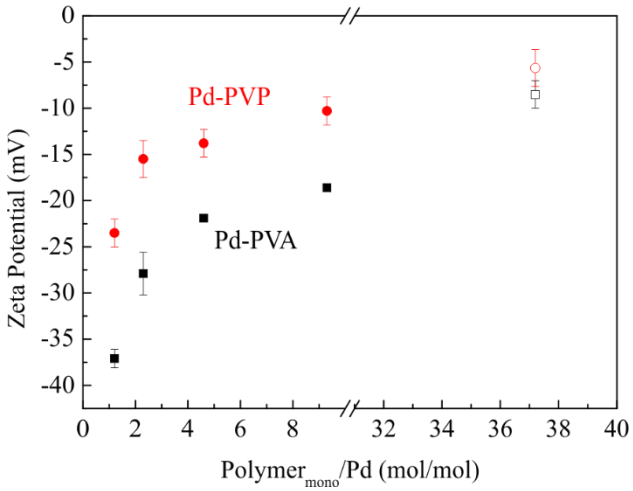

Figure. 3.3. Zeta potential of Pd colloid with different $polymer_{mono}$/Pd mole ratio in reaction slurry at pH = 8.5 ± 0.1 at 25°C. The solid symbols (■ and ●) represent as-prepared Pd-polymer colloid, while the open symbols (□ and ○) represent colloids added with additional polymer to as-prepared colloid with $polymer_{mono}$/Pd mole ratio of 1.2.

3.3. ATR-IR of CO chemisorption

Figure. 3.4 shows ATR-IR spectra of irreversibly chemisorbed CO on thin layers of Pd-PVA and Pd-PVP colloid on a ZnSe wafer, collected in Ar flow after CO adsorption. Two distinct peaks are assigned to linearly chemisorbed CO on Pd surface atoms (CO_L) at higher wavenumber (1960 – 2100 cm^{-1}), and CO chemisorbed on bridged or hollow Pd sites (CO_{B+H}) at lower wavenumber (1950 – 1750 cm^{-1}), respectively. These peak assignments are in agreement with previously reported results for Pd-PVA and Pd-PVP colloids [28-30].

However, the wavenumbers of these peaks presented here were lower than what is generally reported for supported Pd catalysts on e.g. Al_2O_3 or SiO_2 at room temperature [31-33]. This observation hints to a significant effect of the polymer on chemisorbed CO molecules.

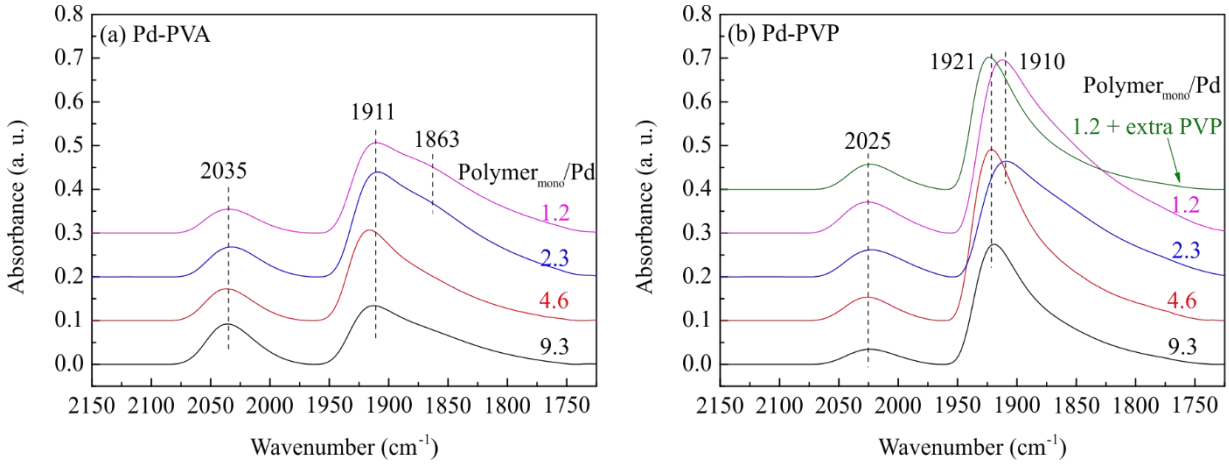

Figure. 3.4. ATR-IR spectra of irreversibly chemisorbed CO on Pd in Ar at 21 ± 1°C: (a) Pd-PVA, (b) Pd-PVP. Note the intensity of the peaks is only qualitatively comparable between samples because the Pd amount was not identical.

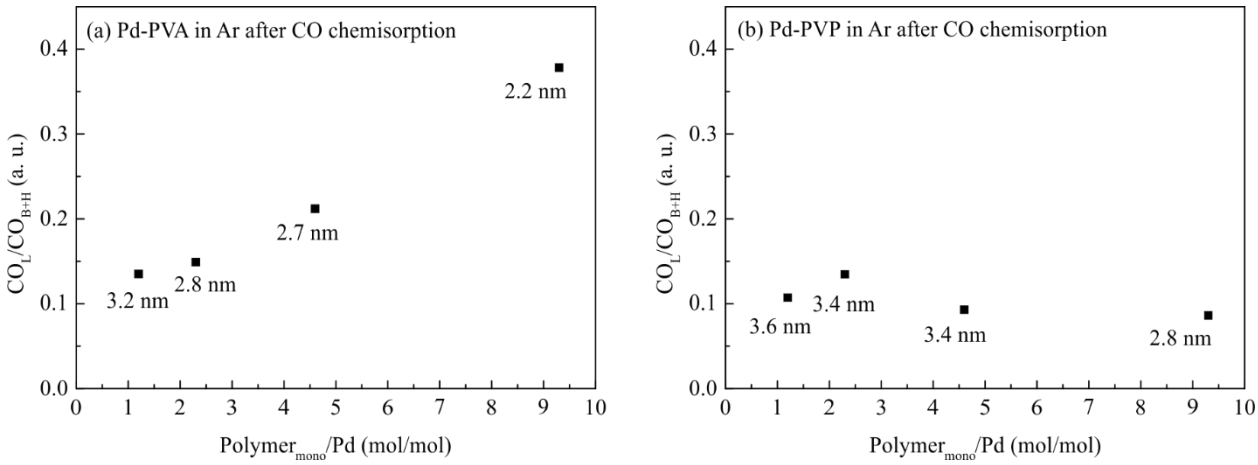

Figure. 3.5. The ratio of integrated area of peaks of CO_L and CO_{B+H} in ATR-IR spectra of irreversibly chemisorbed CO on Pd in Ar at 21 ± 1°C (as shown in Fig. 4) as function of the mole ratio of polymer monomer and Pd.

The position of the CO_L peak was not influenced by the polymer amount. In contrast, the position of the CO_{B+H} peak was red shifted with decreasing $polymer_{mono}$/Pd ratio for Pd-PVP colloid as shown in Figure. 3.4(b). Remarkably, extra PVP added to the Pd-PVP colloid with $polymer_{mono}$/Pd of 1.2, after colloid synthesis, caused a blue shift of the CO_{B+H} peak to the same position observed for the colloid prepared with higher $polymer_{mono}$/Pd ratios. Note that position of the CO_{B+H} peak did not vary at all with the PVA $polymer_{mono}$/Pd ratio in Figure. 3.4(a).

The ratios of integrated peak area of irreversibly adsorbed CO_L and CO_{B+H} are compared in Figure. 3.5. The CO_L/CO_{B+H} ratio increased with decreasing Pd particle size with Pd-PVA colloid (Figure. 3.5a), agreeing well with extensively reported similar trends for supported Pd nanoparticles in the range of 2 – 4 nm in diameter, which is rationalised based on a higher fraction of low coordinated Pd atoms in the surface of smaller particles, favourable for linearly adsorbed CO [34-37]. In contrast, no significant change in the CO_L/CO_{B+H} ratio was observed with Pd-PVP (Figure. 3.5b), indicating a significant effect of PVP on chemisorbed CO with the bonding configuration.

3.4. CO chemisorption in aqueous phase

As shown in Figure. 3.6, the amount of CO chemisorbed on the Pd NPs tends to first decrease and then increased with increasing of $polymer_{mono}$/Pd ratio for both Pd-PVA and Pd-PVP colloid. The decrease is unexpected, whereas the increase is probably due to the concurrent decrease of Pd particles size and increase of dispersion. Importantly, addition of extra PVA or PVP to colloid with the largest particles (3.2 and 3.6 nm respectively) caused the amount of chemisorbed CO to decrease, indicating enhanced blocking by both polymers.

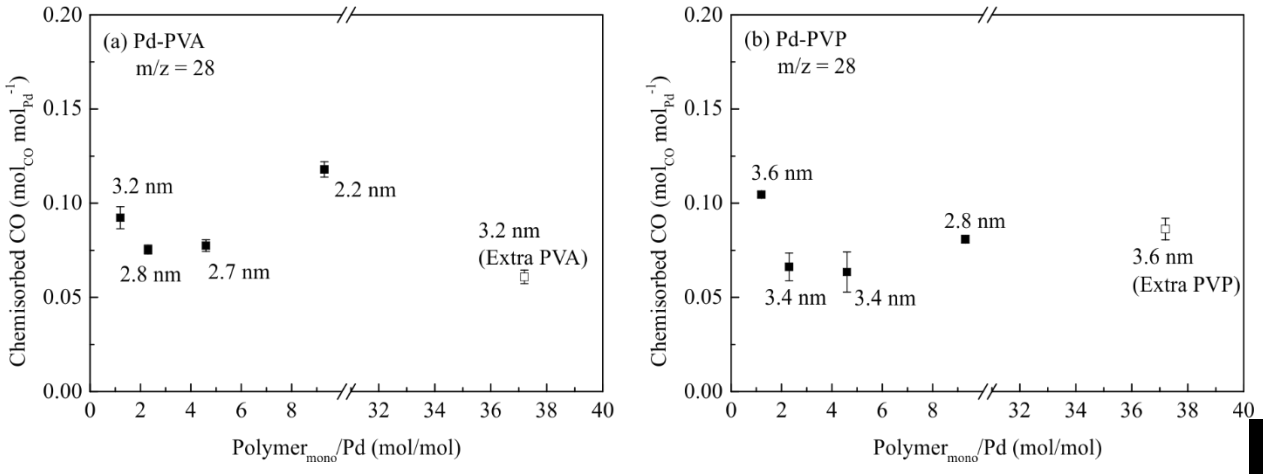

Figure. 3.6. Amount of chemisorbed CO on Pd colloid in aqueous phase (pH = 8.5 ± 0.5, T = 21 ± 1°C) determined by MS with m/z ratio = 28: (a) Pd-PVA colloid, (b) Pd-PVP colloid. The open squares are results for colloid with additional polymer. Error bars represent error margin of 95% confidential interval.

3.5. Nitrite hydrogenation

Figure. 3.7(a) and (b) show how the initial reaction rates were influenced by the polymer$_{mono}$/Pd mole ratio, changing as well the Pd particle sizes. The shape of both curves is rather similar to the shape in Figure. 3.6, observing a minimum at intermediate polymer$_{mono}$/Pd ratios. The activity of the largest PVA stabilized Pd NPs (3.2 nm) was found to decrease on adding additional PVA after colloid synthesis, whereas no change observed for smallest Pd NPs (2.2 nm) with additional PVA. Remarkably, the same experiment with both the largest and smallest PVP stabilized Pd NPs (3.6 nm and 2.8 nm, repectively) did not cause a significant change in initial activity.

The selectivity to ammonium using different Pd colloids is compared in Figure. 3.8; other products ending up in the gas-phase, comprising mainly N_2 and possibly some N_2O, are not analysed [38, 39]. As shown in Figure. 3.8(a) and 8(b), ammonium selectivity increased with nitrite conversion level, thus selectivity to ammonium should be compared at the same nitrite conversion level. Therefore, Figure. 8(c) and (d) present the selectivity to ammonium for all samples at 50% nitrite conversion. The selectivity to ammonium tends to decrease with increasing amount of polymer and decreasing Pd particle size. This effect is clearly significant for Pd-PVA and much less so for Pd-PVP. Generally, Pd-PVP results in lower selectivity to

ammonium as compared to Pd-PVA. Remarkably, ammonium selectivity unchanged when adding extra PVA to the Pd-PVA colloid with both the largest and the smallest particle size (3.2 nm and 2.2 nm, respectively, Figure. 8(a)), whereas ammonium selectivity was found to decrease when adding extra PVP with only the largest Pd NPs (Figure. 3.8(b)).

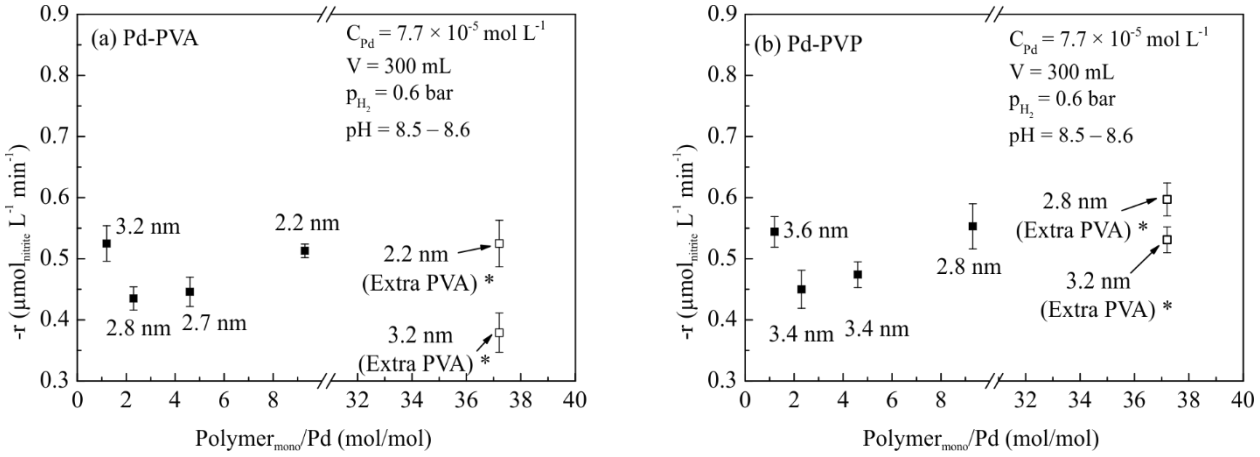

Figure. 3.7. Initial reaction rates of nitrite hydrogenation using (a) Pd-PVA and (b) Pd-PVP colloids with different polymer$_{mono}$/Pd mole ratios in nitrite hydrogenation in aqueous phase at 21 ± 1ºC. The pH was controlled at 8.5 ± 0.1 by phosphoric buffer. Please note the total amount of Pd was identical for all reactions. (* Extra polymer added, after formation of Pd colloid originally prepared with polymer$_{mono}$/Pd = 9.3 and 1.2.)

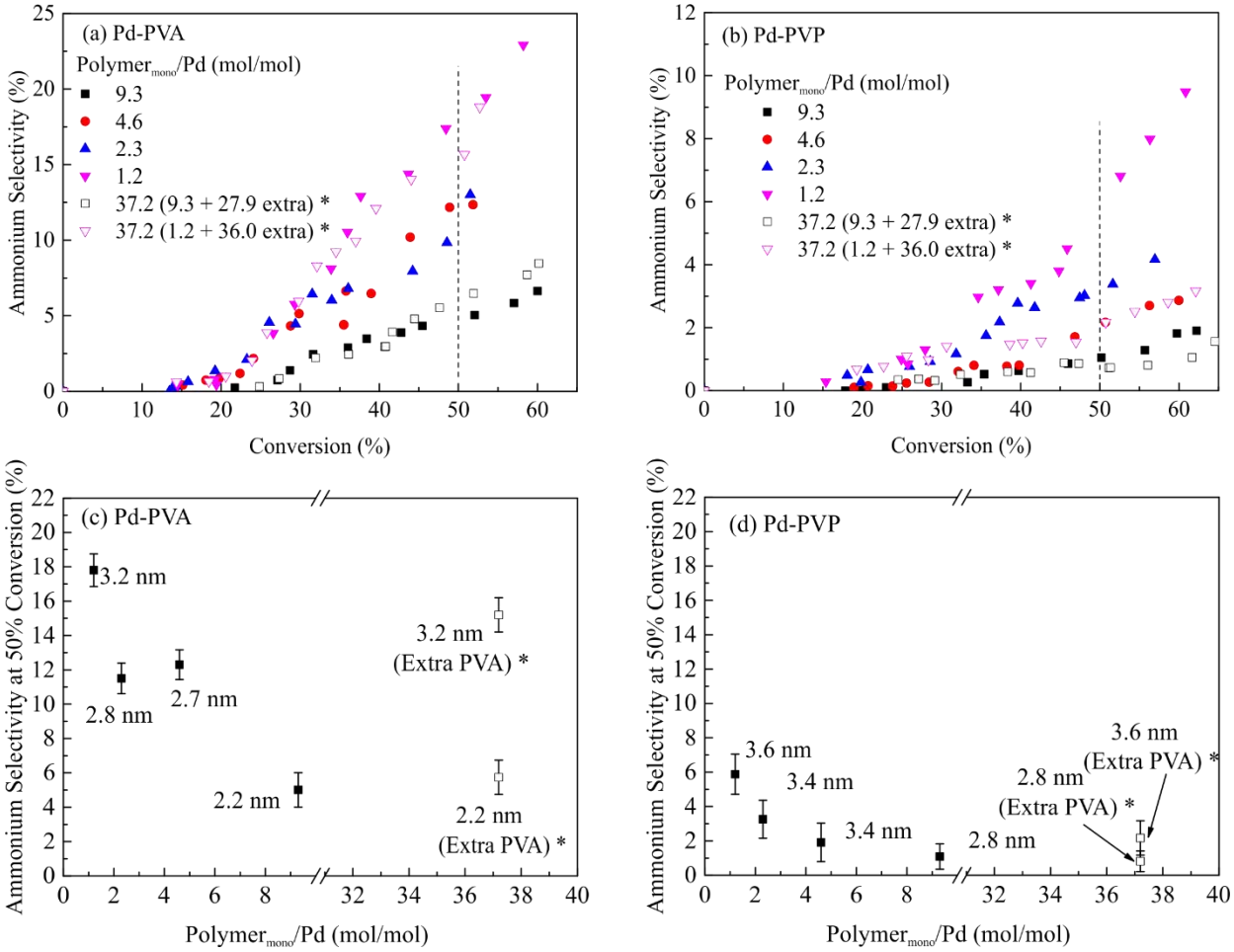

Figure. 3.8. Selectivity to ammonium as function of nitrite conversion for (a) Pd-PVA and (b) Pd-PVP colloids; ammonium selectivity at 50% conversion as function of the polymer$_{mono}$/Pd ratio for (c) Pd-PVA and (d) Pd-PVP colloids. Please note the reaction conditions are identical with the ones in Fig. 7. (* Extra polymer added, after formation of Pd colloid originally prepared with polymer$_{mono}$/Pd = 9.3 and 1.2.)

4. Discussion

4.1. Activity of Pd-PVA and Pd-PVP colloids for Nitrite Hydrogenation

Figure. 3.1 shows that the Pd particle size increased when decreasing the amount of polymer used in colloid preparation. As Pd particle sizes were increased from 2.2 nm to 2.8 nm and from 2.8 nm to 3.4 nm for Pd-PVA and Pd-PVP, respectively, the number of active sites accessible for CO (Figure. 3.6) as well as the observed initial reaction rates decreased (Figure. 3.7). These observations are very similar to what is generally observed for nitrite hydrogenation

with Pd catalysts with clean metal surface: both metal surface area and overall activity increase with decreasing particle size [38, 40]. Surprisingly, the number of active sites as well as observed activity increased when the Pd particle size was further increased, by decreasing the amount of stabilizer, to 3.2 nm for Pd-PVA and 3.6 nm for Pd-PVP colloid, as shown in Figure. 3.6 and 3.7. When extra polymer was added, after colloid preparation, the number of active sites decreased for Pd-PVA and to lesser extent also for Pd-PVP.

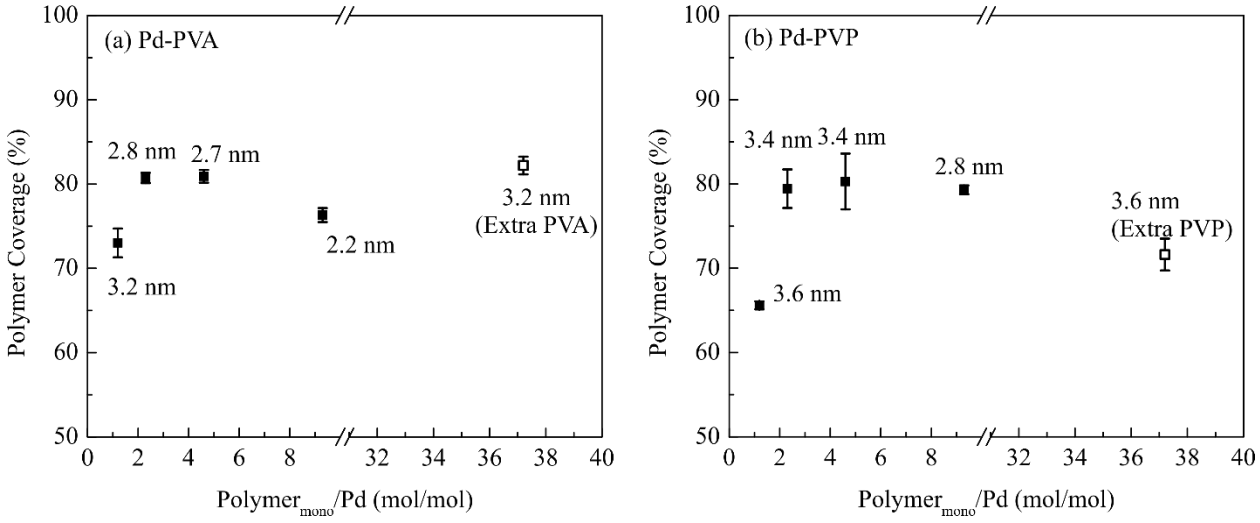

Figure. 3.9. Polymer coverage as function of polymer amount: (a) Pd-PVA; (b) Pd-PVP. Hollow squares represent sample with extra polymer after Pd nanoparticle formation. The polymer coverage was estimated by subtracting number of surface Pd atoms estimated based on TEM and number of Pd available for chemisorbed CO in aqueous phase. The error bars represent 95% confidential intervals.

These observations indicate that the polymer blocks part of active sites, in agreement with many previous studies [10, 11, 41]. The coverage of the Pd surface by polymer can now be estimated based on the CO-chemisorption data, in aqueous phase, and the TEM observations (Figure. 3.1), resulting in Figure. 3.9. It is assumed that the Pd particles are spheres with an average size as determined with TEM. The CO-Pd stoichiometry is assumed to be one, which obviously may induce a systematic error. In any case, it seems that the coverage of the Pd surface with polymer was significantly high for all colloids, while relatively low coverage existed with the colloid prepared with the lowest amount of polymer resulting in relatively large particle sizes (3.2 nm for Pd-PVA and 3.6 nm for Pd-PVP colloid).

The CO chemisorption data in aqueous phase also allow estimation of the turn-over-frequency (TOF) based on the initial reaction rates reported in Figure. 3.7. Figure. 3.10(a) shows a constant TOF for Pd-PVA colloid, independent of particle size and polymer concentration, except for the catalyst with the smallest particle size (2.2 nm). The constant TOF agrees well with the claim in literature that nitrite hydrogenation is structure independent, based on studies with supported Pd catalyst with Pd particle size ranging from 1.5 to 20 nm [38, 40]. It is not clear at this point why very small particles stabilized with PVA seem to deviate.

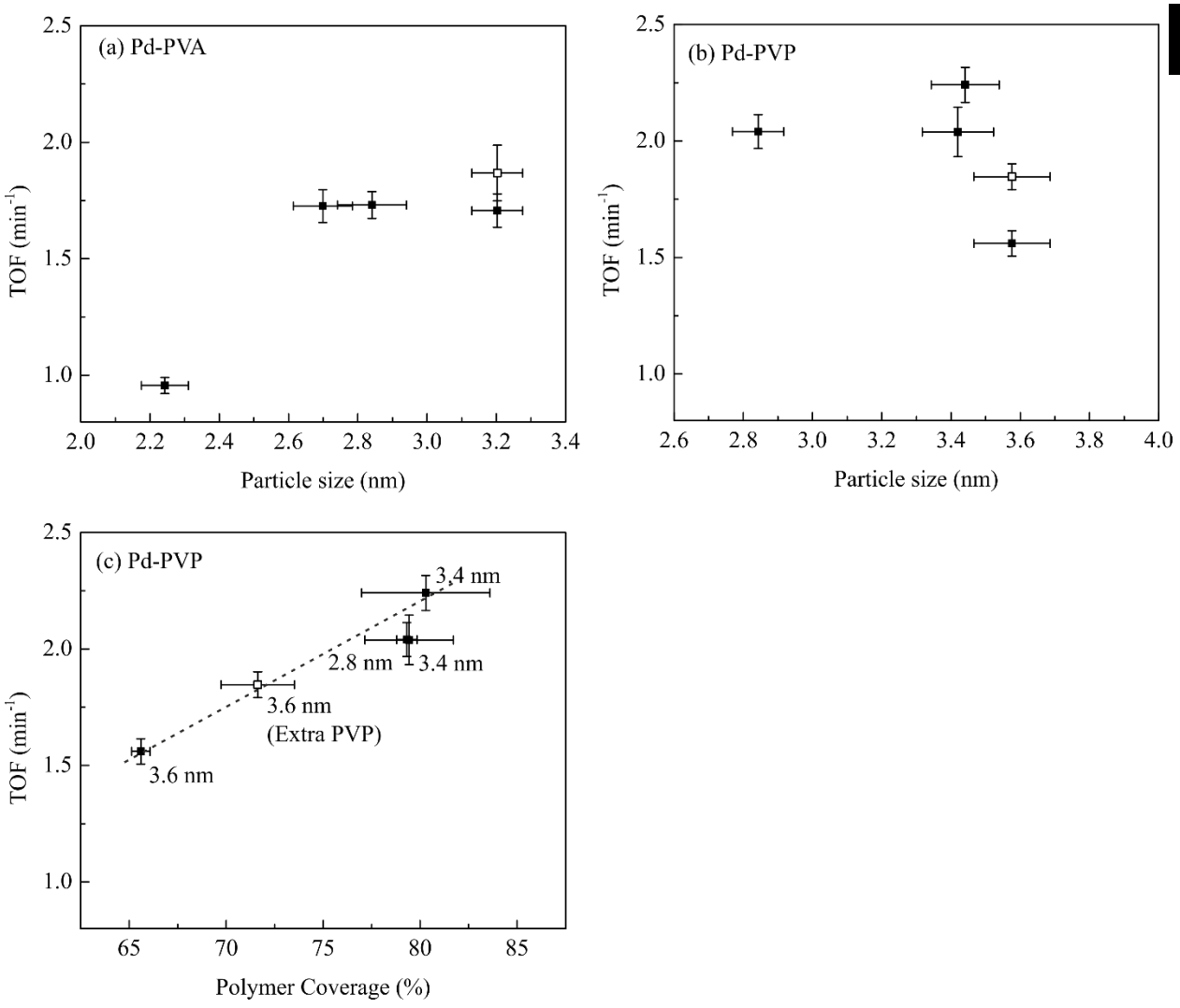

Figure. 3.10. Initial activity per active site: TOF as function of particle sizes of (a) Pd-PVA and (b) Pd-PVP colloid; TOF as function of polymer coverage of Pd-PVP colloid. TOF was calculated based on number of active sites determined by CO chemisorption in aqueous phase. The error bars represent 95% confidential intervals.

Figure. 3.10(b) shows that no correlation is found between particle size and TOF in the case of Pd-PVP. Instead, Figure. 3.10(c) shows that the TOF increases with the PVP coverage. In other words, the activity of the accessible sites increases when fewer sites are accessible.

In summary, the catalytic activity of Pd-PVA and Pd-PVP colloid for nitrite hydrogenation is determined by Pd particle size as well as polymer coverage on the Pd surface. In the case of PVA, Pd surface sites are simply blocked and the remaining sites reveal constant activity. In contrast, PVP induces two competing effects: first, blocking of sites decreases the overall activity and second, the activity of the remaining sites increases with PVA coverage.

4.2. Selectivity to ammonium of Pd-PVA and Pd-PVP colloids for nitrite hydrogenation

As shown in Figure. 3.8(c), ammonium selectivity at 50% nitrite conversion decreased with decreasing Pd-PVA particle size, remaining constant when extra PVA was added, clearly indicating that Pd particle size rather than polymer concentration determines the selectivity of Pd-PVA colloid. Thus selectivity to ammonium of Pd-PVA colloid is only dependent on Pd particle size and large particles are more favourable for ammonium formation than small particles.

This observation agrees with Mendez et al., reporting higher ammonium selectivity with large Pd NPs (10 nm) than with small Pd NPs (2 nm) supported on γ-Al_2O_3 in a batch experiment [42]. They suggested the small size of Pd NPs restricts formation of β-hydride suppressing nitrite deep hydrogenation to ammonium. This could also be the case in this study; however, it cannot be ruled out that particle size influences also the relative concentration of adsorbed species, as it has been reported that the ratio of adsorbed nitrogen-containing species (i.e. adsorbed nitrite as well as other reaction surface intermediates) and adsorbed hydrogen influences the ration of rate of formation of N_2 and NH_4^+ [39, 43, 44].

On the other hand, the opposite effect of Pd particle size on ammonium selectivity has been reported by Yoshinaga et al.; ammonium selectivity decreased with increasing Pd particle size on Pd/activated carbon in a trickle-bed experiment [45]. Also Shuai et al. also reported the same trend with Pd NPs supported on carbon nanofibers in a batch experiment [38]. In both cases, the authors suggested that low coordination sites are responsible for deep hydrogenation to ammonium.

The confusion in the above observations can probably be explained as follows. First, both Mendez et al. and Yoshinaga et al. compared the ammonium selectivity at very different conversion levels. Figure. 3.8 clearly demonstrates that selectivity is strongly influenced by the conversion level, which is caused by the fact that the concentrations of nitrite, hydrogen and protons vary in time in a batch experiment, and along the reactor axis in a fixed bed reactor [39, 46]. Second, G-L mass transfer limitation was not excluded by both Mendez et al. and Yoshinaga et al., inducing further variation of the local concentrations of nitrite, hydrogen and protons, at the active sites. Therefore concentration gradients will influence the selectivity. On the other hand, internal mass transfer limitation is also likely to influence the performance of supported catalysts in case of large diffusion distances and in case of narrow pores. This might be especially relevant when depositing Pd NPs in the internal nano-pore in carbon nanofibers as reported by Shuai et al. [38].

Interestingly, Shuai et al. recently reported that the influence of particle size of Pd-PVP on the TOF depends on the nitrite concentration [47]. In other words, the structure-performance relationship depends on the nitrite concentration. The nitrite concentration in this study is right in between the concentration considered in Ref. [47]. Unfortunately, it is not known whether the relationship between particle size and selectivity depends on the nitrite concentration, and possibly this causes the discrepancy between our observation and the results of Shuai et al. in [38].

The selectivity to ammonium for Pd-PVP colloid was lower as compared to Pd-PVA colloid in general, as shown in Figure. 3.8, and adding extra PVP after colloid formation reduced the formation of ammonium while no influence was observed when adding extra PVA. The effect of PVP on suppressing ammonium formation is in good agreement with observation reported by Hähnlein et al. [48]. In short, PVP not only influences the overall reaction rate per active site as discussed above, but also influences selectivity.

4.3. General discussion

The fact that PVA does not influence the TOF of the accessible sites, as well as the observation that additional PVA does not influence the selectivity, is in agreement with ATR-IR results. Figure. 3.4(a) shows that the positions of the bands assigned to CO_L and CO_{B+H} do not shift when varying the polymer amount. Furthermore, CO_L/CO_{B+H} peak area ratios

decreased with increasing Pd particle size as shown in Figure. 3.5(a), similar to what is reported for supported Pd catalyst with clean Pd surface [34-37]. These observations indicate that PVA has no influence on adsorbed CO; therefore, it is reasonable to assume the same is true for adsorbed nitrite and other surface intermediates during nitrite hydrogenation.

In contrast, PVP is found to influence both the TOF as well as the selectivity to ammonium as discussed above. Three possible explanations can be proposed. First, a direct interaction of PVP with adsorbed species might take place, thus influencing the reactivity of these adsorbed species. Second, PVP might interact preferentially with specific surface sites, influencing or even inhibiting their catalytic activity [47]. Third, interaction of PVP with the Pd surface may influence the electronic structure of Pd surface atoms [49]. Such an electronic effect has been reported for PVP stabilized Au nanoclusters, smaller than 1.5 nm, resulting in high activity for aerobic oxidation of alcohol [22]. However, it remains unclear if this effect is also relevant for relatively large Pd NPs in this study (2 – 4 nm).

In any case, ATR-IR studies in Figure. 3.4 (b) show that PVP influences chemisorbed CO, as the position of the CO_{B+H} band shifted to a lower wavenumber when decreasing the $polymer_{mono}$/Pd ratio. Addition of extra PVP after colloid synthesis causes the band to shift back to a higher wavenumber, confirming the shift is induced by the polymer rather than the size of the Pd particle. Apparently, PVP interacts with adsorbed CO, influencing the C-O bond strength, via one of the mechanisms proposed above. This is further supported by the observation that the CO_L/CO_{B+H} peak area ratio remains constant when varying the Pd particle size for Pd-PVP as shown in Figure. 3.5(b), in contrast to what is observed for clean Pd particles in classical supported Pd catalysts as well as Pd-PVA, as discussed above. It is plausible that a similar interaction with adsorbed reactants like nitrite or NO is responsible for the effect of PVP on the TOF and selectivity. Further investigation would be needed to distinguish whether PVP interacts directly with adsorbed reactants or indirectly via influencing the Pd surface.

Finally, the charge of Pd-PVP colloids in reaction media is less negative as compared to that of Pd-PVA colloids with same $polymer_{mono}$/Pd mole ratio, as shown in Figure. 3.3. This may also contribute to the suppression of the reaction to ammonium by increasing the local N/H ratio at the active sites because of less repulsing of the nitrite anion, favouring nitrite adsorption.

5. Conclusions

Pd colloids with different particle sizes have been prepared by varying the amount of PVA or PVP used as stabilizer. CO chemisorption in aqueous phase reveals that the coverage of Pd surface with polymer is in the order of 80%. It is concluded that PVA does not significantly influence adsorbed species on the Pd surface, and therefore the catalytic properties of the remaining sites are not influenced in terms of TOF and selectivity. In contrast, PVP influences adsorbed species significantly, resulting in increasing TOF and decreasing ammonium formation with increasing the coverage of Pd surface with PVP.

Appendix

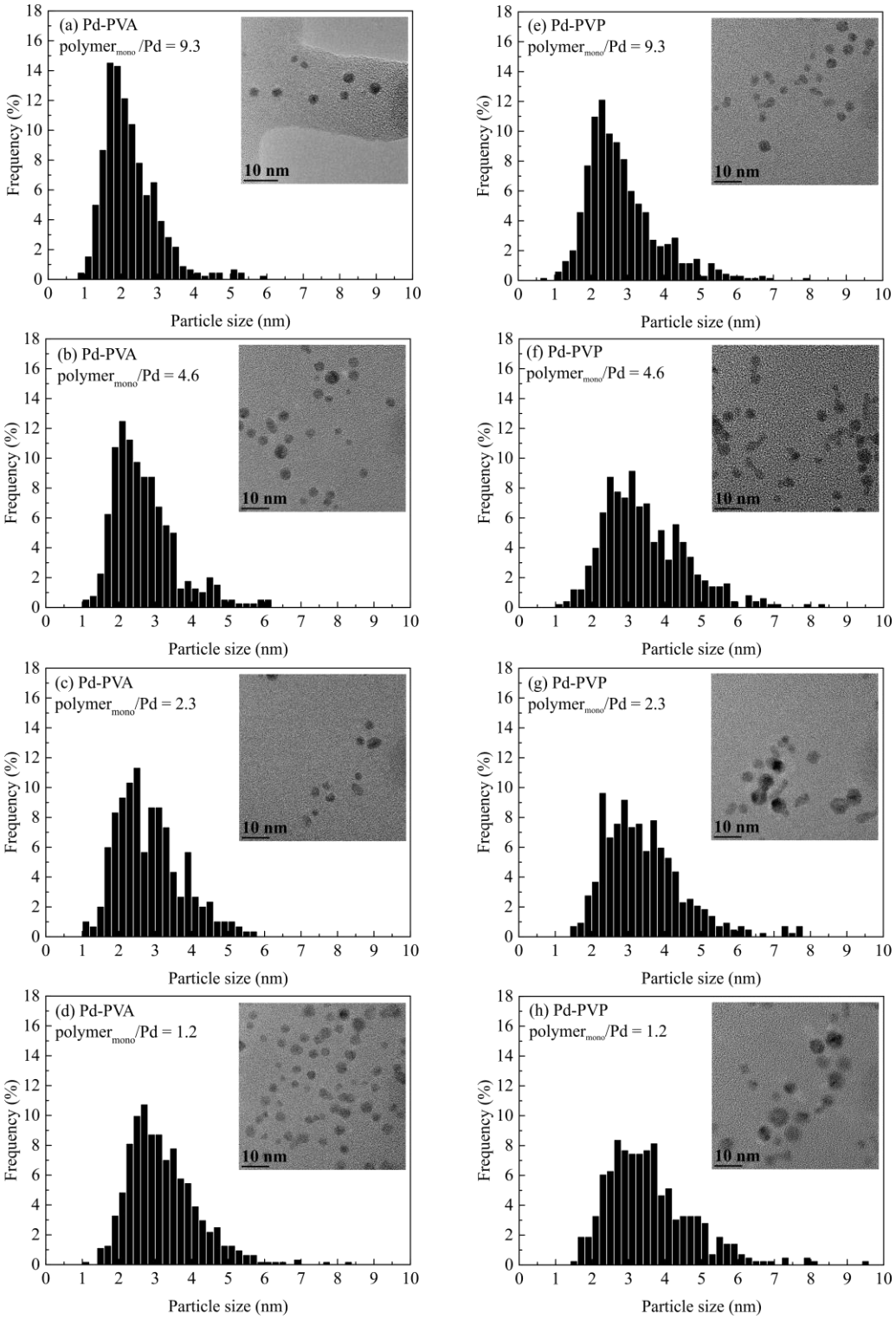

Figure. A3.1. TEM and particle size distribution of (a) – (d) Pd-PVA and (f) – (h) Pd-PVP colloids.

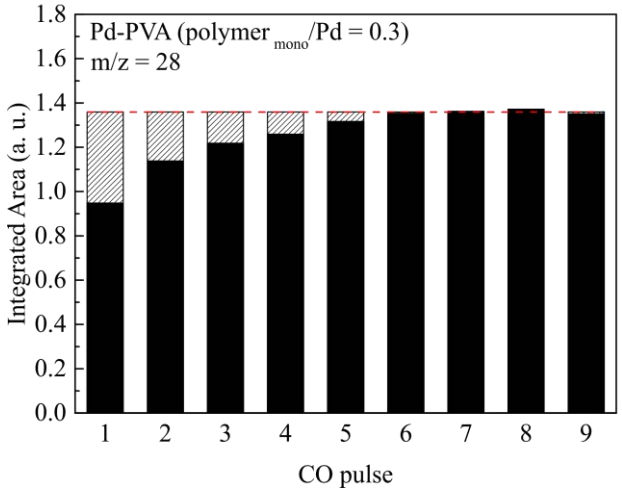

Figure. A3.2. Integrated area of CO pulse peaks of typical mass spectrometry during CO chemisorption of Pd colloid in aqueous phase. The shallow bars represent amount of CO adsorbed by Pd colloid.

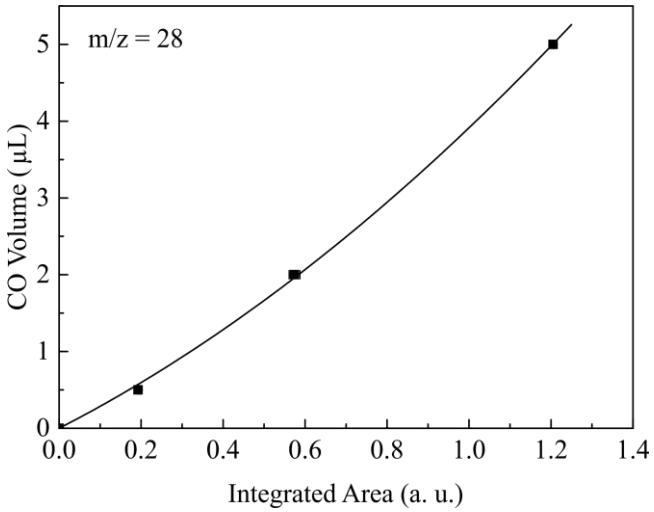

Figure. A4.3. Volume of CO for one pulse as function of integrated area. The curve represents 2nd order fitting of the data points. (R^2 = 0.9997)

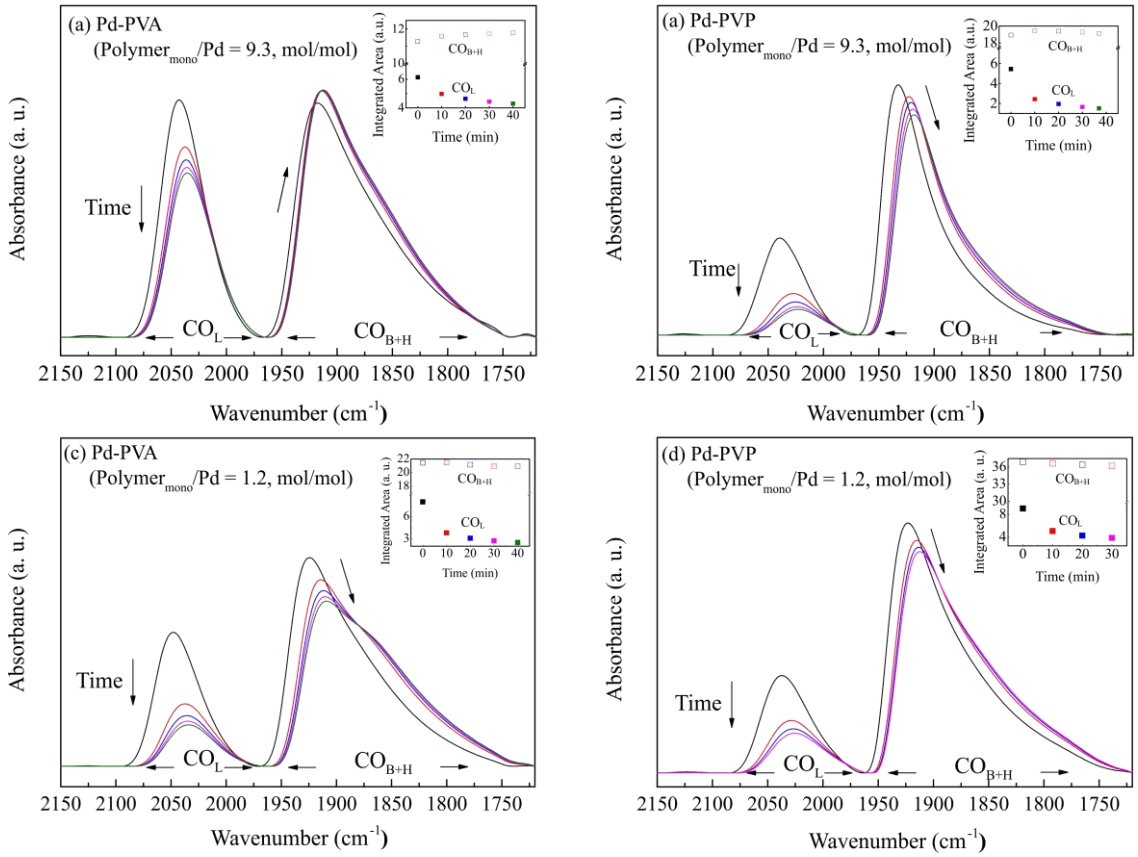

Figure.A3.4. ATR-IR spectra of chemisorbed CO on Pd-PVA and Pd-PVP colloid in Ar atmosphere after CO chemisorption. The peaks showed red shift in Ar flow, while the integrated area of CO_L peaks decreased with slightly increasing of the integrated area of CO_{B+H} peaks with both Pd-PVA and Pd-PVP colloid. The CO_{B+H} peaks also became boarder in Ar flow as compared with in CO flow. These phenomena indicated (1) partly desorption of CO weakly adsorbed on Pd surface and (2) relocation of CO_L into bridge or hollow sites with decreasing CO partial pressure.

Nitrite Hydrogenation at pH = ~5.5

Typically, 70 mL colloidal suspension was added into 230 mL H_2O. The mixed suspension was then stirred vigorously in H_2/He/CO_2 atmosphere (H_2/He/CO_2 = 6/3/1 by volume flow rate, total flow rate = 100 mL min^{-1}, total pressure = 1 bar) for at least 1 h. CO_2 was used as a buffer according to reaction shown in Eq. A3.1 and A3.2 to supply the protons consumed by nitrite hydrogenation.

$$CO_2 + H_2O \longrightarrow HCO_3^- + H^+ \quad \text{(Eq. A3.1)}$$

$$HCO_3^- + H_2O \longrightarrow CO_3^{2-} + H^+ \quad \text{(Eq. A3.2)}$$

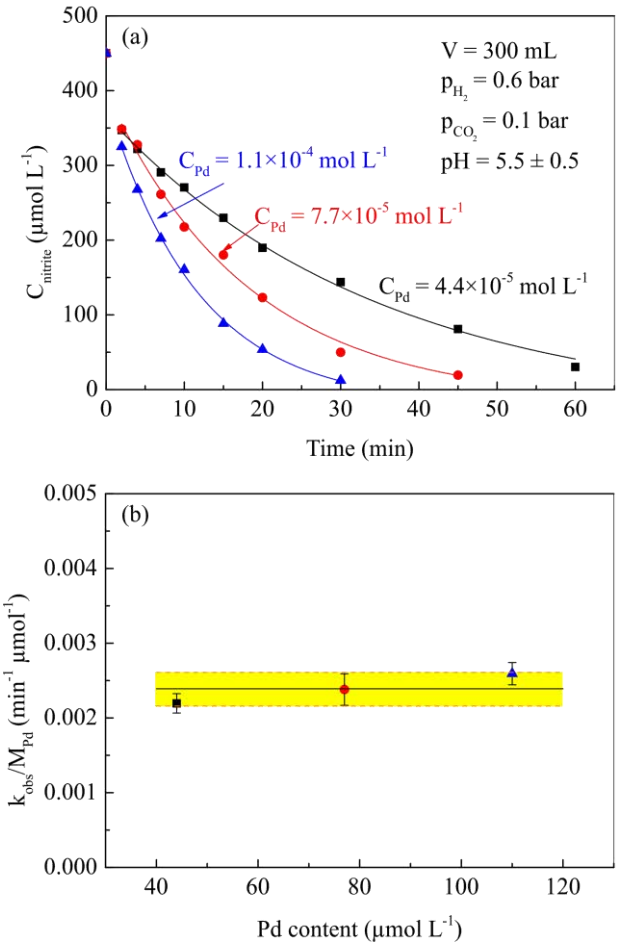

Figure. A3.5. (a) Nitrite concentration vs. time using Pd-PVA colloid ($polymer_{mono}$/Pd = 2.4, mol/mol) as catalyst of different Pd concentration. CO_2 was used as a buffer (pH = 5.5). The lines are first-order fits to the data points. **(b)** The observed reaction rate constant calculated with first-order fits normalized by total amount of Pd. The yellow area with orange margins represents the 95% confidence interval of the average.

Then 3 mL 4.4 mmol L^{-1} $NaNO_2$ solution was introduced, from when the reaction started. 1 mL of reaction suspension was taken by syringe for each time of sampling, and then the sample was filtered through 40 mg of α-Al_2O_3 inside of the syringe and a syringe filter (PTFE, 0.2 µm) to remove Pd nanoparticles. The sample was then injected into IC to determine the content of nitrite and ammonium.

The absence of significant G-L mass transfer limitation was ensured experimentally by varying the catalyst concentration. The nitrite hydrogenation activity per mole total Pd remained constant at pH = 5.5±0.5 using CO_2 as buffer, as shown in Figure. A3.5. All experiments in this study performed using a phosphate buffer (pH = 8.5 – 8.6) showed much lower reaction rates as compared with using CO_2 buffer. This is caused by the lower proton concentration at the higher pH, agreeing with the observations in many previous studies [4, 39, 50, 51]. In any case, G-L mass transfer limitation can be excluded in this study.

References

[1] K. An, G.A. Somorjai, Chemcatchem, 4 (2012) 1512-1524.

[2] N. Semagina, L. Kiwi-Minsker, Catal. Rev., 51 (2009) 147-217.

[3] A.V. Gaikwad, in: Faculty of Science, University of Amsterdam, Amsterdam, 2009.

[4] K.A. Guy, H. Xu, J.C. Yang, C.J. Werth, J.R. Shapley, J. Phys. Chem. C, 113 (2009) 8177-8185.

[5] S.C. Kim, S.C. Jung, Y.K. Park, H.G. Ahn, S.G. Seo, J. Nanosci. Nanotechnol., 13 (2013) 1961-1965.

[6] H. Hirai, N. Yakura, Polym Advan Technol, 12 (2001) 724-733.

[7] T. Teranishi, M. Miyake, Chem. Mater., 10 (1998) 594-600.

[8] L.S. Ott, R.G. Finke, Coord. Chem. Rev., 251 (2007) 1075-1100.

[9] H. Thiele, H.S. von Levern, Journal of Colloid Science, 20 (1965) 679-694.

[10] A. Villa, D. Wang, D.S. Su, L. Prati, Chemcatchem, 1 (2009) 510-514.

[11] A. Quintanilla, V.C.L. Butselaar-Orthlieb, C. Kwakernaak, W.G. Sloof, M.T. Kreutzer, F. Kapteijn, J. Catal., 271 (2010) 104-114.

[12] Y. Li, M.A. El-Sayed, J. Phys. Chem. B, 105 (2001) 8938-8943.

[13] C. Aliaga, J.Y. Park, Y. Yamada, H.S. Lee, C.-K. Tsung, P. Yang, G.A. Somorjai, J. Phys. Chem. C, 113 (2009) 6150-6155.

[14] E.G. Rodrigues, S.A.C. Carabineiro, J.J. Delgado, X. Chen, M.F.R. Pereira, J.J.M. Órfão, J. Catal., 285 (2012) 83-91.

[15] Y. Borodko, H.S. Lee, S.H. Joo, Y. Zhang, G. Somorjai, J. Phys. Chem. C, 114 (2009) 1117-1126.

[16] R.M. Rioux, H. Song, J.D. Hoefelmeyer, P. Yang, G.A. Somorjai, J. Phys. Chem. B, 109 (2004) 2192-2202.

[17] P. Dash, T. Bond, C. Fowler, W. Hou, N. Coombs, R.W.J. Scott, J. Phys. Chem. C, 113 (2009) 12719-12730.

[18] L.R. Baker, G. Kennedy, J. Krier, M. Spronsen, R. Onorato, G. Somorjai, Catal. Lett., 142 (2012) 1286-1294.

[19] Y. Zhao, L. Jia, J.A. Medrano, J.R.H. Ross, L. Lefferts, ACS Catal., 3 (2013) 2341-2352.

[20] J.A. Lopez-Sanchez, N. Dimitratos, C. Hammond, G.L. Brett, L. Kesavan, S. White, P. Miedziak, R. Tiruvalam, R.L. Jenkins, A.F. Carley, D. Knight, C.J. Kiely, G.J. Hutchings, Nat. Chem., 3 (2011) 551-556.

[21] C. Evangelisti, N. Panziera, A. D'Alessio, L. Bertinetti, M. Botavina, G. Vitulli, J. Catal., 272 (2010) 246-252.

[22] H. Tsunoyama, N. Ichikuni, H. Sakurai, T. Tsukuda, J Am Chem Soc, 131 (2009) 7086-7093.

[23] N.K. Chaki, H. Tsunoyama, Y. Negishi, H. Sakurai, T. Tsukuda, J. Phys. Chem. C, 111 (2007) 4885-4888.

[24] S.D. Ebbesen, B.L. Mojet, L. Lefferts, Langmuir, 22 (2005) 1079-1085.

[25] J.A. Baeza, L. Calvo, M.A. Gilarranz, A.F. Mohedano, J.A. Casas, J.J. Rodriguez, J. Catal., 293 (2012) 85-93.

[26] M. Králik, A. Biffis, J. Mol. Catal. A: Chem., 177 (2001) 113-138.

[27] T. Ashida, K. Miura, T. Nomoto, S. Yagi, H. Sumida, G. Kutluk, K. Soda, H. Namatame, M. Taniguchi, Surf. Sci., 601 (2007) 3898-3901.

[28] J.S. Bradley, E.W. Hill, S. Behal, C. Klein, A. Duteil, B. Chaudret, Chem. Mater., 4 (1992) 1234-1239.

[29] M.R. Mucalo, R.P. Cooney, Chem. Mater., 3 (1991) 1081-1087.

[30] M. Crespo-Quesada, J.-M. Andanson, A. Yarulin, B. Lim, Y. Xia, L. Kiwi-Minsker, Langmuir, 27 (2011) 7909-7916.

[31] S.D. Ebbesen, B.L. Mojet, L. Lefferts, Phys Chem Chem Phys, 11 (2009) 641-649.

[32] W. Juszczyk, Z. Karpiński, I. Ratajczykowa, Z. Stanasiuk, J. Zieliński, L.L. Sheu, W.M.H. Sachtler, J. Catal., 120 (1989) 68-77.

[33] L.F. Liotta, G.A. Martin, G. Deganello, J. Catal., 164 (1996) 322-333.

[34] G. Cabilla, A. Bonivardi, M. Baltanás, Catal. Lett., 55 (1998) 147-156.

[35] R.F. Hicks, A.T. Bell, J. Catal., 90 (1984) 205-220.

[36] L.R. Becerra, C.P. Slichter, J.H. Sinfelt, J. Phys. Chem., 97 (1993) 10-12.

[37] R. Van Hardeveld, F. Hartog, Surf. Sci., 15 (1969) 189-230.

[38] D. Shuai, J.K. Choe, J.R. Shapley, C.J. Werth, Environ Sci Technol, 46 (2012) 2847-2855.

[39] A. Pintar, G. Berčič, J. Levec, Aiche J., 44 (1998) 2280-2292.

[40] J.K. Chinthaginjala, J.H. Bitter, L. Lefferts, Appl. Catal., A, 383 (2010) 24-32.

[41] X. Wang, P. Sonström, D. Arndt, J. Stöver, V. Zielasek, H. Borchert, K. Thiel, K. Al-Shamery, M. Bäumer, J. Catal., 278 (2011) 143-152.

[42] C.M. Mendez, H. Olivero, D.E. Damiani, M.A. Volpe, Appl. Catal., B, 84 (2008) 156-161.

[43] S.D. Ebbesen, B.L. Mojet, L. Lefferts, J. Catal., 256 (2008) 15-23.

[44] J.K. Chinthaginjala, L. Lefferts, Appl. Catal., B, 101 (2010) 144-149.

[45] Y. Yoshinaga, T. Akita, I. Mikami, T. Okuhara, J. Catal., 207 (2002) 37-45.
[46] A. Pintar, J. Batista, J Hazard Mater, 149 (2007) 387-398.
[47] D. Shuai, D.C. McCalman, J.K. Choe, J.R. Shapley, W.F. Schneider, C.J. Werth, ACS Catal., 3 (2013) 453-463.
[48] M. Hähnlein, U. Prüße, J. Daum, V. Morawsky, M. Kröger, M. Schröder, M. Schnabel, K.D. Vorlop, Stud. Surf. Sci. Catal., 118 (1998) 99-107.
[49] Y. Borodko, S.M. Humphrey, T.D. Tilley, H. Frei, G.A. Somorjai, J. Phys. Chem. C, 111 (2007) 6288-6295.
[50] I. Mikami, Y. Sakamoto, Y. Yoshinaga, T. Okuhara, Appl. Catal., B, 44 (2003) 79-86.
[51] M. Al Bahri, L. Calvo, M.A. Gilarranz, J.J. Rodriguez, F. Epron, Appl. Catal., B, 138–139 (2013) 141-148.

Chapter 4

Adsorption Species on Pd Catalyst for Nitrite Hydrogenation at Close-to-complete Conversion

1. Introduction

Nitrate and nitrite are harmful compounds often found in underground drinking water supplies, especially in agricultural areas using nitrogen-rich fertilizers. In later 1980s, the pioneering work by Vorlop and co-works have shown that nitrate can be reduced to nitrogen (N_2) using bimetallic hydrogenation catalysts, with nitrite as intermediate and ammonium as by-product, via reaction shown in Eq. 1.1 to 1.3 [1-3]. Since then, various metals have been tested in order to optimize activity and selectivity to N_2, minimizing the formation of ammonium [4-8].

$$NO_3^- + H_2 \xrightarrow{\text{Pd-Cu}} NO_2^- + H_2O \qquad \text{(Eq. 1.1)}$$

$$2NO_2^- + 3H_2 + 2H^+ \xrightarrow{\text{Pd}} N_2 + 4H_2O \qquad \text{(Eq. 1.2)}$$

$$NO_2^- + 3H_2 + 2H^+ \xrightarrow{\text{Pd}} NH_4^+ + 2H_2O \qquad \text{(Eq. 1.3)}$$

Palladium has been found as most active catalyst for nitrite hydrogenation (Eq. 1.2 and 1.3), with the best selectivity to N_2 [2, 7]. Studies have been extensively performed in order to understand the mechanism of the reaction with Pd catalysts. It has been well accepted that the turn-over-frequency (TOF) of the reaction is independent of the Pd particle size [9-11]. Yoshinaga et al. first declaimed a relationship between the structure of Pd nanoparticles (NPs) and the selectivity, with supported Pd catalyst in fixed bed reaction [12]. Our previous work with unsupported Pd colloids showed that a large Pd particle size is favorable for the formation of ammonium in semi-batch reaction with continuous hydrogen flow [11]. However, there has hardly been any literature explaining the reason of the generally very high selectivity to N_2 (above 80%) with Pd catalyst.

In this chapter, nitrite hydrogenation was studied with Pd catalyst prepared via colloidal methods as well as impregnation method. The study will focus on the selectivity to ammonium at close-to-complete conversion level. It will show an independent ammonium formation beside of the major reaction converting nitrite to N_2, and the mechanism will be discussed.

2. Experimental

2.1. Chemicals

Sodium tetrachloropalladate (II) ($Na_2PdCl_4 \geq 99.995\%$), polyvinyl alcohol (PVA, average MW = 13000 – 23000, 87% – 89% hydrolyzed), and sodium borohydride ($NaBH_4$, ≥ 96% (gas-volumetric) were purchased from Sigma-Aldrich. Palladium acetylacetonate ($Pd(acac)_2 \geq 99\%$) was purchased from Alfa Aesar, and acetone (> 99%) and 2-propanol (> 99%) was purchased from Merck. γ-Al_2O_3 (S_{BET} = 205 m^2 g^{-1}) was supplied by BASF. Sodium nitrite (> 99%) was purchased from Merck. All the aqueous solutions were prepared using ultra purified water obtained on water purification system (Millipore, Synergy).

2.2. Pd-PVA colloid

The preparation of palladium nanoparticles via colloidal method has been described in Chapter 2, which can be summarized as follows. PVA was dissolved in water at 70°C with stirring for at least 2 hours. The solution (2 wt %) was then cooled down to room temperature. Aqueous solution of Na_2PdCl_4 (20 mL, containing 0.086 mmol Pd) and 1.76 mL of freshly prepared PVA solution were added to 240 mL water, obtaining a yellow-brown solution. After 3 min, $NaBH_4$ solution (1.72 mL, 0.172 mmol) was added under vigorous stirring. The brown Pd colloid solution was immediately formed. The final pH was typically 8 – 8.5.

2.3. Pd-PVA/Al_2O_3

γ-Al_2O_3 (38 – 42 μm) was calcined in air flow at 600°C for 4 h before adding 1.5 g γ-Al_2O_3 to 520 mL as-prepared Pd-PVA colloidal suspension ($C_{Pd} = 3.3 \times 10^{-4}$ mol L^{-1}) without any pH adjustment. After stirring with a mechanical 6-blade-stirrer (ϕ 44 mm, 1000 rpm) with the propeller positioned at the centre of liquid for 2 h, the catalyst was filtered and dried in a vacuum oven at 40°C.

2.4. Pd/Al_2O_3

Pd nanoparticles supported on the same calcined γ-Al_2O_3 was also prepared via wet impregnation method in order to compare with Pd-PVA/Al_2O_3. Typically, 0.95 g of γ-Al_2O_3

was added into 80 mL acetone solution containing 4.7×10^{-4} mol L^{-1} $Pd(acac)_2$. Then the suspension was stirred with a magnetic stirrer (500 rpm) for 3 h, followed by drying using a rota evaporator (IKA Labortechnick) under sub-atmospheric pressure at 80ºC. The resulting sample was calcined at 300ºC in air flow for 3 h, and subsequently reduced in H_2 at the same temperature for 3 h.

The prepared catalysts were stored in air. No further pre-treatment was performed before any experiments described in below.

2.5. Characterization

Pd particle size distribution was determined using TEM (Philips CM300ST-FEG) with a resolution of 1 nm. The AC supported catalysts were firstly ground into sub-micron fragments and dispersed in ethanol. Then the suspension was dropped on a copper grid covered with hollow carbon for taking TEM images. At least five of these ground fragments were randomly selected for determination of Pd particle sizes, and typically 300 Pd particles were measured. Note that information on the spatial distribution of nanoparticles through the support cannot be obtained as the samples were ground. The metal loading on the supports were analyzed by XRF. The total surface area of samples were calculated based on N_2 physisorption data, using the BET method with a typical error margin of 5%.

The zeta potential of the catalysts dispersed in aqueous phase was measured with a Zetasizer Nano ZS ZEN3600 instrument (Malvern Instruments) at 25ºC using a laser with wavelength of 633 nm. The pH was adjusted to 6 with HCl and NaOH solution.

CO chemisorption at room temperature was used to determine the metal surface area that is accessible in gas phase. Typically, the sample was pre-reduced at room temperature in hydrogen and then flushed in He at the same temperature. Then CO was introduced as pulses and the responses were recorded using a TCD detector. We assumed that the stoichiometric ratio of number of adsorbed CO molecules and number of accessible Pd surface atoms is 1 : 1. The Pd dispersion (*Pd disp.*) was defined as

$$Pd\ disp. = \frac{\text{number of Pd atoms in the surface of NPs}}{\text{number of Pd atoms in total}}$$

2.6. Nitrite and ammonium adsorption in aqueous phase

Adsorption isotherms for nitrite and ammonium were determined using a home-built apparatus containing a flat bottom flask (250 mL) with a magnetic stirrer at room temperature. Typically 50 mg catalyst was added to 100 mL H_2O and stirred, dispersing 10% CO_2/Ar (1 bar, 40 mL min^{-1}) in the suspension for at least 1 hour. Then 1 mL of concentrated sodium-nitrite or ammonium-chloride solution was injected into the suspension, repeatedly every 15 minutes. Adsorption equilibrium was achieved within 5 minutes and one sample of 1 mL was taken after each injection, using a syringe equipped with a filter (PTFE, 0.2 μm) to remove the catalysts. The samples were analyzed for nitrite or ammonium with ion chromatography (IC, DIONEX, ICS 1000). The amount of nitrite or ammonium adsorbed was calculated by subtracting the amount of free nitrite or ammonium, calculated based on the equilibrium concentration, from the total amount of nitrite or ammonium added.

2.7. ATR-IR of nitrite hydrogenation

A suspension containing 0.1 g Pd/Al_2O_3 dispersed in 25 mL 2-propanol was spray coated on a trapezoidal ZnSe crystal (52.5 mm × 20 mm × 2 mm, facet angle 45°, Anadis instruments BV), resulting in about 5 mg catalyst on the crystal, which was then mounted in a home-build *in-situ* Attenuated Total Reflection Infrared Spectroscopy (ATR-IR) cell which has been described in detail elsewhere [13]. The chamber above the ATR crystal in the cell was about 0.77 mL in volume. The cell was mounted in the sample compartment of an infrared spectrometer (Bruker Tensor 27) equipped with a MCT detector. All the measurements were done at room temperature (21 ± 1°C) with a resolution of 4 cm^{-1}. Nitrite hydrogenation on the catalyst was performed via a multi-step titration method:

(1) Typically the catalyst was first flushed with water saturated with hydrogen (flow rate = 1 mL min^{-1}, p_{H2} = 1 bar) for 4 h in order to remove adsorbed oxygen from Pd surface.

(2) Followed by flowing water saturated with argon for 30 minutes, in order to remove any physisorbed hydrogen on the catalyst as well as residual hydrogen in liquid phase.

(3) After that, nitrite solution (0.025 mol L^{-1}, argon saturated, 1 mL min^{-1}) flow was introduced into the cell during 30 min in order to saturate the catalyst with nitrite.

(4) Argon saturated water was then used again for 10 min to remove residual nitrite in solution as well as any physisorbed nitrite on the catalyst.

(5) Finally, water saturated with hydrogen was introduced, reacting with nitrogen-containing-species (N-species) adsorbed on the catalyst, until the IR signals from nitrogen containing species either adsorbed on the catalyst or present in the liquid became constant.

All the liquid flows were pumped by a peristaltic pump (Masterflex) downstream of the ATR-IR cell and then directed to a container.

After completion of the five steps described above, a circulation flow study was performed in order to mimic a semi-batch reaction at almost-complete-conversion level. The H_2/H_2O flow was stopped, while the flow downstream of the ATR-IR cell was directed back to the entrance of the ATR-IR cell, passing through a porous alumina tube (inner diameter 1.0 mm, outer diameter 1.8 mm, length 65 mm), coated with polydimethylsiloxane (PDMS) membrane. The function of the semi-permeable membrane tube is to introduce additional H_2 to the recirculating liquid, by allowing H_2 molecules to diffuse through the PDMS membrane from H_2 containing gas outside of the tube. The amount of liquid in the cell, the tubes and the pump is about 2.5 ml in total. The recirculation flow was maintained during 150 minutes, and ATR-IR spectra were taken using the same resolution and speed as described above.

2.8. Nitrite hydrogenation

The reaction was performed in a home-build semi-batch reactor including a glass tank reactor (ϕ 98 mm with four 5 mm baffles), equipped with a mechanical 6-blade-stirrer (ϕ 44 mm, 1000 rpm) with the propeller positioned at the centre of liquid. Typically, 50mg catalyst was dispersed in 300 mL H_2O. The mixed suspension was then stirred vigorously in $H_2/He/CO_2$ atmosphere ($H_2/He/CO_2$ = 6/3/1, total flow rate = 100 mL min^{-1}, total pressure = 1 bar) for at least 1 h. CO_2 was used as a buffer to control pH to 5.5±0.5.

The reaction was initiated by injecting 3 mL $NaNO_2$ solution (4.4 mmol L^{-1}). Samples of the reaction suspension of 1 mL were taken with syringes equipped with filters (PTFE, 0.2 μm) to remove the catalyst. Samples were taken every 5 minutes and then injected into the IC (DIONEX, ICS 1000) to determine the concentration of nitrite and ammonium.

3. Results

3.1. TEM

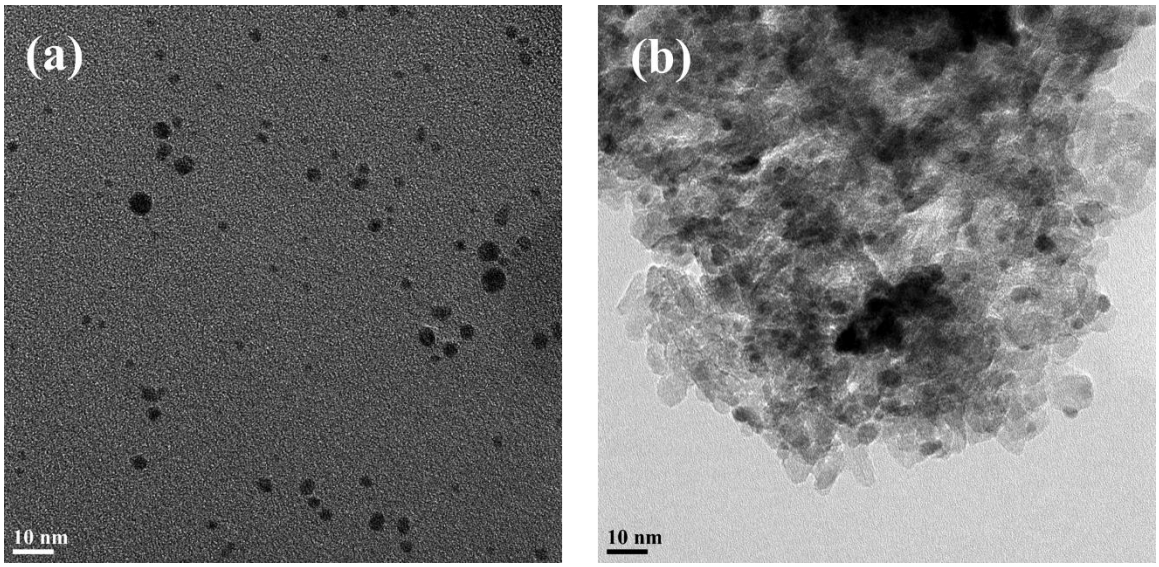

Figure 1. TEM images: (a) Pd-PVA colloid; (b) Pd-PVA/Al_2O_3

Figure 1 shows typical TEM images of unsupported Pd-PVA and Pd-PVA supported on Al_2O_3. Unsupported Pd-PVA showed sphere-like shaped particles with an average size of 2.2 nm (Table 1), whereas Pd NPs deposited on Al_2O_3 seem somewhat distorted, suggesting hemi-spherical shaped particles with an apparent particle size of 3.0 nm. The changes of Pd particle size and shape indicate that the PVA stabilized particles interact significantly with alumina.

Table 1 Physical properties of samples in this study

Sample	Pd loading (wt %)	$D_{Pd,\ TEM}$ (nm)	S_{BET} ($m^2\ g^{-1}$)	Pd disp. (%)	$\zeta_{pH=6}$ (mV)
Pd-PVA		2.2 ± 0.7		9 [a]	-34.5
Al_2O_3			205		26.5
Pd-PVA/Al_2O_3	0.4	3.0 ± 0.8		14.5	30.5
Pd/Al_2O_3	5.0	2.1 ± 0.4		16	

[a] According to CO chemisorption in aqueous phase. [11]

3.2. Zeta potential

As shown in Table 1, the zeta potential of unsupported Pd-PVA colloid was negative at pH 6, whereas the colloid supported on Al_2O_3 was positively charged at the same pH.

3.3. Adsorption

3.3.1. Nitrite adsorption

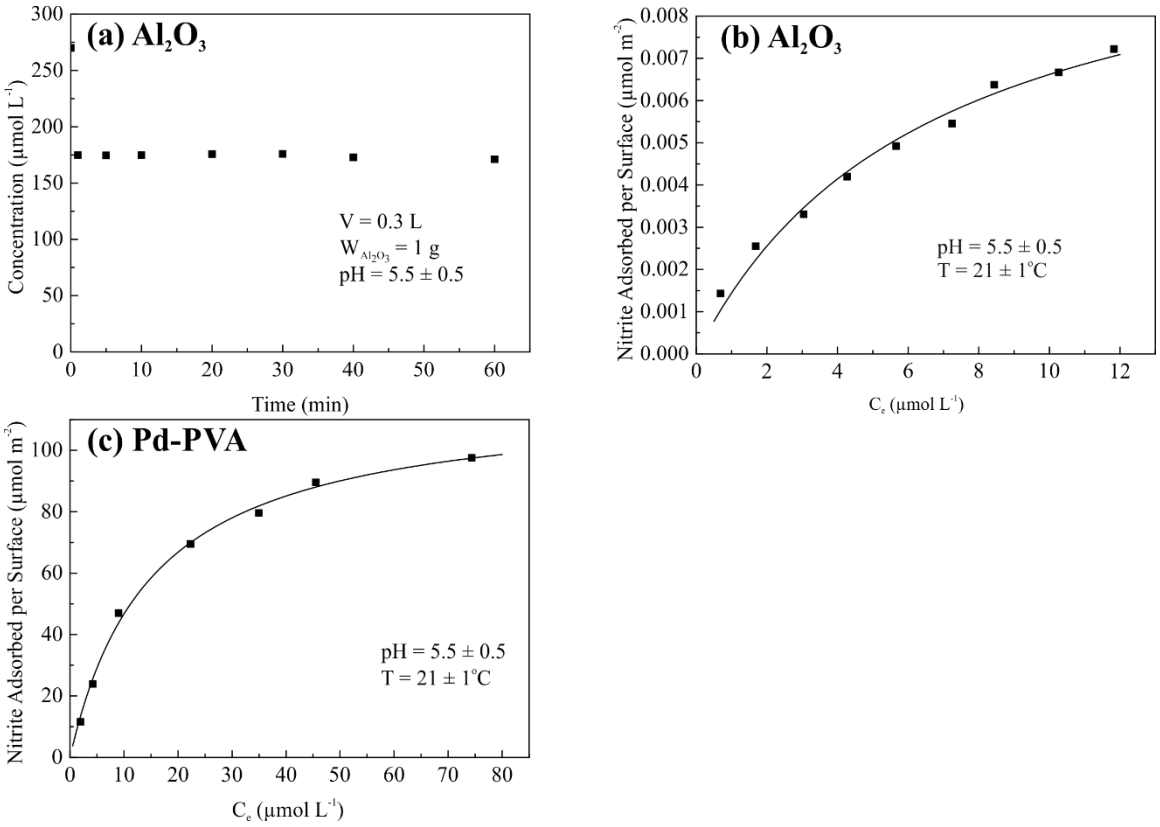

Figure 2. Adsorption of nitrite by Al_2O_3: (a) nitrite concentration with Al_2O_3 as function of time; nitrite adsorption isotherm with (b) Al_2O_3 and (c) Pd-PVA colloid. The lines represent Langmuir fitting of the data. The surface area of Pd colloid was determined by CO chemisorption in aqueous phase [11], and surface area of Al_2O_3 was determined by N_2 physisorption with BET method (Table 1).

Figure 2(a) shows that equilibrium of nitrite adsorption on Al_2O_3 was reached rapidly within 1 min; the initial concentration was 275 μmol L^{-1}, rapidly decreasing to the equilibrium concentration (175 μmol L^{-1}). Similar fast equilibrium was observed with Pd-PVA.

The coverage of alumina surface by NO_2^- ($\Gamma_{NO_2^-}$) can be estimated with the following equation

$$\Gamma_{NO_2^-} = \frac{M_{NO_2^-,\,surface}}{(S_{surface}/S_{NO_2^-})/(6\times10^{23})} \times 100\% \qquad \text{(Eq. 4.1)}$$

where $M_{NO_2^-,\,surface}$ is the amount of nitrite adsorbed on Al_2O_3 in moles, which can be estimated based on the data in Figure 2(b). $S_{surface}$ is the specific area as determined by N_2 physisorption with the BET method (Table 1). $S_{NO_2^-}$ is the area occupied by a NO_2^- ion, estimated at 4×10^{-20} m^2, assuming the size of NO_2^- ion is 0.2 nm. Figure 2(b) shows the amount of nitrite adsorbed per surface area is about 8×10^{-4} μmol m^{-2} at equilibrium concentration of nitrite close to the IC detect limitation (0.5 μmol L^{-1}), resulting in a surface-coverage of NO_2^- ions on alumina as low as 0.002%. The maximal coverage achieved in Figure 2(b) is still as low as 0.02%.

In contrast, nitrite adsorption on Pd-PVA (figure 2(c)) results in a much higher coverage, assuming that CO chemisorption in aqueous phase is a good measure for the number of Pd surface atoms available for interaction with nitrite [11]. For example, 8% of the Pd surface sites accessible, as described above, is covered with NO_2^- when in equilibrium with 0.5 μmol L^{-1}. The estimated coverage can be as high as 240% in equilibrium with nitrite concentration equal to 80 μmol L^{-1}. Note that the samples were used without pre-reduction with H_2, and we cannot rule that oxygen chemisorbed on the Pd surface reacts with nitrite. However, there was no NO_3^- was detected by IC in the solution in all experiments. Probably, the nitrite adsorption on PVA contributes significantly. In any case, the surface coverage of NO_2^- on Pd is clearly significant.

3.3.2. Ammonium adsorption

Figure 3(a) shows that ammonium adsorption on Al_2O_3 also equilibrated rapidly within a few minutes. Figure 3(b) shows the adsorption isotherm of ammonium on Al_2O_3. The result in terms of surface coverage is similar to the results with nitrite, revealing very weak interaction of alumina with both nitrite and ammonium.

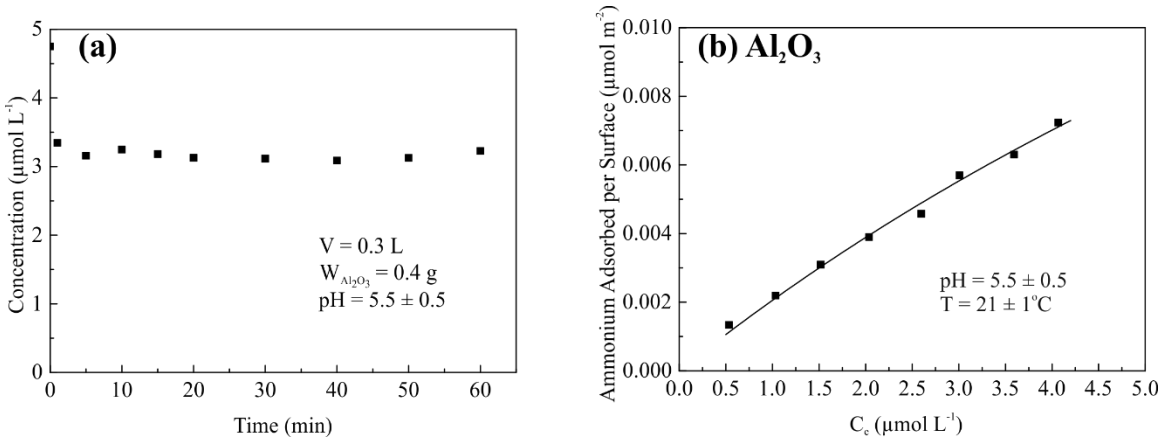

Figure 3. Adsorption of ammonium by Al_2O_3: (a) ammonium concentration as function of time; (b) Ammonium adsorption isotherm. The line represents Langmuir fitting of the data. Surface area of Al_2O_3 was determined by N_2 physisorption with BET method (Table 1).

3.4. ATR-IR

Figure 4(a) to (c) shows typical spectra of nitrogen-containing species adsorbed on Pd/Al_2O_3 catalyst during exposure of a hydrogen covered Pd catalyst to nitrite. The species identified by IR spectra including linear- and multi-bonded NO (NO (L) and NO (M)) on Pd at 1710 cm^{-1} and 1580 cm^{-1}, respectively, as well as a NO_xH_y intermediate at 1490 cm^{-1}. The peak at 1450 cm^{-1} is assigned to NH_4^+, produced exclusively initially. The peak at 1235 cm^{-1} represent free nitrite ions in aqueous phase. These assignments have been discussed in detail in previous work [14] and [15] and were recently partly revised [16].

Also, the changes in integrated areas of fitted peaks with time during adsorption of nitrite, as well as during flushing with inert and reducing of adsorbed species in H_2 containing water, as shown in Figure 4(d), has been discussed in detail previously [16]. In short, linearly and multi bonded NO, together with NO_xH_y were detected as stable N-containing species chemisorbed on the Pd surface by reactive adsorption of nitrite. NH_4^+ was formed initially when nitrite was introduced to the H_2 pre-treated Pd surface, decreasing rapidly because of exhaustion of adsorbed hydrogen as well as weak interaction of NH_4^+ with the catalyst [15]. Flushing with Ar/H_2O induced removal of nitrite in solution. Subsequent exposure to H_2/H_2O induces removal of NO (L) and NO (M) first, followed by consumption of NO_xH_y, accompanied by formation of ammonium. All this has been discussed in detail [16] and is

actually not essential for this study. However, the sequence is needed to generate a catalyst that mimics the situation at the end of a batch experiment, as will be discussed later.

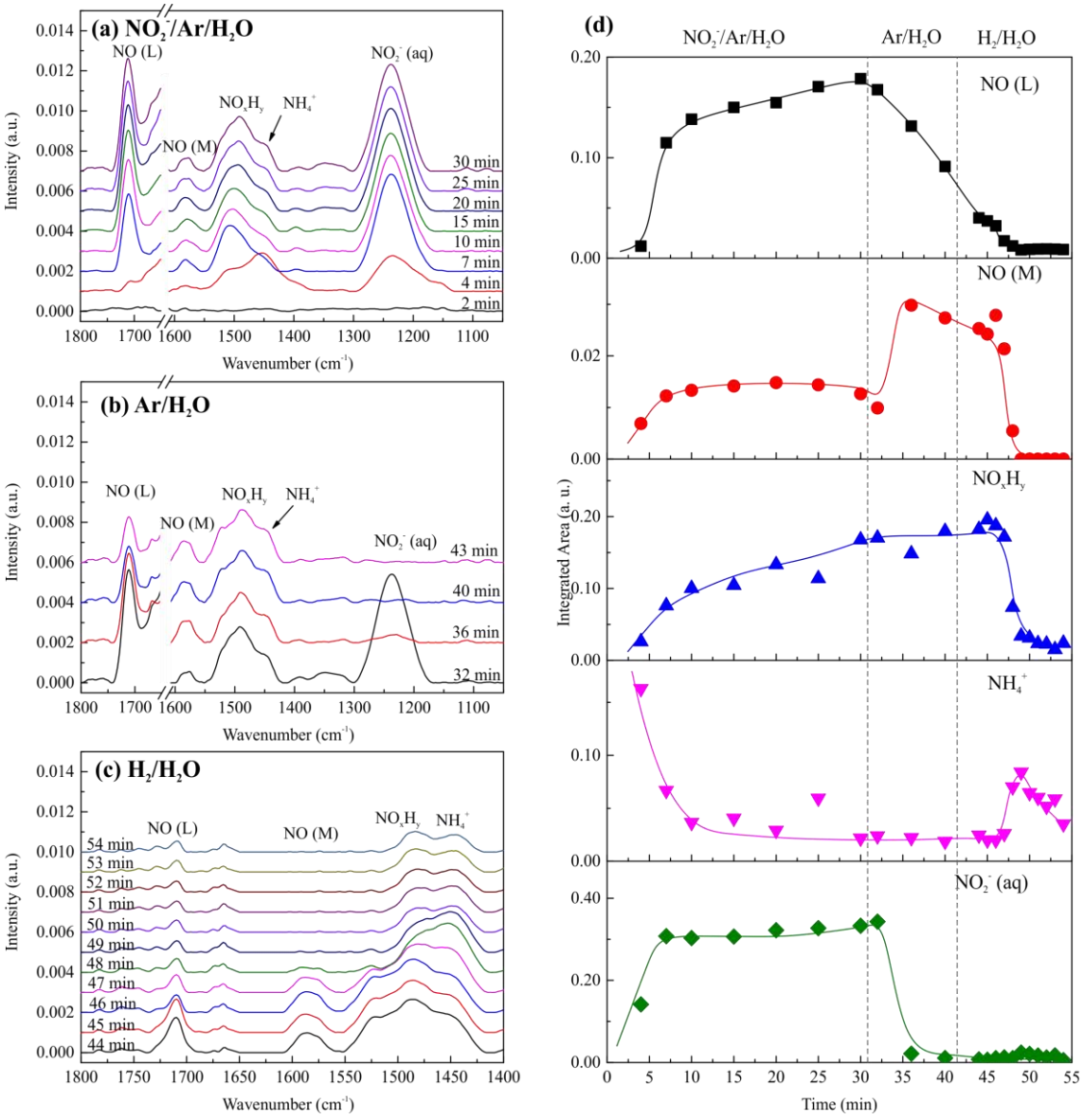

Figure 4. ATR-IR spectra of N-species on Pd/Al_2O_3 catalyst: spectra with N-species during (a) nitrite adsorption on H_2 pre-reduced Pd/Al_2O_3, followed by (b) flushed by Ar/H_2O, and then (c) titration with H_2/H_2O. (d) Summary of change of integrated peak areas during the three steps. The experiment was performed at T = 21 ± 1°C, pH = 7 for all solutions.

Figure 4(d) shows that the NO (L) and NO (M) species, as well as free NO_2^- in aqueous phase were completely removed after flushing with H_2 saturated H_2O for 10 min, while most

of NO_xH_y species was also consumed and the integrated area became stable. The decrease of NH_4^+ indicates a decrease of the formation rate. After 10 minutes flushing with H_2/H_2O, only NH_4^+ and NO_xH_y were detectable by ATR-IR. Then the flow was changed to recycling as described in experimental.

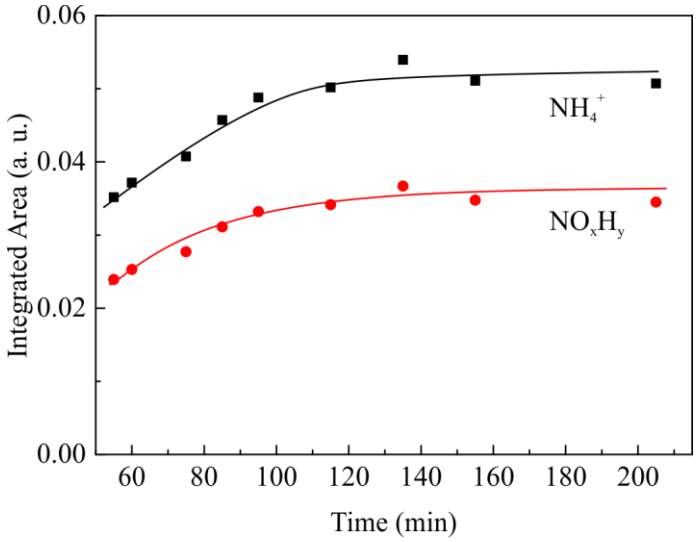

Figure 5. Integrated area of fitted peaks of NO_xH_y and NH_4^+ catalyst in ATR-IR spectra with Pd/Al_2O_3 during recirculation.

Figure 5 shows both the amount of adsorbed NO_xH_y and the amount of NH_4^+ increased during the circulation with hydrogen continuously supplied by H_2 diffusion via the semi-permeable membrane tube. The concentrations of both species reached maximum during recirculation for 3 h.

3.5. Nitrite hydrogenation

Figure 6 shows the concentration of nitrite and ammonium as function of time with unsupported Pd-PVA colloid and Pd-PVA supported on Al_2O_3. The concentration of Pd in the experiments was summarized in Table 2. As shown in Figure 6(a), nitrite concentration decreased from 435 μmol L^{-1} to 0.5 μmol L^{-1} within 1 h. In the same time, ammonium concentration increased to 1.4 μmol L^{-1} as can be seen in Figure 6(c) and Table 2. The change in the slope in the inset of Figure 6(c) also shows that the formation rate of ammonium

decreased significantly, from 0.043 μmol L^{-1} min^{-1} to 0.008 μmol L^{-1} min^{-1}, at the moment that nitrite is exhausted after about 65 minutes, when the concentration of nitrite decreased below the detect limit of the IC (~0.5 μmol L^{-1}). Ammonium formation continued during the following 40 h, despite the fact that nitrite is exhausted, reaching a final ammonium concentration of 7.4 μmol L^{-1}.

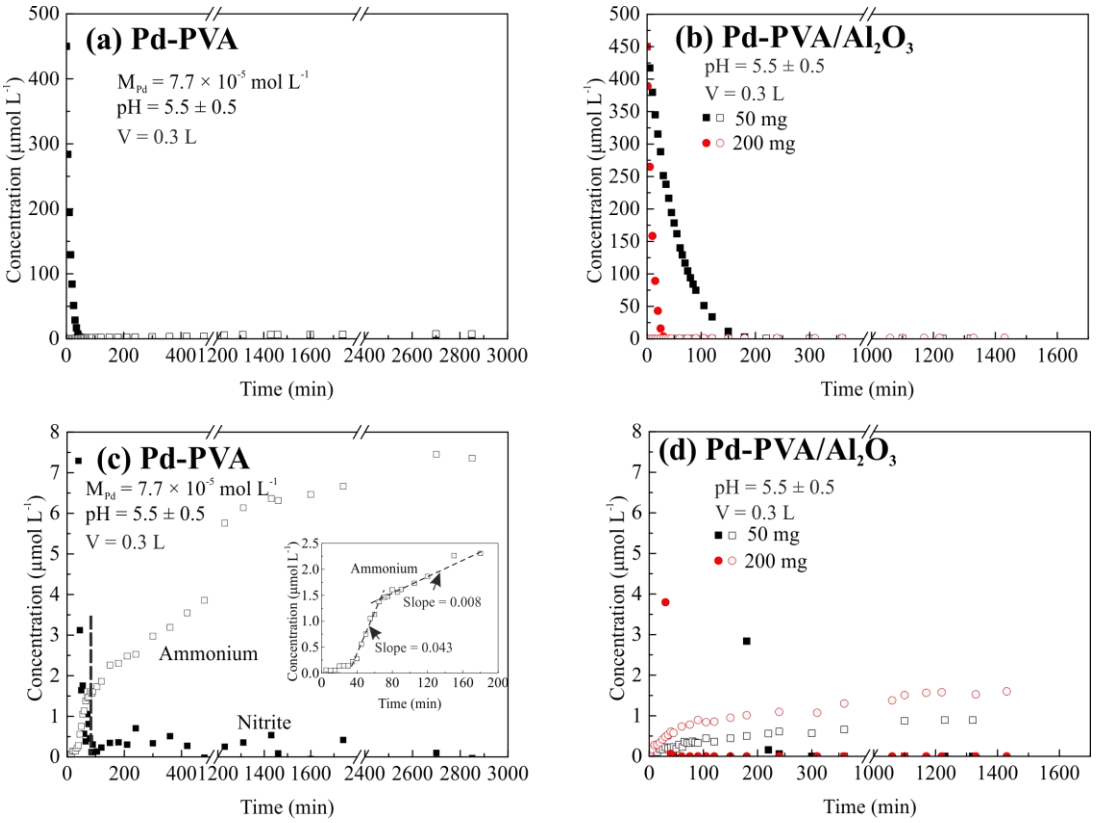

Figure 6. Concentration of nitrite (solid symbols) and ammonium (open symbols) as function of time with (a) unsupported Pd-PVA colloid and (b) Pd-PVA supported on Al_2O_3. (c) and (d) represent the same data of (a) and (b), respectively, with a zoomed-in concentration scale. Note that the time axis in interrupted.

Similar results are obtained with Pd-PVA supported on Al_2O_3; again, final ammonium concentration was reached after at least 20 h, whereas nitrite was completely consumed much earlier, as shown in Figure 6(b) and (d). The final ammonium concentrations increased with increasing weight of Pd-PVA/Al_2O_3 catalyst from 50 mg to 200 mg, as shown in Figure 6(d) and Table 2.

Table 2.

Sample	W_{cata} (mg)	C_{Pd} (μmol L^{-1})	$M_{Pd,\ surface}$ (μmol)	TOF [a] (min^{-1})	$C_{NH_4^+,\ final}$ (μmol L^{-1})	$\Delta M_{NH_4^+}$ (μmol) [b]	$M_{NH_4^+,\ ad}$ (μmol) [c]	$\frac{\Delta M_{NH_4^+}}{M_{Pd,\ surface}}$
Pd-PVA		77	2.1 [d]	17	7.4	1.8		0.86
Pd-PVA/Al_2O_3	50	6.4	0.11	74	0.9	0.09	0.01	0.82
	200	25	0.42	95	1.6	0.30	0.04	0.71
Pd/Al_2O_3	50	79	3.9	86	28	3.6		0.92

[a] Based on initial reaction rate with $C_{nitrite}$ = 450 μmol L^{-1}.
[b] The increase of ammonium amount after exhaustion of nitrite (concentration < 0.5 μmol L^{-1})
[c] Amount of ammonium adsorbed by Al_2O_3 at final ammonium concentration of reaction according to Figure 3(b).
[d] According to CO chemisorption in aqueous phase.

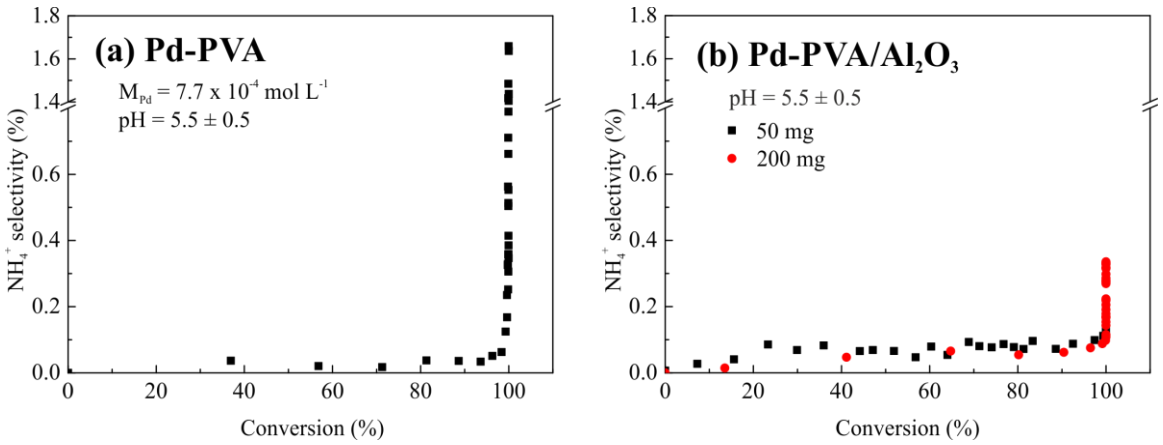

Figure 7. Ammonium selectivity as function of nitrite conversion: (a) unsupported Pd-PVA; (b) Pd-PVA supported on Al_2O_3.

Figure 7 is based on the data presented in Figure 6, showing graphically that the selectivity to ammonium remained very low until the nitrite conversion approached 100%, suddenly inducing a significant increase in the selectivity to ammonium. The selectivity to ammonium is not influenced by the amount Pd-PVA/Al_2O_3 catalyst, until the conversion approaches 100%, as shown in Figure 7(b), inducing in increase in selectivity to ammonium when increasing the amount of catalyst.

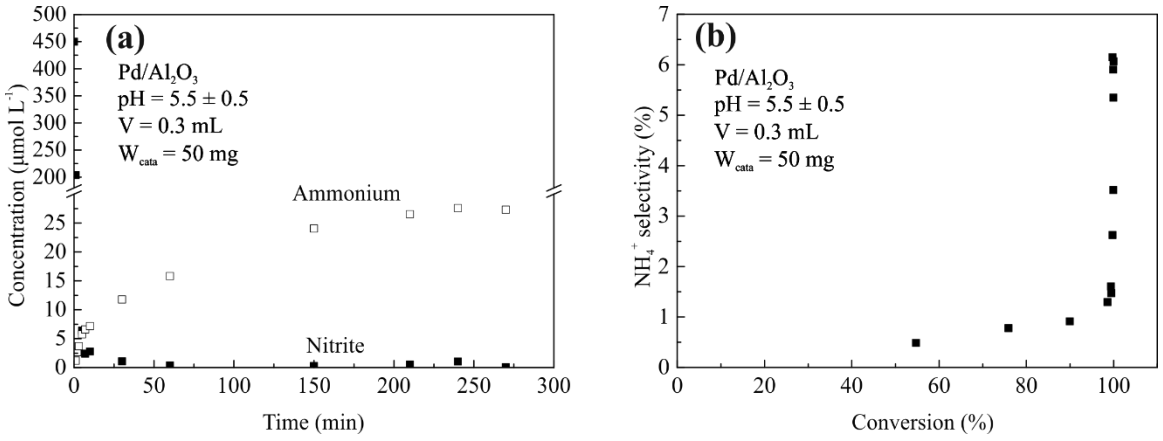

Figure 8. Concentration of nitrite (solid symbols) and ammonium (open symbols) as function of time with Pd/Al_2O_3 without PVA capping.

Similar experiments were performed with Pd/Al_2O_3 and the results are presented in Figure 8 and Table 2. Figure 8(a) shows again rapid conversion of nitrite as well as formation of ammonium after 30 minutes. After exhaustion of nitrite, the ammonium concentration continued to increase for another 3 hours to 25 μmol L^{-1}. The selectivity to ammonium increased slowly to 1% at 99% nitrite conversion. Significant increase in selectivity to ammonium was observed when approaching complete conversion of nitrite beyond 99%, as shown in Figure 8(b).

4. Discussion

4.1. Nitrite hydrogenation at low conversion level

Table 2 shows that the TOFs are quite similar for Pd-PVA/Al_2O_3 and Pd/Al_2O_3 catalysts, confirming that PVA has no influence on the intrinsic activity of Pd as discussed in Chapter 3 [11]. However, a much lower TOF was observed for unsupported Pd-PVA. Two possible explanations can be proposed. First, significant interaction between Pd NPs and the Al_2O_3 surface, based in the TEM images in Figure 1, influencing the shape of the Pd particles, might influence the activity. Second, accessibility of the Pd surface for nitrite may be influenced by the negative charge surrounding the Pd NPs (Table 1). This negative charge in likely to repulse nitrite ions, whereas positive charge of Pd-PVA/Al_2O_3 favours the adsorption of nitrite.

Figure 7 and 8(b) shows that the selectivity to ammonium increased mildly with nitrite conversion for unsupported Pd-PVA colloid, Pd-PVA/Al_2O_3 as well as Pd-Al_2O_3 catalysts. Similar increase of selectivity to ammonium with nitrate conversion with Pd-Cu/Al_2O_3 catalyst was reported by Pintar et al. [17, 18]. Kinetic studies on nitrite hydrogenation agreed that formation of ammonium over N_2 is favored at low nitrite/hydrogen ratios [19, 20]. Ebbesen et al. confirmed that decreasing nitrite/hydrogen ratio enhances the formation of intermediates responsible for the formation of ammonium, based on studies using ATR-IR [14, 15]. Hence, the increase in selectivity to ammonium with nitrite conversion can be simply explained based on kinetics, for conversion levels below 99.9% ($C_{nitrite}$ > 0.5 μmol L^{-1}). Another explanation proposed in literature, i.e. the pH decreases with conversion enhancing ammonium formation, is not relevant here because CO_2 was used to buffer [19].

4.2. Reaction after exhaustion of dissolved nitrite

Surprisingly, the selectivity to ammonium increased significantly when approaching complete conversion for all three catalysts, as shown in Figure 7 and 8(b). Figure 6(c) and Table 2 show that ammonium formation continued during tens of hours after nitrite exhaustion (<0.5 μmol L^{-1}) with unsupported Pd-PVA colloid. The ammonium concentration increased by 6.0 μmol L^{-1} in this time window, which clearly shows that the reactant involved cannot be dissolved nitrite. Similar deviations in the mass balance were found with Pd-PVA/Al_2O_3 and Pd/Al_2O_3 catalysts as shown in Figure 6(d), Figure 8, and Table 2. In all cases, the amount of ammonia formed after exhaustion of nitrite exceeds significantly the detection limit of nitrite. Apparently, the extra nitrogen must origin from adsorbed species on the catalysts, which is

further confirmed by the increase of ammonium formation after nitrite exhaustion with increasing Pd-PVA/Al_2O_3 catalyst amount, as shown Figure 6(d) and Table 2. Two options would seem reasonable to explain this observation: nitrite may adsorb on Pd, alumina or PVA, whereas N-containing intermediate species are likely to be adsorbed on Pd. We will first consider adsorption of nitrite.

Nitrite adsorption on Al_2O_3 can be neglected as compared to the amount of nitrite adsorbed on Pd and PVA, as shown in Figure 2. The low surface coverage of nitrite on alumina is at least an order of magnitude too small to account for the formation of ammonia after nitrite exhaustion. Furthermore, the increase of ammonium concentration after exhaustion of nitrite exceeds significantly the detection limit of nitrite (0.5 μmol L^{-1}) with both unsupported Pd-PVA as well as Pd-PVA/Al_2O_3 catalyst, as shown in Figure 6 and Table 2, indicating the presence of Al_2O_3 is not relevant with the formation of extra ammonium. Similarly, PVA should also not relevant with the formation of extra ammonium after dissolved nitrite exhausted, as comparing the results with Pd-PVA/Al_2O_3 and Pd/Al_2O_3, as shown in Figure 6(d) and Figure 8(a).

It is well known that adsorption of nitrite on Pd in the presence of hydrogen results in the formation of adsorbed species including NO and NO_xH_y, based on our previous ATR-IR studies [14]. These nitrogen-containing species are relevant for the formation of the extra ammonium after nitrite exhaustion. This is further supported by the fact that the molar ratio of the extra ammonium formed and the number Pd surface atoms ($\Delta M_{NH_4^+}/M_{Pd,\ surface}$) are in the range between 0.7 and 0.9 for all the catalysts, as shown in Table 2. It is interesting to note that these ratios are so high, indicating that the nitroge- containing species covered most of the Pd surface, which is apparently not blocked by the polymer.

In summary, significant amount of ammonium formed with the last percentage of conversion of nitrite hydrogenation in semi-batch reactor, causing mass unbalance of nitrogen in the aqueous phase during this period. The extra nitrogen released into the aqueous phase is caused by adsorbed species on the Pd surface.

4.3.Nitrogen-containing species on Pd NPs

ATR-IR study with circulation flow was performed in order to study the role of the nitrogen-containing-species in producing ammonium, after exhaustion of nitrite in the batch

experiment. As show in Figure 5, only NO_xH_y and NH_4^+ were detected [15]. The peak area of NO_xH_y and NH_4^+ increased in the same time, whereas no other nitrogen-containing species were detected on the catalyst surface. NO_xH_y species is an intermediate in the pathway to NH_4^+ formation [14]. Apparently, formation of NO_xH_y and NH_4^+ originates from a nitrogen-containing species on Pd surface that cannot be detected with IR. We propose that nitrogen atoms on the Pd surface are responsible for the effect as any species containing N and either O or H would be IR active

It should be noted that the experiment in Figure 5 was performed during only 3 hours because of experimental limitations, significantly shorter than the time needed to obtain the final amount of ammonium in a batch experiment (Figure 6). It is expected that after longer times the surface coverage of NO_xH_y would decrease under formation of additional ammonia.

As discussed above, Table 2 shows $\Delta M_{NH_4^+}/M_{\text{Pd, surface}}$ ratios are in the range of 0.7 to 0.9 for all catalysts, indicating that the surface coverage of nitrogen atoms is significant. Figure 6(c) shows that the formation rate of ammonium significantly decreased after exhaustion of nitrite, indicating that the reaction rate of adsorbed N atoms to ammonium is much slower than the rate of the main reaction, i.e. nitrite hydrogenation reaction producing N_2, via NO species on Pd surface [14]. Furthermore, the active sites for the main reaction seem to be minority sites, as the surface coverage of N atoms seems significant. Apparently, these minority sites mainly catalyze the reaction from nitrite to N_2. On the other hand, the majority of Pd sites covered with N atoms, are much less active, catalyzing the reaction to ammonium, explaining that Pd catalysts are generally very selective to N_2.

5. Conclusion

Nitrite hydrogenation was studied with Pd catalysts prepared with colloid method and impregnation. Significant increase of the selectivity to ammonium appeared after dissolved nitrite exhausted, and ammonium formation continues for tens of hours with catalysts prepared with colloidal method. It is concluded that nitrogen atoms covers about 80% of the accessible Pd surface area. These N atoms convert to ammonium at a very low rate. In contrast, NO species on a limited number of Pd sites react rapidly with hydrogen, producing mainly N_2.

References

[1] K.-D. Vorlop, T. Tacke, Chemie Ingenieur Technik, 61 (1989) 836-837.

[2] T. Tacke, Dissertation, Technischen Universität Carolo-Wilhelmina (1991).

[3] S. Hörold, K.D. Vorlop, T. Tacke, M. Sell, Catal. Today, 17 (1993) 21-30.

[4] J.C. Fanning, Coord. Chem. Rev., 199 (2000) 159-179.

[5] M. Shrimali, K.P. Singh, Environ Pollut, 112 (2001) 351-359.

[6] A. Kapoor, T. Viraraghavan, Journal of Environmental Engineering, 123 (1997) 371-380.

[7] N. Barrabés, J. Sá, Appl. Catal., B, 104 (2011) 1-5.

[8] F. Gauthard, F. Epron, J. Barbier, J. Catal., 220 (2003) 182-191.

[9] J.K. Chinthaginjala, J.H. Bitter, L. Lefferts, Appl. Catal., A, 383 (2010) 24-32.

[10] D. Shuai, J.K. Choe, J.R. Shapley, C.J. Werth, Environ Sci Technol, 46 (2012) 2847-2855.

[11] Y. Zhao, J.A. Baeza, N. Koteswara Rao, L. Calvo, M.A. Gilarranz, Y.D. Li, L. Lefferts, J. Catal., 318 (2014) 162-169.

[12] Y. Yoshinaga, T. Akita, I. Mikami, T. Okuhara, J. Catal., 207 (2002) 37-45.

[13] S.D. Ebbesen, B.L. Mojet, L. Lefferts, Langmuir, 22 (2005) 1079-1085.

[14] S.D. Ebbesen, B.L. Mojet, L. Lefferts, J. Catal., 256 (2008) 15-23.

[15] S.D. Ebbesen, B.L. Mojet, L. Lefferts, Langmuir, 24 (2008) 869-879.

[16] N. Koteswara Rao, A. van Houselt, B.L. Mojet, L. Lefferts, Under preparation.

[17] A. Pintar, M. vetinc, J. Levec, J. Catal., 174 (1998) 72-87.

[18] A. Pintar, J. Batista, J Hazard Mater, 149 (2007) 387-398.

[19] A. Pintar, G. Berčič, J. Levec, Aiche J., 44 (1998) 2280-2292.

[20] J.K. Chinthaginjala, L. Lefferts, Appl. Catal., B, 101 (2010) 144-149.

Chapter 5

Pd Colloid Supported on Activated Carbon: An Optimization of Preparation

1. Introduction

Our previous study in Chapter 2 has shown HCl can remove PVA from Pd surface when Pd-PVA colloid adsorbed on activated carbon (AC) with the presence of oxygen in air. In this chapter, different concentrations of HCl were used for Pd-PVA colloid immobilization on AC, and resulted catalysts were then reduced by H_2 at 200^{o}C. It will be shown that concentration of HCl influences catalytic performance of as-prepared and reduced catalysts.

2. Experimental

2.1. Chemicals

Sodium tetrachloropalladate(II) (Na_2PdCl_4 ≥ 99.995% (metal basis)), polyvinyl alcohol (PVA, average MW = 13000 – 23000, 87% – 89% hydrolyzed), sodium borohydride ($NaBH_4$, ≥ 96% (gas-volumetric)), and formic acid (98% – 100%) were purchased from Sigma-Aldrich. Sodium nitrite (>99%) was purchased from Merck. Activated carbon (AC, S_{BET} = 1000 $m^2 g^{-1}$) was supplied by Norit. AC were sieved in the range of 38 – 45 μm in diameter before used as catalyst support. All the aqueous solutions were prepared using ultra purified water obtained on water purification system (Millipore, Synergy).

2.2. Pd colloid preparation

The preparation of palladium nanoparticles via colloidal method has been described in Chapter 2, which can be summarized as follows. PVA was dissolved in water at 70°C with stirring for at least 2 hours. The solution (2 wt%) was then cooled down to room temperature. Aqueous solution of Na_2PdCl_4 (20 mL, containing 0.086 mmol Pd) and 1.76 mL of freshly prepared PVA solution were added to 240 mL water, obtaining a yellow-brown solution. After 3 min, NaBH4 solution (1.72 mL, 0.172 mmol) was added under vigorous stirring. The brown Pd colloid solution was immediately formed. The final pH was typically 8 – 8.5.

2.3. Colloid immobilization

Typically, 0.75 g AC or graphite was added to the Pd colloid solution (260 mL, 3.3×10^{-4} mol L^{-1}) immediately after preparation. Hydrochloric acid (HCl) was added to adjust pH to either 1, 2 or 3. The slurry was stirred by a mechanical 6-blade-stirrer (ϕ 44 mm, 1000 rpm) with the propeller positioned at the centre of liquid in air for 2 h at room temperature, filtered and thoroughly washed with water. After that, the catalysts were dried in vacuum at 40°C overnight.

2.4. Catalyst reduction

Catalysts prepared as described above were carefully treated in a tube furnace. In a typical procedure, the temperature was raised to 200°C at a rate of 5°C min^{-1}, then kept for 1 h at 200°C, in 10 vol% H_2/90 vol% N_2. Then the sample was flushed in N_2 for 30 min at 200°C, and cooled down at a rate of 20°C min^{-1} to room temperature in the same atmosphere. The catalysts were flushed in N_2 for 24 h before exposure to air. In the following, the sample notation will be used as shown in Table 1.

Table 1. Sample notations and details of corresponding preparation procedure

Sample	Preparation Procedure
Pd_AC_1_A	Pd-PVA colloid immobilized on AC using HCl to adjust pH to 1
Pd_AC_2_A	Pd-PVA colloid immobilized on AC using HCl to adjust pH to 2
Pd_AC_3_A	Pd-PVA colloid immobilized on AC using HCl to adjust pH to 3
Pd_AC_1_R	Pd_AC_1_A reduced in H_2/N_2 at 200°C
Pd_AC_2_R	Pd_AC_2_A reduced in H_2/N_2 at 200°C
Pd_AC_3_R	Pd_AC_3_A reduced in H_2/N_2 at 200°C

2.5. Characterization

Pd particle size distribution was determined using TEM (Philips CM300ST-FEG) with a resolution of 1 nm. The AC supported catalysts were firstly ground into sub-micron fragments and dispersed in ethanol. Then the suspension was dropped on a copper grid covered with hollow carbon for TEM image taking. At least five of these ground fragments were randomly selected for determination of Pd particle sizes, and typically 300 Pd particles were measured. Note that information on the spatial distribution of nanoparticles through the support cannot be obtained as the samples were ground. The metal loading on the supports were analyzed by XRF. The total surface area of samples were calculated based on N_2 physisorption data, using the BET method for p/p_0 values between 0.03 and 0.13 for catalysts prepared with AC following the recommendations of Rouquerol *et al*. [1], with a typical error margin of 5%.

Re-dissolution of Pd by HCl was detected by UV-vis spectroscopy of the colloidal suspension in a UV-spectrometer (Perkin Elmer Lambda 850) at room temperature. The pH of freshly prepared unsupported Pd-PVA colloid suspension was adjusted to 1, 2 and 3 by adding HCl solution, followed by stirring the suspension in air atmosphere for 2 h. Then 500 μL of the

treated suspension was introduced in a quartz cell (QS1000) for spectrum analysis, with wavelength from 200 to 800 nm and a scanning speed of 266.75 nm min^{-1}.

CO chemisorption at room temperature was used to determine the metal surface area that is accessible in gas phase. Typically, the sample was pre-reduced at room temperature in hydrogen and then flushed in He at the same temperature. Then CO was introduced as pulses and the response was recorded using a TCD detector. We assumed that the stoichiometric ratio of number of adsorbed CO molecules and number of accessible Pd surface atoms is 1 : 1. The Pd dispersion (*Pd disp*.) was defined as

$$Pd\ disp. = \frac{\text{number of Pd atoms in the surface of NPs}}{\text{number of Pd atoms in total}}$$

The surface composition of the catalysts was analyzed by X-ray photoelectron spectroscopy (XPS, Quantera SXM, Al *K*α (1486.6 eV)). The powder samples were stored in air without any further pretreatment before analysis. Typically a few microgram sample was pressed into an indium foil, and four spots (600×300 μm^2) on the sample were randomly selected for measurements to rule out any inhomogeneity in the catalysts. The accuracy of the resulting peak positions was within 0.2 eV. The spectra were fitted using the software "Multipak v.9.4.0.7". Typically, the binding energy in all spectra was first calibrated using the carbon 1s peak at 284.8 eV as an internal reference. The spectra detected from the four spots of one sample were averaged in order to improve the signal-to-noise ratio, followed with Shirley background subtraction. The Pd peaks were fitted using an asymmetric model, necessary because of interaction of the photoelectrons with the valence band electrons [2], whereas the S and Cl peaks were fitted using mixed Gaussian-Lorentzian model, as suggested by Handbook of X-ray Photoelectron Spectroscopy [3]. The peaks for each sample (Pd 5d, Cl 2p and S 2p) were fitted with sets of doublets with identical FHWM. Both width and peak position were allowed to optimize. The distance within the doublets was fixed, according to the data suggested in the handbook [3].

2.6. Nitrite hydrogenation

The reactions involved in nitrite hydrogenation are given in Eq. (1.2) and (1.3).

$$2NO_2^- + 3H_2 + 2H^+ \xrightarrow{Pd} N_2 + 4H_2O \qquad \text{(Eq. 1.2)}$$

$$NO_2^- + 3H_2 + 2H^+ \xrightarrow{Pd} NH_4^+ + 2H_2O \qquad \text{(Eq. 1.3)}$$

The reaction was performed in a home-build apparatus including a glass tank reactor (ϕ 98 mm with four 5 mm baffles), equipped with a mechanical 6-blade-stirrer (ϕ 44 mm, 1000 rpm) with the propeller positioned at the centre of liquid. Typically, 50 mg catalyst was added into 300 mL H_2O. The mixed suspension was then stirred vigorously in H_2/He/CO_2 atmosphere (H_2/He/CO_2 = 6/3/1 by volume flow rate, total flow rate = 100 mL min^{-1}, total pressure = 1 bar) for at least 1 h. CO_2 was used as a buffer according to reaction shown in Eq. A3.1 and Eq. A3.2 to supply the protons consumed by nitrite hydrogenation.

$$CO_2 + H_2O \longrightarrow HCO_3^- + H^+ \quad \text{(Eq. A3.1)}$$

$$HCO_3^- + H_2O \longrightarrow CO_3^{2-} + H^+ \quad \text{(Eq. A3.2)}$$

Then 3 mL 4.2 mmol L^{-1} $NaNO_2$ solution was introduced, starting the reaction. Samples of 1 mL were taken with a syringe every 5 min. Catalysts were removed using a syringe filter (PTFE, 0.2 μm)before injecting into ion chromatograph (DIONEX, ICS 1000) to determine the content of nitrite and ammonium.

3. Results

3.1. Elemental analysis

Table 2. XRF and CO chemisorption results

Sample	C_{Pd} (wt %)	C_{Cl} (wt %)	Pd disp. (%) CO chemisorption [a]	TEM [b]
Pd_AC_1_A	1.2	1.1	12 ± 3	30
Pd_AC_2_A	1.2	0.8	12 ± 2	32
Pd_AC_3_A	1.2	0.6	8 ± 2	29
Pd_AC_1_R	1.3	n.d.	32 ± 5	22
Pd_AC_2_R	1.2	n.d.	30 ± 4	30
Pd_AC_3_R	1.2	n.d.	18 ± 4	28

[a.] The sample was reduced in H_2 flow for 1 h at 21 ± 1°C.
[b.] Estimated by assuming Pd NPs are sphere shaped with clean surface.

Table 2 shows Pd loading was independent with pH used for colloid immobilization, while chlorine concentration decreased with increasing pH (less HCl used). In any case, no chlorine was detected by XRF after reduction in H_2/N_2 at 200°C, indicating the chlorine contents were lower than the detecting limitation, i.e. 0.05 wt %.

3.2. TEM

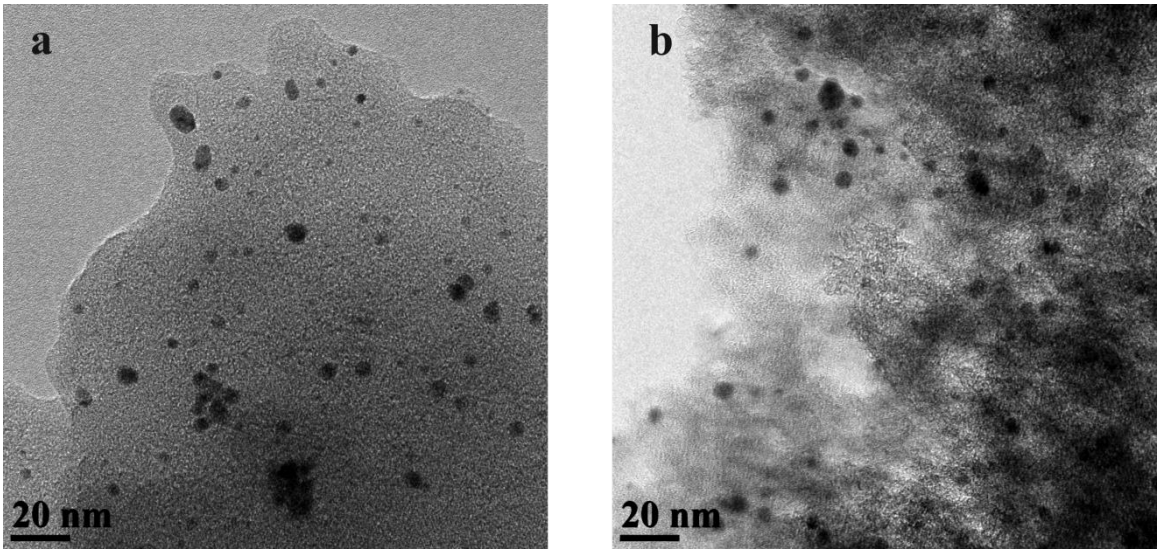

Figure 1. Typical TEM images of Pd-PVA supported on AC: (a) Pd_AC_1_A; (b) Pd_AC_1_R.

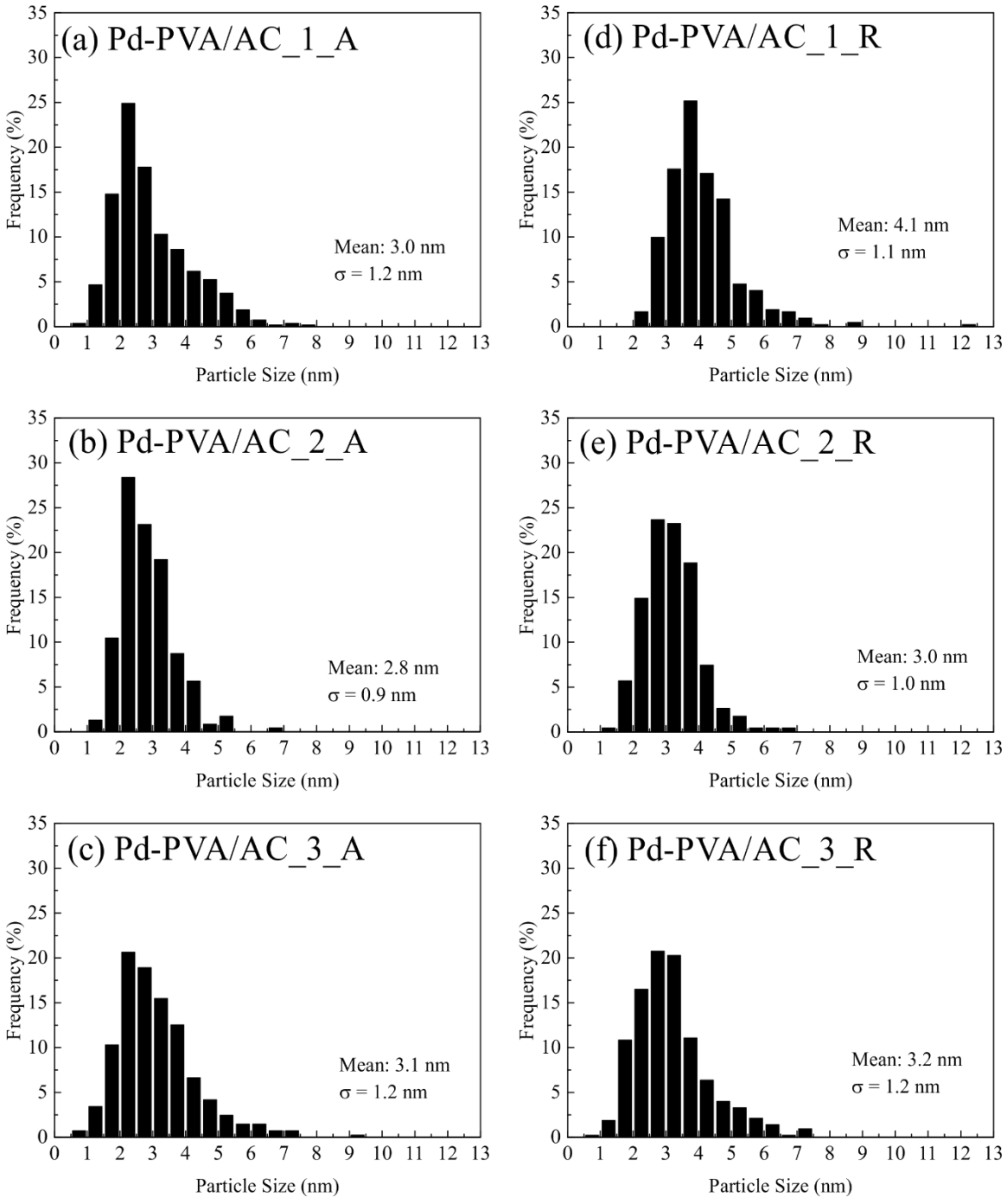

Figure 2. Particle size distribution of Pd-PVA supported on AC with different pH, before and after reduction.

Figure 1 shows a typical TEM image of Pd-PVA colloid supported on activated carbon, presenting sphere-shaped NPs on carbon sheets; similar morphology was observed with all other catalysts. Figure 2 shows the average particle sizes were identical with narrow size distribution for all as-prepared catalysts, independent with the pH value during colloid

immobilization. The particle size distribution remained narrow after reduction in 10% H_2/N_2 at 200°C; however, the average particle size increased after the reduction for catalyst prepared at pH=1, indicating sintering of the NPs.

3.3. Physisorption

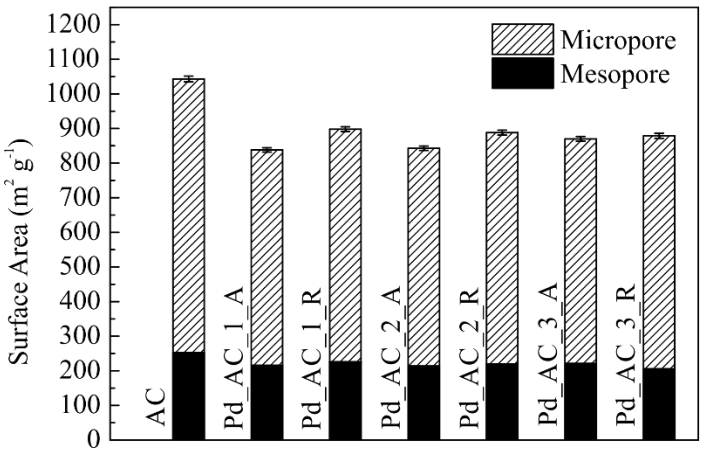

Figure 3. Surface area of micro- and mesopores: Pd-PVA supported on AC prepared with different pH. The surface area of micropores was calculated by t-plot method using data of N_2 physical adsorption. The mesopore surface area was estimated based on the difference between BET surface area and micropore surface area.

Figure 3 shows no significant change of mesopore surface area for AC after Pd colloid immobilization with different pH. Instead, micropore surface area of the supports decreased after colloid immobilization, which is probably caused by blocking or filling of micropores with PVA. In any case, the surface area increased after reduction in H_2/N_2 at 200°C.

3.4. UV-vis spectroscopy

Figure 4 shows partial re-dissolution of Pd on unsupported Pd-PVA colloid stirred in air at different pH adjusted by HCl. No Pd-Cl complex was detected in as-prepared colloid suspension, indicating complete reduction of Pd^{2+} during colloid preparation. After stirring in air for 2 h, $[PdCl_3(H_2O)]^-$ (207 nm and 236 nm) was the only detected Pd-Cl complex in the

colloid suspension at pH = 3, adjusted by HCl; $[PdCl_4]^{2-}$ (278 nm) started to appear in the suspension at pH = 2 and became the majority Pd-Cl complex (222 nm and 278 nm) when the pH was further decreased to 1.

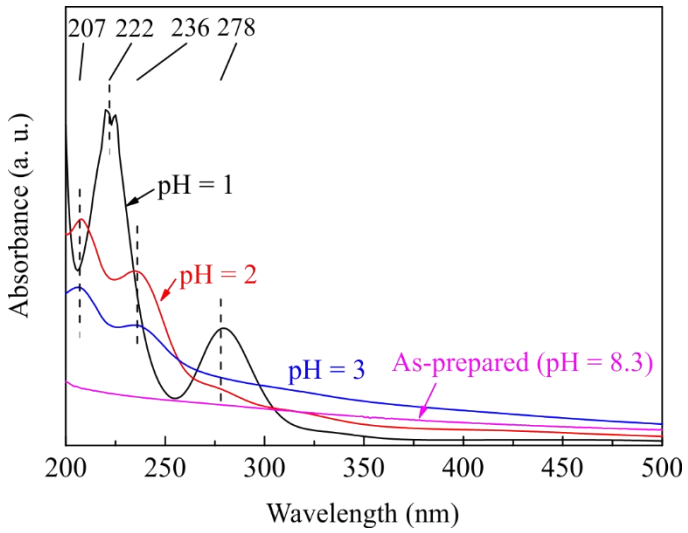

Figure 4. UV-vis spectra of unsupported Pd-PVA colloid suspension after stirred in air for 2 h at different pH adjust by HCl. The absorption peaks at 207 nm and 236 nm can be attributed to $[PdCl_3(H_2O)]^-$ and peaks at 222 nm and 278 nm to $[PdCl_4]^{2-}$. These assignments are consistent with the literature [4, 5]. The total amounts of Pd in mole are semi-quantitatively comparable.

3.5.CO chemisorption

As shown in Table 2, the metal dispersion for as-prepared catalysts kept identical with different pH during colloid immobilization. Note that the samples were first reduced in H_2 flow at room temperature, before CO was chemisorbed. After reduction in H_2/N_2 at 200°C, the metal dispersion was significantly increased; however, the dispersion of the catalyst prepared with pH = 3 was lower as compared with catalysts prepared with pH= 1 and 2.

3.6. XPS

Figure 5 shows the effect of reduction at 200ºC on the oxidation state of Pd in catalyst prepared at pH 2; similar results have also been observed with catalyst prepared at pH 1 and 3, as shown in Supporting Information. Table 3 presents the full data set of peak positions resulting from the fitting procedure as well as the ratio values for Pd^{2+}/Pd^{0} , showing that the as-prepared catalyst contained 38% Pd^{2+} for catalyst prepared with pH 1 and 2, whereas only 7% of Pd^{2+} appeared after using pH 3. After reduction in H_2/N_2 at 200ºC, Pd^{2+} decreased significantly. Pd was almost completely reduced with catalyst prepared with pH = 2 and 3 for colloid immobilization; however, 12% of Pd^{2+} still existed in catalyst prepared with pH = 1.

On the other hand, two types of chlorine were detected with formal charge Cl^{-}, as shown in Figure 5 and Table 3, which can be attributed to Cl bonded to Pd (*ca.* 198 eV) and Cl in organic compounds (*ca.* 200 eV), respectively [6]. After thermal treatments at 200ºC in H_2/N_2, the relative amount of Cl bonded to palladium decreased caused by reaction with H_2. Furthermore, the molar ratio of $Cl(Pd)/Pd^{2+}$ was in the range of 2 – 3 for all samples, both before and after reduction.

Table 3. XPS results of Pd and Cl oxidation-states and surface concentration

Sample	Pd^{2+}/Pd	Cl(Pd)/Cl	$Cl(Pd)/Pd^{2+}$ (mol/mol) [a]
Pd_AC_1_A	0.38	0.75	1.7
Pd_AC_2_A	0.38	0.79	1.8
Pd_AC_3_A	0.07	0.72	3.0
Pd_AC_1_R	0.12	0.37	2.1
Pd_AC_2_R	0.03	0.43	3.1
Pd_AC_3_R	0.03	0.36	1.7

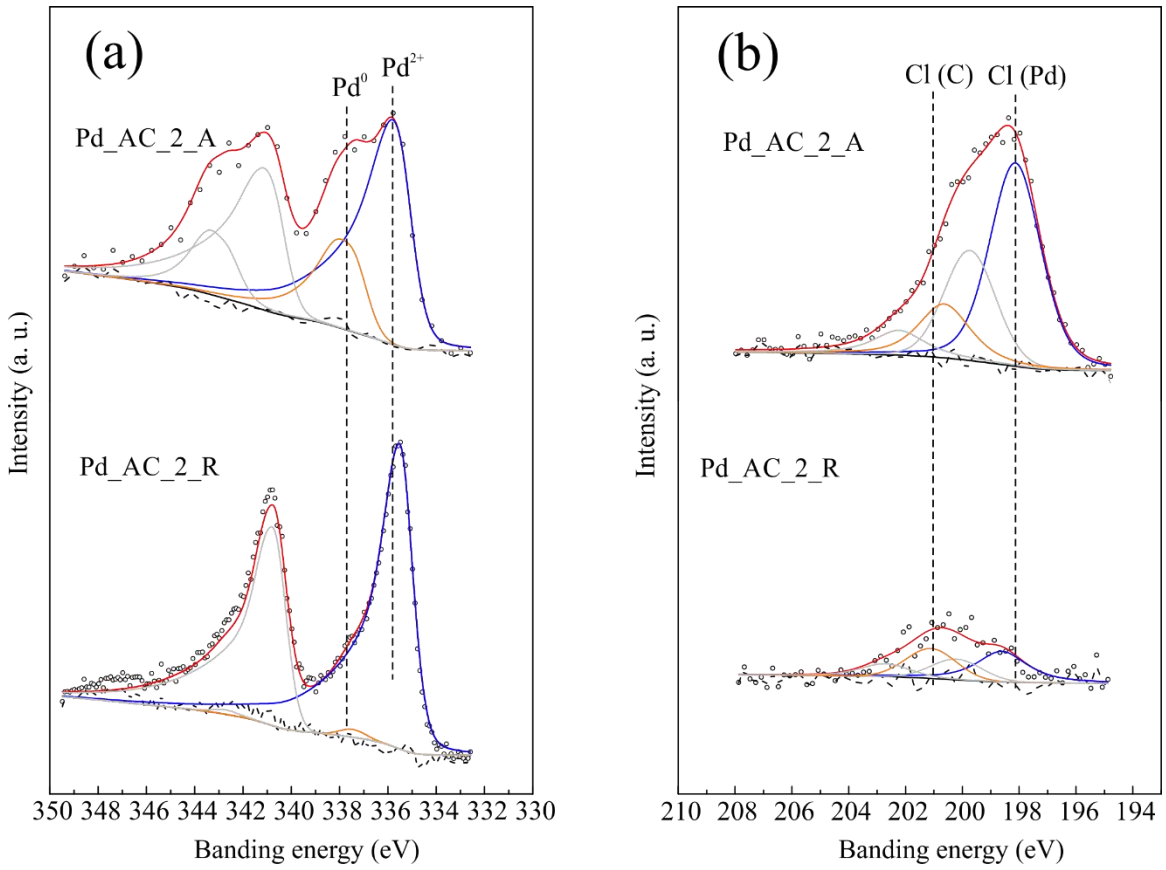

Figure 5. XPS spectra of activated carbon supported Pd-PVA colloids prepared at pH = 2: (a) Pd 3d spectra, (b) Cl 2p spectra. Original data (hollow dots) was subtracted with Shirley background (black line) and fitted using method described in section 2.5. The fitted Pd 3d5/2 peaks, and Cl 2p3/2 peaks are highlighted (blue and orange) for comparison. The sum of all fitted peaks showed as red line with error showed as dash line.

3.7. Nitrite hydrogenation

Figure 6(a) and (b) present concentrations of nitrite and ammonium as function of time. The initial rate per total Pd can be estimated using the Pd loading as determined by XRF in Table 1, as shown in Figure 6(c). Alternatively, Figure 6(d) shows the initial rate per surface Pd, where the amount of surface Pd was determined by XRF results together with CO chemisorption results in Figure 4. In any case, the reaction rate showed no significant change with variation of the pH during colloid immobilization for as-prepared Pd-PVA/AC catalysts in Figure 6(d). For the reduced catalysts, an increase of reaction rate was observed with increasing the pH-value.

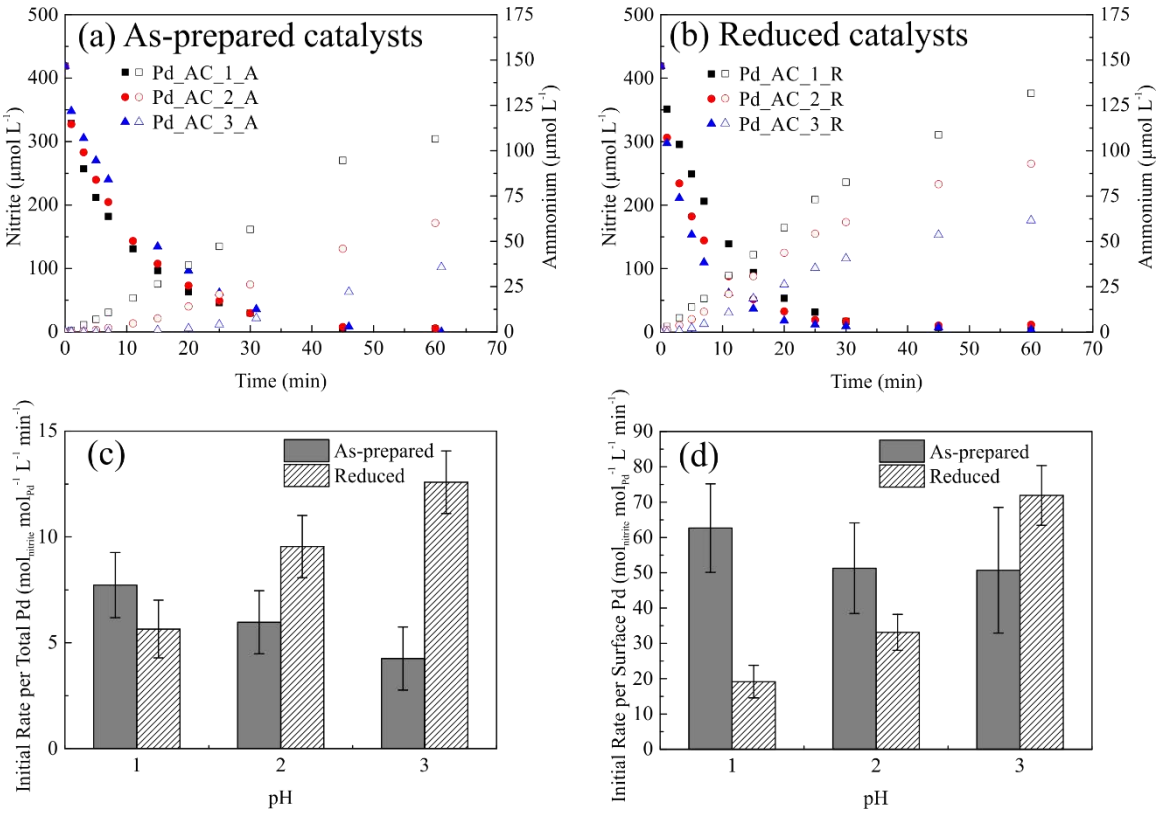

Figure 6. Activity of Pd-PVA supported on AC before and after reduction at 200°C in H_2/N_2: concentration of nitrite (solid symbols) and ammonium (open symbols) with (a) as prepared and (b) reduced catalysts; initial reaction rate (c) per total Pd or (d) per surface Pd with catalysts prepared at different pH. The error bars represent standard deviation.

Figure 7 shows that selectivity to ammonium decreased with increasing pH during colloid immobilization, for both as-prepared and reduced catalysts. The reduction treatment at 200°C in H_2/N_2 resulted in higher selectivity to ammonium, regardless the amount of HCl was used for immobilization.

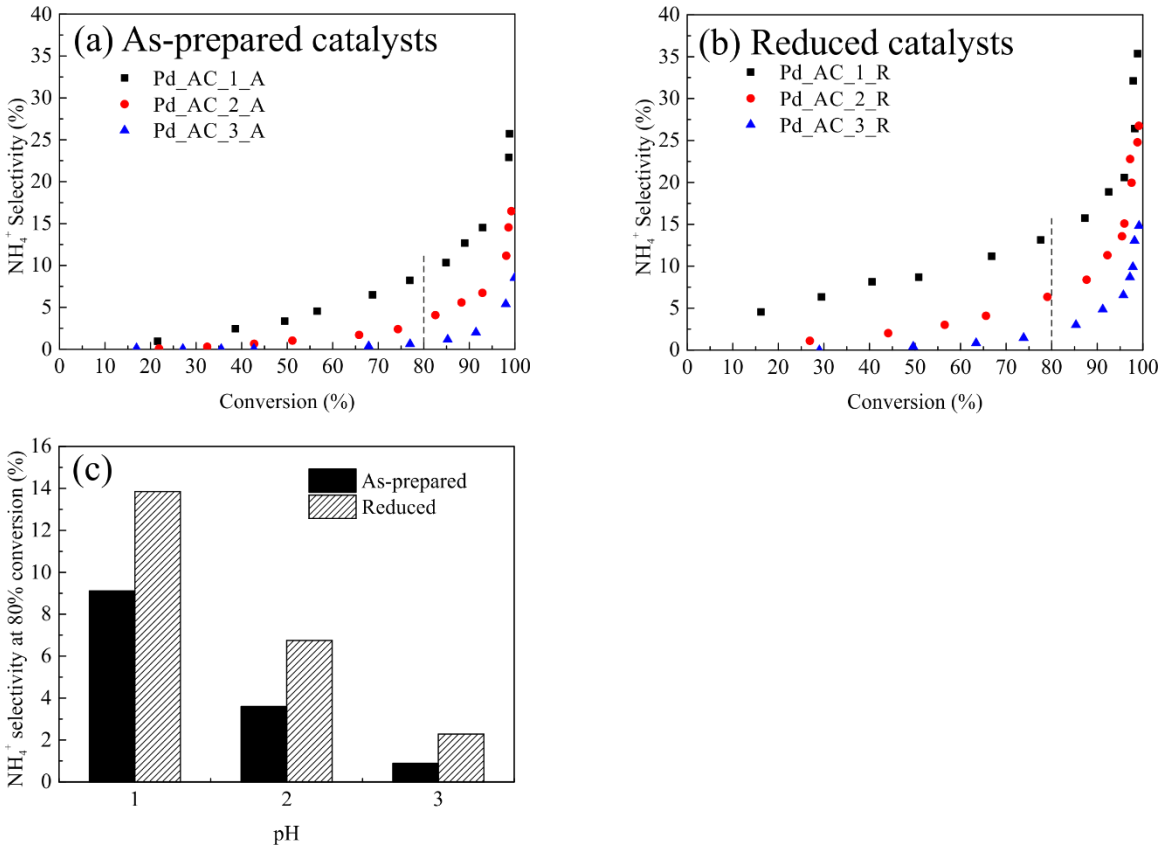

Figure 7. Selectivity to ammonium for nitrite hydrogenation with Pd-PVA supported on AC: (a) selectivity to ammonium as function of nitrite conversion with as-prepared catalysts; (b) selectivity to ammonium as function of nitrite conversion with catalysts reduced at 200ºC in H_2/N_2; (c) comparison of ammonium selectivity at 80% nitrite conversion with catalyst prepared at different pH.

Table 4. Summary of reaction rate and selectivity to ammonium related to chlorine concentration

Sample	$M_{Cl,\ cata}$ (µmol)	$M_{Cl,\ solu}$ (µmol)	Initial rate per total Pd ($mol_{nitrite}\ mol_{Pd}^{-1}\ L^{-1}\ min^{-1}$)	Initial rate per surface Pd ($mol_{nitrite}\ mol_{Pd}^{-1}\ L^{-1}\ min^{-1}$)	NH_4^+ selectivity at 80% conversion (%)
Pd_AC_1_A	16	16			9.1 ± 0.5
Pd_AC_2_A	11	11			3.6 ± 0.4
Pd_AC_3_A	8.4	8.0	4.2 ± 1.5	50.7 ± 17.8	0.8 ± 0.2
Pd_AC_3_R	-	0.3	12.6 ± 1.5	71.9 ± 8.5	2.3 ± 0.3
Pd_AC_3_R with extra NaCl	-	9.2	13.3 ± 1.5	76.1 ± 8.5	1.1 ± 0.2

The amount of Cl introduced by the catalysts ($M_{Cl,\ cata}$) can be calculated using the XRF results in Table 2, as shown in Table 4. Cl- released from the catalyst to solution during the 1 h pre-reduction treatment before the beginning of reaction, and the Cl- constant remained

constant during the whole reaction. The amounts of Cl^- in solution ($M_{Cl,\ solu}$) were also shown in Table 4. In all cases, the values of $M_{Cl,\ cata}$ and $M_{Cl,\ solu}$ are quite similar, indicating that almost all the chlorine on the catalyst transferred into the solution during the batch reaction. In order to reveal the influence of the free Cl^- in reaction solution on catalyst performance, NaCl was added in reaction slurry before the reaction with Pd_AC_3_R, as shown in Table 4. No significant change of activity of Pd_AC_3_R with NaCl added in reaction slurry; however, selectivity to ammonium of the catalyst decreased significantly with extra Cl added.

4. Discussion

4.1. Influence of HCl on Pd accessibility

CO chemisorption results in Table 2 show significant increase of accessible Pd surface after reduction in H_2/N_2 at 200°C for the catalyst prepared at pH 1 and 2, resulting the Pd dispersion equal to or higher than the observation of TEM. This agrees with the observations described in Chapter 2, that the blocking of Pd surface by PVA can be suppressed by HCl in the presence of air, according to the following reaction:

$$2Pd + Cl^- + O_2 + 4H^+ \longrightarrow 2PdCl_2 + 2H_2O(l) \quad \Delta G = -269.57 \text{ kJ} \quad \text{(Eq. 2.3)}$$

The presence of $PdCl_2$ on the Pd surface weakens the interaction between PVA and Pd NPs, thus PVA can be completely removed from the Pd surface. Reaction at 200°C is necessary to remove chlorine from the Pd surface.

On the other hand, CO chemisorption results also show a smaller increase in Pd dispersion after reduction for catalyst prepared at pH 3, lower than what is expected from TEM. This indicates that the amount of Cl^- and H^+ is probably not sufficient in induce complete removal of PVA at this pH.

UV-vis spectra in Figure 4 show the presence of Pd-Cl complex anion in the unsupported colloid suspension after stirring in air with different pH, and the complexes converted from $[PdCl_3(H_2O)]^-$ to $[PdCl_4]^{2-}$ with adding HCl to decrease the pH, indicating re-dissolution of Pd from the metallic nanoparticles with the following reaction:

$$Pd \xrightarrow[O_2,\ H^+]{+\ Cl^-} PdCl_2 \xrightarrow[+\ H_2O]{+\ Cl^-} [PdCl_3(H_2O)]^- \xrightarrow[-\ H_2O]{+\ Cl^-} [PdCl_4]^{2-} \quad \text{(Eq. 5.1)}$$

Apparently, a high Cl^- concentration is preferable for this re-dissolution. On the other hand, XRF results in Table 2 clearly show no difference of Pd loadings for all the catalyst supported on AC, regardless the pH during colloid immobilization. This indicates that the majority of the dissolved Pd-Cl complex anions adsorbed on AC. Simonov et al. have declared that a low pH causes a strong interaction between carbon support and $[PdCl_4]^-$, resulting highly dispersed $(PdCl_2)_n$ clusters [6, 7]. These $(PdCl_2)_n$ clusters agglomerate during reduction, resulting in sintering, as confirmed by TEM for catalyst prepared with pH 1, where the Pd particle size increased from 3 to 4 nm after reduction at 200°C for 2 h. On the other hand, we cannot rule

out the possibility of the formation of very small Pd clusters (< 1 nm) at the same time, which are not visible with TEM, resulting in under-estimation of Pd dispersion based on TEM images. XPS results in Table 3 show 12% of Pd atoms remained oxidized after reduction for catalyst prepared at pH 1, whereas catalysts prepared at pH 2 and 3 can be almost completely reduced. This indicates incomplete reduction of $(PdCl_2)_n$ clusters at 200°C in H_2/N_2 in gas phase.

In summary, excess amount of HCl (pH 1) used for Pd colloid immobilization on AC causes partial re-dissolution of Pd NPs, probably resulting in ultra-highly dispersed $(PdCl_2)_n$ clusters and Pd clusters. In contrast, insufficient amount HCl (pH 3) causes less extent of Pd re-dissolution, but also can not prevent the blocking of Pd surface by PVA. The pH we have chosen in Chapter 2 is an optimized value in order to minimize both negative effects.

4.2. Influence of HCl on activity

4.2.1. Influence of Chlorine on activity in general

For as-prepared catalysts, Pd particle sizes were identical with different pH during colloid immobilization, as shown by TEM in Figure 2 (a) – (c). And Table 1 shows similar values for apparent Pd dispersion according to CO chemisorption. Furthermore, the data in Table 4 show that chlorine is almost completely released into aqueous phase during the reaction, indicating very few chlorine bonded to the Pd surface during the reaction. As a result, the number of accessible active sites for all as-prepared catalysts prepared with different pH should be identical.

As shown in Figure 6(c) and (d), all as-prepared catalysts showed identical activity, regardless the different chlorine concentrations in the slurry reactor. Furthermore, no significant change of activity for Pd_AC_3_R was found, with increasing chlorine concentration from 1 to 30 μmol L^{-1} by adding extra NaCl. These observations do not agree with the results reported by Pintar, et al., where the reaction rate decreased with adding chloride in slurry phase nitrate hydrogenation on powdered Pd/Al_2O_3 [8]. The authors explained this by the repulsion between Cl^- and unconverted nitrate in the Helmholtz layer [9-11]. However, the effect on nitrite hydrogenation was not reported. On the other hand, Chaplin et al. reported that the influence of Cl^- on nitrite hydrogenation is much weaker as compared with nitrate hydrogenation on $Pd\text{-}Cu/Al_2O_3$; nevertheless, and the activity of nitrite hydrogenation still decreased to half with adding high concentration of NaCl (1 $g_{chlorine}$ L^{-1}, or 28 mmol L^{-1}) [12].

However, only bimetallic catalysts were studied and Cu dissolution was also observed by adding NaCl, thus it is difficult to compare these results with our study. Additionally, high concentration of chlorine was used by both Pintar et al. and Chaplin et al., between 5 to 30 mmol L^{-1}, much higher than the chlorine concentration in this study (1 – 50 μmol L^{-1}). In any case, chlorine released from the as-prepared catalysts would not influence the reaction rates significantly.

4.2.2. Activity per total Pd

Reduction in H_2/N_2 at 200°C caused an increase of the reaction rate per total Pd for the catalysts prepared at pH 2, as shown in Figure 6(c), together with no significant change in particle size as observed by TEM in Figure 2, as well as complete reduction of Pd according to XPS results in Table 3. Similar increase of activity per total Pd have been reported in the study of Chapter 2, using the same catalyst in fixed bed operation. This cannot be explained by chlorine removal effect as discussed above. Probably, PVA molecules remained in the pore structure of AC after removal from Pd surface by chlorine. These residential PVA might take a role of blocking Pd surface after chlorine removal during the pre-reduction treatment before reaction. On the other hand, hydrogenolysis of PVA catalyzed by Pd during reduction at 200°C, according to reaction in Eq. 2.4 as discussed in Chapter 2. This reaction changes the structure of PVA, probably also preventing the remained molecules influencing the reaction.

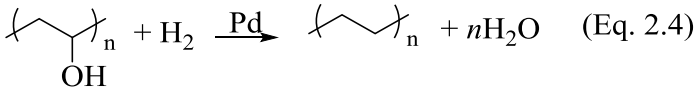

(Eq. 2.4)

4.2.3. Activity per surface Pd

The reaction rate per surface Pd decreased as a result of reduction at 200°C for catalyst prepared at pH 1 and 2, as shown in Figure 6(d). Concurrently, Pd dispersion increased according to CO chemisorption results in Table 2, and Pd_AC_1_R cannot be completely reduced according to XPS results in Table 3. Particle size effect on the activity per surface Pd can be ruled out according to our previous study in Chapter 3 as well as in literatures, showing that nitrite hydrogenation on Pd catalyst is size independent with the range between 2.5 to 30 nm [13, 14]. The reaction is also independent of chlorine concentration for the concentration used in this study as discussed above. The results are similar as observed with fixed bed operation as reported in Chapter 2, explained by reduction of Pd^{2+} during the reaction, and

consequently the number of active sites on Pd surface was underestimated based on CO chemisorption in gas phase.

Reaction rate per Pd surface decreased with decreasing pH during colloid immobilization for reduced catalysts, as shown in Figure 6(d). Concurrently, more Pd dissolved with decreasing pH, meaning increasing of HCl concentration, according to UV-vis spectra in Figure 4. As discussed in Section 4.1, these dissolved Pd may redispersed on AC with such small size at invisible by TEM. It is well known that nanoclusters containing only a few number of atoms have unique structures and often perform different catalytic properties as compared with nanoparticles large than 2 nm. In Chapter 3, it has shown an exclusive low TOF with the smallest Pd NPs of 2.2 nm as compared with Pd NPs larger than 2.5 nm. Probably the low activity per Pd surface was caused by very small Pd particles redispersed on AC, caused by Pd dissolution with HCl, for reduced catalyst prepared at pH 1.

In summary, catalyst prepared with pH = 3 performs highest activity after reduction in H_2/N_2, regardless the residential blocking of Pd surface by PVA. The re-dissolution of Pd by HCl in the presence of air results in decreasing of the activity of the reduced catalysts. On the other hand, both particle size and the presence of chlorine have no influence on the activity per surface Pd.

4.3. Effect of HCl on selectivity

Reduction in H_2/N_2 at 200°C increases the selectivity to ammonium as shown in Figure 7(c), together with removal of chlorine content as detected by XRF in Table 2 and XPS in Table 3. On the other hand, table 4 shows the selectivity decreases with adding extra NaCl in Pd_AC_3_R catalyst. This indicating that Cl^-, no matter whether released from the catalyst during the reaction or externally added in the aqueous phase, decreases the selectivity to ammonium. Similar decrease of selectivity to ammonium caused by Cl was also reported by Chaplin et al., with Pd-Cu/Al_2O_3 catalysts used in slurry phase [12]. In contrast, Pinter et al. reported the presence of NaCl increases of the selectivity to ammonium with Pd/Al_2O_3 sphere catalysts (1.7 mm, Pd layer 120 μm thick) in a fixed bed reactor [10]. Mass transfer limitation was not excluded by the authors, inducing concentration gradients influencing the catalyst selectivity [14]. In this study, probably the presence of free chlorine close to Pd surface inhibits

the accessibility of active sites for NO_2^-, consequently decreasing the N/H ratio close to active sites, resulting in enhanced selectivity to ammonium.

Surprisingly, the selectivity to ammonium increased when the pH during colloid immobilization was decreased, for both as-prepared and reduced catalysts, as shown in Figure 7. Table 4 shows that catalysts prepared with lower pH induced higher chlorine concentration during the reaction. This indicates other effects also influence the selectivity, besides free chlorine effect.

Any effect with Pd particle size can be excluded as particle sizes were identical expect for Pd_AC_1_R. Also, PVA is not able to influence the selectivity, as discussed in Chatper 3. Therefore, we speculate that the redistribution of Pd via Pd dissolution by HCl caused formation of ultrafine dispersed Pd nanoclusters, which were responsible for the change in selectivity. However, the exact role of these nanoclusters remains unclear and further investigation is needed.

5. Conclusions

Pd-PVA colloids have been immobilized on AC with different HCl concentration in the presence of air. UV-vis spectra show Pd re-dissolution by HCl in the presence of air. The catalyst prepared with pH 3 exhibits highest reaction rate as well as a relatively low selectivity to ammonium after reduction at 200^{o}C, despite an incomplete removal of PVA from the Pd surface according to CO chemisorption. This indicates the higher importance of preventing excess amount of HCl as compared with polymer blocking, in order to limit the formation of ammonium during nitrite hydrogenation with Pd-PVA/AC catalysts.

References

[1] F. Rouquerol, J. Rouquerol, K. Sing, in: Adsorption by Powders and Porous Solids, Academic Press, London (1999), pp. 237-285.

[2] David Briggs, J.T. Grant, Surface Analysis by Auger and X-Ray Photoelectron Spectroscopy, IM Publications, in Chichester (2003).

[3] J. F. Moulder, W. F. Stickle, P. E. Sobol, K.D. Bomben, Handbook of X-ray Photoelectron Spectroscopy, Perkin-Elmer Corporation, in Eden Prairie (1992).

[4] L.I. Elding, Inorg Chim Acta, 6 (1972) 647-651.

[5] C. Drew Tait, D.R. Janecky, P.S.Z. Rogers, Geochim Cosmochim Ac, 55 (1991) 1253-1264.

[6] P.A. Simonov, A.V. Romanenko, I.P. Prosvirin, E.M. Moroz, A.I. Boronin, A.L. Chuvilin, V.A. Likholobov, Carbon, 35 (1997) 73-82.

[7] P. Simonov, S. Troitskii, V. Likholobov, Kinet. Catal., 41 (2000) 255-269.

[8] A. Pintar, M. vetinc, J. Levec, J. Catal., 174 (1998) 72-87.

[9] A. Pintar, J. Batista, Appl. Catal., B, 63 (2006) 150-159.

[10] A. Pintar, J. Batista, J Hazard Mater, 149 (2007) 387-398.

[11] A. Pintar, J. Batista, I. Muševič, Appl. Catal., B, 52 (2004) 49-60.

[12] B.P. Chaplin, E. Roundy, K.A. Guy, J.R. Shapley, C.J. Werth, Environ Sci Technol, 40 (2006) 3075-3081.

[13] D. Shuai, J.K. Choe, J.R. Shapley, C.J. Werth, Environ Sci Technol, 46 (2012) 2847-2855.

[14] J.K. Chinthaginjala, J.H. Bitter, L. Lefferts, Appl. Catal., A, 383 (2010) 24-32.

Chapter 6

Concluding Remarks and Recommendations

Studying catalysis using model catalysts prepared via colloidal method has become attractive because monodispersed metallic nanoparticles (NPs) can be prepared with accurately manipulated size and shape. However, the complexity brought by residential stabilizer on the metal surface remains a challenge for application of colloids, including surface blocking and influencing the catalytic performance of the catalysts.

The work presented in this thesis aimed at a better understanding of nitrite hydrogenation in aqueous phase using monodispersed Pd nanoparticles (NPs) as model catalysts, prepared via colloidal methods. We first discussed the possibility of complete removal of polymer stabilizer from the Pd surface and the subsequent influence on the catalytic performance. Secondly, unsupported and supported Pd colloids were also used directly as model catalysts, without removal of the polymer, focusing on the effects of the polymer on catalyst performance.

6.1. Polymer removal from Pd NPs prepared via colloidal method

Monodispersed Pd NPs were prepared using polyvinyl alcohol (PVA) and polyvinylpyrrolidone (PVP) as stabilizer dissolved in aqueous phase. The Pd precursor, Na_2PdCl_4, was rapidly reduced with $NaBH_4$ to Pd NPs within a few seconds. The rapid reduction resulted in sphere-like Pd NPs with sizes in the range of 2 – 4 nm, which can be manipulated by changing the polymer/reducer ratio. The resulting colloidal suspension is stable during a few days and then agglomerated slowly. XPS results indicated that Pd can be reduced completely, but re-oxidize partly when exposed to air at room temperature. Therefore, Pd-PVA and Pd-PVP colloid is recommended to be prepared freshly when used as catalyst or catalyst precursor.

The pH of freshly prepared Pd-PVA colloid was about 8 – 9 because of the decomposition of $NaBH_4$, and the colloidal NPs were negatively charged even at very low pH (e.g., pH 1). As a result, it is necessary to adjust the pH to create a positive surface charge on the support materials, in order to adsorb the colloidal NPs.. The shape of the NPs kept sphere-like on activated carbon (AC) according to TEM, whereas changed into hemisphere-like on Al_2O_3, indicating a weaker interaction between Pd NPs with AC than with Al_2O_3. There is a lack of direct evidence on the existence of polymer layer between the “bottom” of the NPs and the support surface in the present study. Both HCl and H_2SO_4 can be used to charge the support positively; however, only HCl showed an additional effect that helps to remove PVA from Pd

NPs supported on activated carbon (AC). CO chemisorption and TEM results show that chlorine, introduced by HCl, effectively suppressed the interaction of the Pd NPs with PVA. Clean and catalytically active Pd NPs were obtained after reduction in H_2/N_2 atmosphere at mild temperature (200ºC) without any significant sintering.

HCl concentration is an important parameter for optimizing the catalytic performance of the resulting Pd/AC catalysts after PVA removal. UV-vis spectra show partly dissolution of Pd by HCl in the presence of air. The catalyst prepared with pH 3, and relatively low Cl^- concentration, exhibits the highest activity as well as relatively low selectivity to ammonium after reduction at 200ºC, despite incomplete removal of PVA from the Pd surface according to CO chemisorption. This indicates that a clean metal surface is not always required for optimizing the selectivity of the catalyst. On the other hand, excess amount of HCl enhanced Pd dissolution, resulting in re-distribution of Pd via dissolved Pd-Cl compounds ($PdCl_x$) the location of polymer stabilizer has rarely been discussed in literature for catalysts prepared via colloidal methods [1-6]. It is also recommended that studies using thermal decomposition or oxidation to remove stabilizers from nanoparticles prepared via colloidal method, addresses the question where the stabilizers are located (on the support or on the metal), when discussing removal of the stabilizers.

6.2. Application of model catalysts prepared via colloidal method for nitrite hydrogenation

Pd NPs supported on AC was applied as model catalysts for nitrite hydrogenation in both fixed bed and slurry phase reactors. The reaction in fixed bed showed that the apparent reaction rate per total Pd was enhanced by using HCl for colloid immobilization instead of H_2SO_4. The results also show that the number of active sites was underestimated with CO chemisorption in gas phase, which is attributed to different configuration of the polymer molecules in absence and presence of liquid water. It is recommended to use CO chemisorption in aqueous phase to estimate the number of active sites.

Impurities such as chlorine bonded on Pd surface can be at least partly removed by the reactant mixture, containing nitrite and hydrogen, in the first hour of operation of the fixed bed. In contrast, any compound released from the catalyst during the reaction in slurry phase, except for the gaseous products like nitrogen (N_2), will remain in the reactor. It has been proved in

this study that the concentration of chlorine in the aqueous phase, ranging between of 0 and 50 μmol L^{-1}, does not influence the activity of the Pd catalysts significantly. On the other hand, the selectivity to ammonium is inhibited when adding chlorine in a low concentration (~30 μmol L^{-1}). Chlorine has been widely used as disinfectant and oxidant in drinking water treatment, with a guideline of 140 μmol L^{-1} as proposed by WHO [7]. However, it is normal practice to supply water with a chlorine residual of a concentration slightly above the guideline value to act as a preservative during distribution. This thesis suggests that a proper concentration of chlorine is necessary to optimize activity and selectivity of Pd catalyst for nitrite hydrogenation in treatment procedure of drinking water. A systemic study of chlorine effect on the activity and the selectivity in a broader chlorine concentration range is also suggested for future study.

For unsupported Pd-PVA and Pd-PVP colloids, CO chemisorption in aqueous phase reveals that the coverage of the Pd surface with polymer is in the order of 80%. Testing in a semi-batch reactor shows that activity and selectivity to ammonium are not influenced by the coverage of the Pd surface by PVA. It is concluded that PVA does not significantly influence adsorbed species on the Pd surface, and therefore the catalytic properties of the remaining sites are not influenced in terms of TOF and selectivity. In contrast, PVP influences adsorbed species significantly; the TOF on the remaining sites, not covered with PVP, increases significantly with increasing the coverage of the Pd surface with PVP whereas the formation ammonium decreases. This clearly suggests that PVP is more suitable as polymer stabilizer than PVA for Pd colloids, in order to achieve high activity together with low selectivity to ammonium. This actually give us a hint that polymers can be candidates of functional assistants to optimize selectivity of catalyst. It would be interesting to investigate the effect on the selectivity with other stabilizers for colloid preparation in future studies.

The particle size effect on activity and selectivity to ammonium of Pd catalyst for nitrite hydrogenation has been discussed in range of 2 – 4 nm, with unsupported Pd-PVA and Pd-PVP colloids. It is confirmed that the TOF is independent with Pd particle size, whereas the selectivity to ammonium decreases with decreasing Pd particle size for unsupported Pd-PVA colloids, ruling out any effect of PVA on the selectivity. According to this, it is recommended that a small Pd particle size is preferable for an optimized catalyst performance for nitrite hydrogenation. As discussed in Chapter 4, this does not agree with some other literatures with Pd catalysts with clean Pd surface [8]. It is noticeable that our study is based on catalysts with significant coverage, typically 80%, by the polymers. It is recommended to investigate the size

dependence with supported Pd NPs prepared via colloidal method, with polymer removal method developed in this study.

The selectivity to ammonium increases with nitrite conversion in a batch reaction, caused by the decrease of N/H ratio on Pd surface. The rate of ammonium formation decreased significantly after 99% nitrite converted, and ammonium kept on converted while no nitrite detected in the reaction suspension for at least 20 h with both unsupported and Al_2O_3 supported Pd-PVA colloid. The amount of ammonium formed after nitrite in aqueous phase consumed turned out to be very close to the number of Pd surface sites estimated by CO chemisorption. ATR-IR results show no N-species was detected consumed for the formation of ammonium during a circulation flow test mimicking batch reaction at nitrite almost-complete conversion level. It is concluded that nitrogen atoms single layer convers most of the Pd surface. These nitrogen atoms convert to ammonium via NO_xH_y species very slowly, thus not involved in the majority conversion of nitrite hydrogenation. In contrast, only a few specific Pd sites, adsorbing NO species, catalyzed most of nitrite hydrogenation to N_2. This also explains why our Pd catalysts were so selectivity to N_2 over ammonium. It is recommended to perform systematic study on the relationship between adsorbed N-species and specific Pd surface sites. Model catalysts with more accurately manipulated size and shape is necessary for this, and in-situ ATR-IR study with unsupported Pd NPs is suggested to use in order to distinguish the surface species.

The mole of Pd surface used in this thesis is typically one magnitude lower than the initial nitrite concentration. The dependence of final ammonium amount with number of Pd surface sites suggests the importance to limit total amount of Pd in a batch reaction, in order to limit the final concentration of ammonium. Alternatively, the batch reaction is suggested to be terminated as early as nitrite concentration lower than detected limitation (~0.5 μmol L^{-1}) to avoid further formation of ammonium. This problem can probably also be avoid by using fixed bed operation, because hydrogen is consumed with the reduction of nitrite, resulting N/H ratio change less significant as compared with a semi-batch reaction. However, it is not clear whether stable nitrogen atom exists in the bed position where nitrite conversion close to complete. A future study with different bed height with high nitrite conversion is suggest to perform.

In summary, the study using model catalyst containing Pd NPs prepared via colloidal method has given us some new understanding for Pd catalysts for nitrite hydrogenation. Polymer stabilizers remaining on Pd NPs are not always necessary to be removed completed,

but rather perform as a functional assistant to increase TOFs and decrease the selectivity to ammonium. An appropriate amount of chlorine in water will inhibit the formation of ammonium without influencing catalyst activity. Small Pd NPs is preferable for low selectivity to ammonium. Low catalyst amount as well as short reaction time is required in order to avoid a slow formation of ammonium.

References

[1] E.G. Rodrigues, S.A.C. Carabineiro, J.J. Delgado, X. Chen, M.F.R. Pereira, J.J.M. Órfão, J. Catal., 285 (2012) 83-91.

[2] C. Aliaga, J.Y. Park, Y. Yamada, H.S. Lee, C.-K. Tsung, P. Yang, G.A. Somorjai, J. Phys. Chem. C, 113 (2009) 6150-6155.

[3] Y. Borodko, H.S. Lee, S.H. Joo, Y. Zhang, G. Somorjai, J. Phys. Chem. C, 114 (2009) 1117-1126.

[4] R.M. Rioux, H. Song, J.D. Hoefelmeyer, P. Yang, G.A. Somorjai, J. Phys. Chem. B, 109 (2004) 2192-2202.

[5] P. Dash, T. Bond, C. Fowler, W. Hou, N. Coombs, R.W.J. Scott, J. Phys. Chem. C, 113 (2009) 12719-12730.

[6] L.R. Baker, G. Kennedy, J. Krier, M. Spronsen, R. Onorato, G. Somorjai, Catal. Lett., 142 (2012) 1286-1294.

[7] World Health Organization, Guidelines for drinking-water quality, 3rd version, 1, in Geneva (2008).

[8] D. Shuai, J.K. Choe, J.R. Shapley, C.J. Werth, Environ Sci Technol, 46 (2012) 2847-2855.

Publications

Journal papers

- Y. Zhao, L. Jia, J.A. Medrano, J.R.H. Ross, L. Lefferts, **Supported Pd Catalysts Prepared via Colloidal Method: The Effect of Acids**, *ACS Catal*., 3 (2013) 2341-2352.
- Y. Zhao, J.A. Baeza, N. Koteswara Rao, L. Calvo, M.A. Gilarranz, Y.D. Li, L. Lefferts, **Unsupported PVA and PVP stabilized Pd nanoparticles as catalyst for nitrite hydrogenation in aqueous phase**, *J. Catal.,* 318 (2014) 162-169.
- Y. Zhao, Y.D. Li, L. Lefferts, **Adsorption Species on Pd Catalyst for Nitrite Hydrogenation at Close-to-complete Conversion**, *Manuscript in preparation* (2014)
- Y. Zhao, L.L. Wang, Y.D. Li, L. Lefferts, **Pd Colloid Supported on Activated Carbon: An Optimization of Preparation**, *Manuscript in preparation* (2014)
- N. Koteswara Rao, Y. Zhao, B.L. Mojet, A. van Houselt and L. Lefferts, **Interaction of PVA stabilized Pd nanoparticles with nitrite isotopes studied with ATR-IR**, *Manuscript in preparation* (2014)
- N. Koteswara Rao, Y. Zhao, B.L. Mojet, A. van Houselt and L. Lefferts, **Particle size effects on nitrite adsorption and reduction on Pd colloidal nanoparticles: ATR-IR studies**, *Manuscript in preparation* (2014)

Presentations

Oral:

- **Unsupported PVA and PVP Stabilized Pd Nanoparticles as Catalyst for Nitrite Hydrogenation**, *8th ICEC*, USA, 2014
- **Unsupported PVA and PVP Stabilized Pd Colloid as Catalyst in Aqueous Phase**, *NCCC XV*, The Netherlands, 2014
- **Remove Polymer Stabilizer Blocking on Colloidal Nanoparticles**, *NCCC XIV*, The Netherlands, 2014

Poster:

- **Suppression of PVA Blocking Effect on the Surface of Supported Pd Nanoclusters,** *11th EuropaCat*, France, 2013

- **Chlorine Suppression Stabilizer Poisoning on Supported Pd Nanoparticles**, *Faraday Discussion 162*, Germany, 2013
- **Polymer Removal from Supported Pd Colloids**, *NCCC XIII*, The Netherlands, 2012
- **Nitrite Selective Hydrogenation over Supported Pd Catalyst in Slurry Phase**, *NCCC XII*, The Netherlands, 2011

Summary

The study on stabilization of colloids, containing nano-sized particles dispersed in liquid, has been lasting for 160 years since the time of Faraday, yet the application of colloidal methods for catalysis has only become extensive in the last 30 years. The most distinguished advantage to use colloidal methods for catalyst preparation is that the size and the shape of nanoparticles can be manipulated easily under good control, which is normally difficult to achieve by using traditional methods, such as impregnation and precipitation. This facilitates studies on structure sensitivity of catalytic reactions, i.e., the relationship between the size of active metal particles and their catalytic activity. However, the challenges of using colloidal methods is also quite obvious: the residing stabilizers on the metal surface are normally difficult to remove completely, inducing complex influences on catalytic reactions taking place on the metal surface.

Nitrate and nitrite contamination of groundwater is threatening the safety for supply of drinking water in many areas all over the world, mainly caused by over-fertilization in modern agriculture. Catalytic nitrate hydrogenation has been developed as an efficient and inexpensive way to remove nitrate and nitrite contamination in drinking water. In these reactions, nitrate can be reduced to nitrogen (N_2) using bimetallic hydrogenation catalysts, with nitrite as an intermediate product and ammonium as by-product. Pd catalysts have been found most efficient for nitrite hydrogenation. A high selectivity to N_2 of the catalyst is required, because ammonium is also harmful in drinking water. It has been proved that the selectivity is influenced by reaction conditions, such as reactant concentration, pH, and temperature. Mass transfer limitation should also be carefully avoided in order to discuss intrinsic catalytic performance and to optimize the performance. There has been disagreement on the influence of Pd particle size on the catalyst performance, and a study with model catalysts with different Pd particle sizes, which can be prepared with colloidal methods, may answer the open question.

A novel method has been developed to remove residing polymer stabilizer (polyvinyl alcohol (PVA)) from Pd surface after immobilization of the colloid on activated carbon (AC), as described in Chapter 2. It is shown that Pd dispersion calculated based on CO chemisorption results is quite similar to estimation based on particle sizes as observed with TEM only when HCl was used during colloid immobilization after Pd nanoparticles prepared, followed by reduction in H_2 at 200^{o}C. XPS results show that the chlorine content on the catalyst influences the oxidation state of Pd. A mechanism is proposed that chlorine fully covers the Pd surface in

presence of air, suppressing the coverage of the Pd surface by PVA. Furthermore, thermal decomposition of PVA in H_2 or inert atmosphere has also been studied, and the results show different decomposition temperature for PVA located on Pd surface as compared to PVA adsorbed on AC. In Chapter 5, it is also shown that chlorine suppress the selectivity to ammonium without a significant effect on activity.

In Chapter 3, unsupported colloidal Pd NPs are used directly as catalyst in aqueous phase in order to rule out any support effect. Polymer stabilizers, PVA and PVP, containing different functional groups, have been used with varying polymer-monomer/Pd molar ratios, in order to achieve different particle sizes and coverages of the Pd surface by polymer. It is found that both PVA and PVP block Pd sites, limiting the apparent activity of the catalyst. However, PVP influences the activity per Pd surface atom not covered with PVP. PVP also influences the selectivity to ammonium, probably by influencing reaction intermediates adsorbed on the available Pd sites. In contrast, PVA shows no such effects.

The selectivity to ammonium changes dramatically when approaching complete nitrite conversion with both unsupported and Al_2O_3 supported Pd-PVA colloid in a semi-batch reactor, as shown in Chapter 4. The increase of ammonium amount after exhaustion of nitrite is quite close to the number of Pd surface sites estimated based on CO chemisorption. ATR-IR results show no consumption of any infrared sensitive N-species at almost-complete conversion level. A mechanism has been proposed that nitrogen atoms cover most Pd surface sites. These N atoms are rather unreactive with hydrogen, converting very slowly to ammonium. Consequently nitrite is converted on a minority Pd site, with high reaction rate and high selectivity to N_2.

Samenvatting

Stabilisatie van nano-deeltjes verspreid in een vloeistof, in het algemeen aangeduid als colloïden, wordt al 160 jaar bestudeerd sinds de tijd van Faraday, maar de toepassing van colloïdale methoden voor bereiding van katalysatoren heeft pas aandacht gekregen in de afgelopen 30 jaar. Het voornaamste voordeel van de toepassing van colloïden voor katalysatorbereiding is dat de grootte en de vorm van nano-deeltjes gemakkelijk en precies kunnen worden gemanipuleerd. Dit is gewoonlijk moeilijk te bereiken met behulp van traditionele methoden, zoals impregnering en precipitatie. Dit faciliteert onderzoek naar de relatie tussen de structuur van katalysatoren en de katalytische eigenschappen, bijvoorbeeld naar de relatie tussen de afmeting van actieve metaaldeeltjes en hun katalytische activiteit. De nadelen van colloïdale methoden is ook heel duidelijk: stabilisatoren zijn gewoonlijk moeilijk volledig te verwijderen van het oppervlak van de metaaldeeltjes en beïnvloeden de katalytische reacties op het metaaloppervlak.

Nitraat en nitriet verontreiniging van het grondwater is een bedreiging voor de veiligheid van de drinkwatervoorziening in veel regio's over de hele wereld, vooral veroorzaakt door overbemesting in de moderne landbouw. Katalytische hydrogenering van nitraat is ontwikkeld als een efficiënte en goedkope manier om nitraat en nitriet vervuiling te verwijderen uit drinkwater. In deze reactie wordt nitraat omgezet tot moleculair stikstof (N_2) middels bimetallische hydrogeneringskatalysatoren, met nitriet als intermediair product en ammonium als bijproduct. Pd katalysatoren bleken het meest efficiënt voor nitriet hydrogenering. Een hoge selectiviteit naar N_2 is vereist, omdat ammonium ook schadelijk is voor de gezondheid en dus niet te tolereren is in drinkwater. Het is bekend dat de selectiviteit wordt beïnvloed door de reactieomstandigheden, zoals reactant concentratie, pH-waarde en temperatuur. Massatransport-limiteringen moet zorgvuldig worden vermeden om de intrinsieke katalytische eigenschappen te kunnen vaststellen, en vervolgens te optimaliseren. Er is onzekerheid en wetenschappelijk debat over de invloed van de Pd deeltjesgrootte op de katalytische prestatie; daarom is onderzoek met model katalysatoren met verschillende en goed beheerste afmeting van de Pd deeltjes met behulp colloïdaal methoden van wetenschappelijk belang.

Hoofdstuk 2 beschrijft een nieuwe methode om polymeer-stabilisatoren (polyvinylalcohol (PVA)) van het Pd oppervlak te verwijderen, nadat het colloïd geïmmobiliseerd is op een actieve-kool dragermateriaal (AC). Er wordt aangetoond dat de Pd dispersie, berekend op basis van CO chemisorptie data, zeer vergelijkbaar is met schattingen op basis van TEM, onder

voorwaarde dat HCl werd gebruikt tijdens immobilisatie van de Pd nano-deeltjes, gevolgd door reductie met H_2 bij 200°C. XPS resultaten laten zien dat het chloorgehalte van de katalysator de oxidatietoestand van Pd beïnvloedt. Een mechanisme is voorgesteld, waarin chloor het Pd oppervlak volledig bedekt in aanwezigheid van lucht, waarmee de interactie van het oppervlak met PVA wordt onderdrukt. Thermische decompositie van PVA in H_2 of inerte atmosfeer werd eveneens onderzocht en de resultaten tonen verschillende ontledingstemperaturen aan van PVA op Pd oppervlak ten opzichte van PVA geadsorbeerd op AC. Het is ook aangetoond in Hoofdstuk 5 dat chloor de selectiviteit naar ammonium onderdrukt, zonder significant effect op de activiteit te hebben.

In Hoofdstuk 3 worden colloïdaal Pd NP's gebruikt als katalysator zonder drager materiaal om de katalytische eigenschappen te bepalen in afwezigheid van mogelijke effecten van het drager materiaal. Polymeer stabilisatoren, PVA en PVP, die verschillende functionele groepen omvatten, zijn gebruikt met variërende molaire verhoudingen van polymeer-monomeer en Pd, om verschillende deeltjesgrootte en bedekking van het Pd oppervlak met het polymeer te bereiken. Het blijkt dat zowel PVA en PVP Pd sites blokkeren en de activiteit van de katalysator beperken. Echter, PVP beïnvloedt de activiteit per Pd atoom dat niet is bedekt met PVP in het oppervlak van de Pd deeltjes. PVP blijkt ook invloed the hebben op de selectiviteit naar ammonium, waarschijnlijk door beïnvloeding van geadsorbeerde reactie-intermediairen op de Pd sites. Daarentegen toont PVA dergelijke effecten niet.

Hoofdstuk 4 laat zien dat de selectiviteit naar ammonium dramatisch toeneemt bij het naderen van compleet conversie van nitriet in semi-batch reactoren, met zowel ongedragen als ook Al_2O_3 gedragen Pd-PVA colloïden. De toename van de hoeveelheid ammonium dat wordt gevormd als nitriet al is uitgeput, is vergelijkbaar met het aantal Pd atomen aan het oppervlak van de metaaldeeltjes, geschat op basis van CO chemisorptie. ATR-IR resultaten laten zien dat op dat moment geen N-houdende oppervlaktespecies aanwezig zijn die te detecteren zijn met IR spectroscopie. Daarom is voorgesteld dat stikstofatomen de meeste Pd oppervlakteplaatsen bedekken, die met een zeer lage reactiesnelheid omgezet kunnen worden naar ammonium. Het dominante snelle reactie-pad van nitriet met hoge selectiviteit naar N_2 wordt blijkbaar gekatalyseerd door een kleine fractie van het Pd oppervlak.

Acknowledgements

On January 14, 2010, I arrived at this quiet, small town in the snow evening. I was pulling two heavy luggage cases, and another big bag on my back, sweating to find the right hotel inside the campus. At that moment, I can hardly imagine how many dear friends I would meet and what kind of memorable journey I would experience. For a long time, I have already regarded Enschede as another hometown. At the end of this thesis, I would like to thank many people I have met in the five years.

I would like to first thank my supervisor Prof. dr. ir. Leon Lefferts. Leon, it has been my great honour to be your student in the last five years. You are a real gentleman and a great motivator. You have guided me to think, and to make right decisions. I will always remember the progress meetings we had, often needed to prolong because of exiting discussions. I will always remember your great patience on improving my writing, making me confident more and more on the output of my work. I will always remember the attitude you have taught me on facing challenges. I would also thank you for the freedom you gave to me on the direction of research.

I would like to thank Dr. Željko Kotanjac and Dr. José Medrano Catalán to supervise me daily during the first three years. Željko, thank you for teaching me to be critical in science. José, thank you for encouraging me to face difficulties with peaceful mind.

Prof. Yongdan Li, I would like to thank you for introducing me the great opportunity to study in The Netherlands. The skills you have taught made me an easier start of my PhD study. I would also like to thank you for your continuous contribution during the study for this thesis.

There are many people with whom I have greatly collaborated along the five years. I would like to express my gratitude to Prof. Julian Ross, Prof. Miguel Ángel Gilarranz Redondo and Dr. Luisa Calvo Hernández for your kind help, inputs and suggestions during the study for this thesis. I would also thank Lijun, José Alberto, and Rao for the exiting collaboration and the nice outputs.

Many thanks to the scientific staff in CPM group: Seshan, Barbara and Arie, I enjoyed and learned a lot from the discussion with you on scientific/non-scientific topics.

Sebine, Lidy and Maaike, thank you so much for all your kind help on administrative issues. Maaike, I especially thank you to give homelike feel to our CPM members.

Bert, my big friend, you are always there whenever I need help in the lab, or need advice on my life. I will always remember the nice borrel time we have spent, with topics on phones, cultures and some other stuffs, although I am too easy to be red. Thank you. ☺

Karin, Tom and Luben, thank you for your technical support in laboratory. And Louise, thank you for the help and discussion on XRF and BET. You are wonderful. I would also like to acknowledge the kind help from Mark Smithers for TEM and Gerard Kip for XPS measurements.

I would special thank my dear officemates Joline, Shilpa and Arturo. I miss the long chats, games, and New Year's Eve we had together. Joline, thank you for always helping with the Dutch translation, and the support on Dutch daily rules. Shilpii, you are small lady but powerful. I know you can achieve whatever you want. Best wishes for you and James with happy life. Really wish I can make you some dumplings again in future. Arturo, you are perfect as my friend, colleague and even teacher. I will always remember the positive attitude you have shared on life. Again, "post-CPM trip" is an excellent idea! ☺

Furthermore, I would like to thank my coworkers Roger, Cristina, Rao and Jie for the help and suggestions. I thank my colleagues Kumar, Cassia, Vijay, Marijana, Sergio, Dennis, Son, Masoud, Raman, Hrudya, Châu, Kamila, Kaisa, Songbo and Yejun for the pleasant time. I miss the great time with you in the group trips, international dinners, BBQs, drinking nights and NCCC conferences.

During the five years I came to know many friend in Enschede, making my life colourful. Lantian, Liu Feng, Songbo, Du Ying, Jiajia, Zhu Dan, Chenxi, Chen Wei and many many more, thank you and hope our friendship last long.

Special thanks to Fred for helping me to translate the summary part into Dutch. Best wishes for you and your girlfriend.

Finally I would like to thank my family:

爸爸妈妈，感谢您们对我出国深造的支持和理解。虽然远隔万里，我知道你们对我的牵挂。这五年，儿子成长了。感谢您们对我无私的爱，我也爱您们！

亲爱的银儿，我曾对你说，荷兰，就是我们两个人的催化剂吧？能够与你相知相爱是我在这五年里最幸运的事情，早上醒来看见你在身边是我一天最美的时刻。我要谢

谢你对我工作进度缓慢的理解，以及你带给我的家的温暖。荷兰是我们的起点，而不管将来我们生活在哪里，我对会努力做的更好，与你携手共行。爱你！

Yingnan Zhao (赵英男) was born in Heze, Shandong, China, in 1984. He graduated from China Petroleum University (East China) with Bachelor degree on Chemical Engineering. Then he finished his master's studies in Industrial Chemistry under the supervision from Prof. Yongdan Li, in Tianjin University, in 2009. He started his PhD study under the supervision of Prof. Leon Lefferts in Catalytic Processes and Materials group (CPM) in University of Twente from 2010. The current work presents part of the outcome of his PhD research.

UNIVERSITY OF TWENTE.